

1-1-2008

Satellite attitude control using environmental forces based on variable structure control

Tarunkumar Patel
Ryerson University

Follow this and additional works at: <http://digitalcommons.ryerson.ca/dissertations>

 Part of the [Aerospace Engineering Commons](#)

Recommended Citation

Patel, Tarunkumar, "Satellite attitude control using environmental forces based on variable structure control" (2008). *Theses and dissertations*. Paper 154.

SATELLITE ATTITUDE CONTROL
USING ENVIRONMENTAL FORCES BASED ON
VARIABLE STRUCTURE CONTROL

by

Tarunkumar Patel
B.Eng., Aerospace Engineering
Ryerson University, 2006

A thesis presented to Ryerson University

in partial fulfillment of the requirements for the degree of

Master of Applied Science

in the Program of

Aerospace Engineering

Toronto, Ontario, Canada, 2008

© Tarun Patel 2008



AUTHOR'S DECLARATION

I hereby declare that I am the sole author of this thesis.

I authorize Ryerson University to lend this thesis to other institutions or individuals for the purpose of scholarly research.

I further authorize Ryerson University to reproduce this thesis by photocopying or by other means, in total or in part, at the request of other institutions or individuals for the purpose of scholarly research.



DEDICATION

This thesis is dedicated to my parents, Rasikbhai and Kailashben, and my wife, Roshni, who have given me all the support I needed during my education towards Master of Applied Science in Aerospace Engineering.

ABSTRACT

SATELLITE ATTITUDE CONTROL USING ENVIRONMENTAL FORCES BASED ON VARIABLE STRUCTURE CONTROL

Tarunkumar Patel, Master of Applied Science, Aerospace Engineering
Ryerson University, Toronto, 2008

The present thesis examines the use of environmental forces for satellite attitude control using variable structure control. The system comprises of a satellite with control flaps to utilize environmental forces such as solar radiation pressure and aerodynamic forces. A variable structure control approach has been adopted to develop control law for suitably rotating the control flaps to achieve desired satellite attitude performance. The detailed numerical simulation of the governing nonlinear system equation of motion including the effects of various system parameters on the controller performance establishes the effectiveness of the proposed control strategy. The numerical simulation matches with the analytical results. Furthermore from analysis, the proposed controller is found to be robust against parameter uncertainties and external disturbances and its performance is superior in comparison to other strategies proposed in the literature. Thus, the robustness of the proposed control strategy and utilizing natural environmental forces for attitude control makes the proposed concept attractive for future space applications.

ACKNOWLEDGMENTS

I would like to first thank my thesis supervisors, Dr. Krishna Dev Kumar and Dr. Kamran Behdinan, for their support and encouragement throughout this research work. I would like to express my deepest gratitude to Dr. Krishna Dev Kumar for providing guidance and advice on the topic of satellite attitude control using environmental forces as well as his personal help other than academic. I would also like to thank Dr. Kamran Behdinan for overseeing my thesis progress and giving very helpful suggestions during my research. I am very thankful to my external examiner members, Dr. Jeffrey Yokota, Dr. Jeff Xi, and Dr. Puren Ouyang, for reviewing my research work and providing useful comments for improving thesis report. I also want to thank for all the graduate students in our SSDC group, who gave me a lot help in academics and life. I would like to thank Godard for helping me to prepare final thesis presentation as well as his valuable suggestions and discussions during this thesis work, which were valuable and positive. I am also very thankful to Kamran Shahid for setting up our SSDC lab and providing complete computer facilities with all tools I needed for research. Finally, but most importantly, to my parents, Rasikbhai and Kailasben, and my wife, Roshni, without whose unconditional love, patience, support, understanding, guidance, and belief in my abilities, I would have never come this far in life.

TABLE OF CONTENTS

AUTHOR'S DECLARATION.....	ii
DEDICATION.....	iii
ABSTRACT.....	iv
ACKNOWLEDGMENTS.....	v
TABLE OF CONTENTS.....	vi
LIST OF FIGURES.....	ix
LIST OF TABLES.....	xii
NOMENCLATURE.....	xiii
ACRONYMS.....	xvi
1. Introduction.....	1
1.1 Introduction.....	1
1.2 Literature Reviews.....	2
1.2.1 Solar Radiation Pressure Torques.....	2
1.2.2 Aerodynamic Torques.....	3
1.2.3 Combination of Environmental Torques.....	4
1.3 Motivation.....	5
1.4 Research Objectives.....	5
1.5 Contributions of Thesis.....	5
1.6 Thesis Organization.....	6
2. Background on Variable Structure Control.....	9
2.1 Introduction.....	9
2.2 Sliding Surface Design.....	12
2.3 Lyapunov Design.....	14
2.4 Design of Reaching Laws.....	14
2.5 Properties of VSC.....	15

2.6	Analytical Proofs for Disturbance Rejection and Parameter Uncertainties	16
2.7	Chattering Phenomenon	20
3.	Application of Solar Radiation Pressure for Satellite Attitude Control.....	21
3.1	Introduction	21
3.2	Proposed System Model.....	21
3.2.1	System Description	21
3.2.2	Equation of Motion	23
3.3	Control Laws	26
3.3.1	Circular Orbit	26
3.3.2	Elliptic Orbit.....	32
3.4	Analytical Solution for Tracking Error	37
3.5	Analytical Proofs for Disturbance Rejection and Parameter Uncertainties	40
3.6	Results and Discussions	43
3.6.1	Circular Orbit	43
3.6.2	Elliptic Orbit.....	55
3.7	Summary	66
4.	Application of Aerodynamic Forces for Satellite Attitude Control.....	69
4.1	Introduction	69
4.2	System Model - I.....	69
4.2.1	System Description	69
4.2.2	Equation of Motion	71
4.2.3	Control Laws	76
4.2.4	Results and Discussions	80
4.3	System Model - II.....	87
4.3.1	System Description	87
4.3.2	Kinematics and Equations of Motion.....	88
4.3.3	Control Laws	96

4.3.4	Results and Discussions	99
4.4	Summary	108
5.	Conclusions.....	109
5.1	Conclusions	109
5.1.1	Solar Radiation Pressure Torques Stabilized Satellite	109
5.1.2	Aerodynamic Torques Stabilized Satellite	110
5.2	Future Works.....	111
	References.....	113
	List of Publications From Present Research	117

LIST OF FIGURES

Figure 2.1:	Variable structure control trajectories.....	10
Figure 3.1:	Geometry of orbit motion for solar radiation pressure torques stabilized satellite	22
Figure 3.2:	Geometry of satellite and proposed solar controller configuration	23
Figure 3.3:	Solar flap deflection and solar flap deflection rate response as affected by mass distribution parameter K : $C=5$, $\psi = 45^\circ$, $i = 0^\circ$, $\varepsilon_s = 23.5^\circ$, $\eta = 0.5$, $p_1 = 16$, $p_2 = 8$, $\alpha_0 = 110^\circ$, $\alpha'_0 = 0$	45
Figure 3.4:	Effect of solar parameter C on solar flap deflection and solar flap deflection rate: $K=0.5$, $\psi = 45^\circ$, $i = 0^\circ$, $\varepsilon_s = 23.5^\circ$, $\eta = 0.5$, $p_1 = 16$, $p_2 = 8$, $\alpha_0 = 110^\circ$, $\alpha'_0 = 0$	46
Figure 3.5:	Effect of solar aspect angle ψ on solar flap deflection and solar flap deflection rate: $K=0.5$, $C=5$, $i = 0^\circ$, $\varepsilon_s = 23.5^\circ$, $\eta = 0.5$, $p_1 = 16$, $p_2 = 8$, $\alpha_0 = 110^\circ$, $\alpha'_0 = 0$	48
Figure 3.6:	Effect of orbit inclination i on solar flap deflection and solar flap deflection rate: $K=0.5$, $C=5$, $\psi = 45^\circ$, $\varepsilon_s = 23.5^\circ$, $\eta = 0.5$, $p_1 = 16$, $p_2 = 8$, $\alpha_0 = 110^\circ$, $\alpha'_0 = 0$	50
Figure 3.7:	Performance of sliding mode control (SMC) under the periodic tracking: $K=0.5$, $C=5$, $\psi = 45^\circ$, $i = 0^\circ$, $\varepsilon_s = 23.5^\circ$, $\eta = 1$, $p_1 = 16$, $p_2 = 8$, $\alpha_0 = 110^\circ$, $\alpha'_0 = 0$	52
Figure 3.8:	Performance of sliding mode control (SMC) and feedback linearization (FL) under the effect of disturbance: $K=0.5$, $C=5$, $\psi = 45^\circ$, $i = 0^\circ$, $\varepsilon_s = 23.5^\circ$, $\eta = 1$, $p_0 = 81$, $p_1 = 108$, $p_2 = 54$, $p_3 = 12$, $\alpha_0 = 0^\circ$, $\alpha'_0 = 0$	53
Figure 3.9:	Performance of sliding mode control (SMC) in presence of parameter uncertainties into the mass distribution parameter (K) and the solar parameter (C): $K=0.5$, $C=5$, $\psi = 45^\circ$, $i = 0^\circ$, $\varepsilon_s = 23.5^\circ$, $\eta = 1$, $p_0 = 81$, $p_1 = 108$, $p_2 = 54$, $p_3 = 12$, $\alpha_0 = 0^\circ$, $\alpha'_0 = 0$	54

Figure 3.10:	Effect of eccentricity on the system performance and control solar flap deflection: $K=0.5$, $C=5$, $\psi = 45^\circ$, $i = 0^\circ$, $\varepsilon_s = 23.5^\circ$, $\eta = 0.5$, $p_1 = 9$, $p_2 = 6$, $\alpha_0 = 100^\circ$, $\alpha'_0 = 0$	56
Figure 3.11:	The system performance and control solar flap deflection response as affected by mass distribution parameter K : $e=0.2$, $C=5$, $\psi = 45^\circ$, $i = 0^\circ$, $\varepsilon_s = 23.5^\circ$, $\eta = 0.5$, $p_1 = 9$, $p_2 = 6$, $\alpha_0 = 100^\circ$, $\alpha'_0 = 0$	57
Figure 3.12:	Effect of solar parameter C on the system performance and control solar flap deflection: $e=0.2$, $K=0.5$, $\psi = 45^\circ$, $i = 0^\circ$, $\varepsilon_s = 23.5^\circ$, $\eta = 0.5$, $p_1 = 9$, $p_2 = 6$, $\alpha_0 = 100^\circ$, $\alpha'_0 = 0$	58
Figure 3.13:	Effect of solar aspect angle ψ on the system performance and control solar flap deflection: $e=0.2$, $K=0.5$, $C=5$, $i = 0^\circ$, $\varepsilon_s = 23.5^\circ$, $\eta = 0.5$, $p_1 = 9$, $p_2 = 6$, $\alpha_0 = 100^\circ$, $\alpha'_0 = 0$	60
Figure 3.14:	Effect of orbit inclination i on the system performance and control solar flap deflection: $e=0.2$, $K=0.5$, $C=5$, $\psi = 45^\circ$, $\varepsilon_s = 23.5^\circ$, $\eta = 0.5$, $p_1 = 9$, $p_2 = 6$, $\alpha_0 = 100^\circ$, $\alpha'_0 = 0$	61
Figure 3.15:	Performance of sliding mode control (SMC) in presence of parameter uncertainties into the orbital eccentricity (e), the mass distribution parameter (K) and the solar parameter (C): $e=0.2$, $K=0.5$, $C=5$, $\psi = 45^\circ$, $i = 0^\circ$, $\varepsilon_s = 23.5^\circ$, $\eta = 0.5$, $p_1 = 9$, $p_2 = 6$, $\alpha_0 = 100^\circ$, $\alpha'_0 = 0$	63
Figure 3.16:	Performance comparison of sliding mode control (SMC) and terminal sliding mode control (TSMC): $K=0.5$, $C=5$, $\psi = 45^\circ$, $i = 0^\circ$, $\varepsilon_s = 23.5^\circ$, $\eta = 0.5$, $p_1 = 9$, $p_2 = 6$, $\alpha_0 = 100^\circ$, $\alpha'_0 = 0$	64
Figure 3.17:	Performance of sliding mode control (SMC) in presence of external disturbance: $K=0.5$, $C=5$, $\psi = 45^\circ$, $i = 0^\circ$, $\varepsilon_s = 23.5^\circ$, $\eta = 0.5$, $p_1 = 9$, $p_2 = 6$, $\alpha_0 = 100^\circ$, $\alpha'_0 = 0$	65
Figure 4.1:	Geometry of orbit motion and proposed aerodynamic controller configuration	70
Figure 4.2:	Geometry of aerodynamic control surface element	72
Figure 4.3:	Effect of K on system performance and control flap deflection: $C_a = 5$, $\eta = 0.5$, $p_1 = 6$, $p_2 = 12$, $p_3 = 8$, $\alpha_0 = 70^\circ$, $\alpha'_0 = 0.01$	82

Figure 4.4:	Effect of aerodynamic parameter C_a system performance and control flap deflection: $K=0.5, \eta = 0.5, p_1 = 6, p_2 = 12, p_3 = 8, \alpha_0 = 70^\circ, \alpha'_0 = 0.01$	83
Figure 4.5:	Performance of sliding mode control (SMC) in presence of parameter uncertainties into the mass distribution parameter (K) and the aerodynamic parameter (C_a): $K=0.5, C_a = 5, \eta = 0.5, p_1 = 6, p_2 = 12, p_3 = 8, \alpha_0 = 70^\circ, \alpha'_0 = 0.01$	85
Figure 4.6:	Performance of sliding mode control (SMC) in presence of external disturbance: $K=0.5, C_a = 5, \eta = 0.5, p_1 = 6, p_2 = 12, p_3 = 8, \alpha_0 = 70^\circ, \alpha'_0 = 0.01$	86
Figure 4.7:	Geometry of orbit motion and proposed aerodynamic controller configuration	88
Figure 4.8:	Detailed schematic diagram of the spacecraft	93
Figure 4.9:	Pico-satellite attitude response.....	100
Figure 4.10:	Pico-satellite control flaps deflections.....	101
Figure 4.11:	Satellite attitude response in presence uncertainties in principle moment of inertia(30% decrease).....	102
Figure 4.12:	Control flaps response in presence of uncertainties in principle moment of inertia(30% decrease).....	103
Figure 4.13:	Satellite attitude response in presence of uncertainties in principle moment of inertia (30% increase)	104
Figure 4.14:	Control flaps response in presence of uncertainties in principle moment of inertia (30% increase)	105
Figure 4.15:	Satellite attitude response in presence of external disturbances	106
Figure 4.16:	Control flaps response in presence of external disturbances	107

LIST OF TABLES

Table 3.1:	Maximum flap deflection and deflection rate for different solar parameter C for circular orbit (transient condition).....	47
Table 3.2:	Min-Max flap deflection for different solar parameter C for circular orbit (steady-state condition).....	47
Table 3.3:	Maximum flap deflection and deflection rate for different solar aspect angle for circular orbit (transient condition).....	49
Table 3.4:	Min-Max flap deflection for different solar aspect angle for circular orbit (steady-state condition).....	49
Table 3.5:	Maximum flap deflection and deflection rate for different orbit inclination for circular orbit (transient condition)	51
Table 3.6:	Min-Max flap deflection for different orbit inclination for circular orbit (steady-state condition).....	51
Table 3.7:	Maximum control solar flap deflection for different solar parameter C.....	59
Table 3.8:	Maximum control solar flap deflection for different solar aspect angle.....	60
Table 3.9:	Maximum control solar flap deflection for different orbit inclination	62
Table 4. 1:	Parameters for Model-I.....	81
Table 4.2:	Maximum control flap deflection for different aerodynamic parameter C_a (transient condition).....	84
Table 4. 3:	Parameters for Model-II.....	99

NOMENCLATURE

a	semi-major axis
A_j	total surface area of control flap
C	$2\rho_s p A r / (I_x \Omega^2)$, a dimensionless solar parameter
C_a	$\frac{\rho \ \vec{V}_R\ ^2 A r}{4 I_z \Omega^2}$, a dimensionless aerodynamic parameter
C_D	aerodynamic drag coefficient
C_L	aerodynamic lift coefficient
e	orbital eccentricity
h_i	control parameters
h_s	Satellite height
i	orbit inclination with respect to the equatorial plane
$\hat{i}, \hat{j}, \hat{k}$	unit vectors along the satellite body-fixed axes X, Y, Z, respectively
I_k	principal centroidal moment of inertia of satellite about k-axis, k=x,y,z
l_f	length of aerodynamic control flap-j
l_s	length of satellite
k, k_j	control parameters
k_{period}	oscillation period for sinusoidal tracking
K	$(I_y - I_z) / I_x$; satellite mass distribution parameter
\vec{n}_j	unit vector along normal to the surface of control flap-j
p	nominal solar radiation pressure constant at 1 astronomical unit from the Sun
p_j	controller parameters
q_j	controller parameters
r	distance between the center of pressure of the solar flap from the system center of mass
r_s	reference length for aerodynamic torque stabilized satellite
r_j	position vector from system center of mass to the center of pressure of the control flaps
R	orbital radius

R_E	Earth radius
\vec{s}_j	unit vector of the incoming light from the sun on the solar flap-j
S	sliding surface
u_j	control input-j
V	Lyapunov function
w	external disturbances
w_s	satellite width, [m]
O	satellite center of mass of
$O-X_0, Y_0, Z_0$	coordinate axes in the local vertical frame
$O-X, Y, Z$	satellite body coordinate frame
ε_s	angle between the equatorial and ecliptic planes
α_L	satellite pitch angle with respect to orbital frame for SRP stabilized satellite
α	satellite pitch angle with respect to inertial frame for SRP stabilized satellite
α_f	final orientation of satellite
α, ϕ, γ	satellite pitch, roll, and yaw angle with respect to orbital frame for aerodynamic torques stabilized satellite
η	control parameter
β_j	angular rotation of the control flap-j
μ	Earth gravitational constant
φ	control parameter
ψ	solar aspect angle or the angle between the direction of the sun and the nodal line
λ_s	desired pole of the closed loop system
ρ	atmospheric density
ζ_j	angle between the relative velocity \vec{V}_R and the outward unit normal vector \vec{n}_j of the aero flap-j
χ_j	angle between the relative velocity \vec{V}_R and the aero flap-j surface
$\rho_d, \rho_s, \rho_t, \rho_a$	a fraction of impinging photons diffusely reflected, specularly reflected, transmitted, and absorbed, respectively
Ω	$\sqrt{\mu/R^3}$, mean orbital rate circular orbits

Ω $\sqrt{\mu/a^3}$, mean orbital rate for elliptic orbit

[] or bold represent matrix

face

$(.)_j$ $(.)$ for j^{th} control flap, $j=1,2$

$(.)_o$ $(.)$ at $\theta=0$ of $t=0$

$(.)'$, $(.)''$ $d(.) / d\theta$ and $d^2(.) / d\theta^2$, respectively

(\dot{q}) , (\ddot{q}) $d(q) / dt$ and $d^2(q) / dt^2$, respectively

$l(.)$ l_{\max} absolute maximum amplitudes of $(.)$

ACRONYMS

ACS	Attitude Control System
FL	Feedback Linearization
GEO	Geosynchronous Earth Orbit
GNC	Guidance, Navigation, and Control
LEO	Low Earth Orbit
SMC	Sliding Mode Control
SRP	Solar Radiation Pressure
TSMC	Terminal Sliding Mode Control
VSC	Variable Structure Control

Chapter 1

Introduction

1.1 Introduction

The attitude stability of a satellite is very important for successful completion of a space mission. The Attitude Control System (ACS) for satellite aims on orienting and stabilizing the satellite in desired setpoint positions. ACS require sensors to measure states of the satellites, actuators to apply torques needed to re-orient the satellite to a desired attitude, and control laws, a set of computations that determine how to command the actuators, based on the sensor measurements. Unfortunately, even though a satellite may be precisely oriented in the beginning, it deviates in time from its preferred orientation under the influence of environmental torques caused by gravity gradient, solar radiation pressure, magnetic, aerodynamic, and free molecular reaction forces [1-2]. However, these forces if properly utilized may stabilize the attitude of the satellite instead of deteriorating it. Several methods of attitude stabilization have been developed over the last four decades. These methods may be broadly classified as active and passive methods. Active stabilization methods require expenditure of propellant or energy, leading to an increase in weight and space requirements. Some of the well known examples are micro-thrusters, reaction wheels, and control momentum gyros. These can assure precise satellite orientation to practically any desired degree of accuracy. On the other hand, passive methods depend on natural forces and they make use of spin stabilization, dual spin, gravity gradient, solar radiation pressure (SRP), aerodynamic, and Earth's magnetic field. These methods are thus low cost and their

development may provide a viable solution to the recent thrust, by space researchers worldwide, on the development of low cost attitude control systems (ACS) and guidance, navigation, and control systems (GNC) for satellites. However, their development poses several challenges including techniques to utilize these forces effectively, low attitude accuracies, and unavailability of forces. The present thesis undertakes these challenges and focuses on the application of SRP forces and aerodynamic forces for attitude control of satellites with a view to achieve the goal of low cost ACSs with higher degree of accuracy for attitude stability of satellite.

1.2 Literature Reviews

The literature review on satellite attitude stabilization using SRP is first presented followed by pertinent literature on the application of aerodynamic forces for satellite attitude stabilization is presented in next section.

1.2.1 Solar Radiation Pressure Torques

The solar radiation pressure (SRP) for attitude control of high altitude satellites and interplanetary probes has been investigated by several researchers [3-27]. For utilizing SRP torque, various configurations have been proposed. These include trailing cone system [3], weathervane type tail surfaces [4], reflector-collector system [5], corner mirror arrays [6], solar paddles [7], grated solar sails [8], and mirror-like surfaces [9-24]. These configurations have been proposed for sun-pointing satellites [7, 8] and gravity-oriented satellites [9-24]. Spinning [6-13] and non-spinning satellites [14-24] were also investigated. The satellite attitude control has been achieved by applying translational motions of single or multiple control surfaces [22-24] or rotating the control surfaces about satellite body-fixed axes [9-21]. There were few missions [25-26] that include the Mariner IV mission [25] employing solar vanes for passive sun pointing attitude, and geostationary communication satellite OTS-2 mission of the European Space Agency [26] using solar flaps for satellite attitude control.

Circular Orbit

The SRP control torque thus can be utilized to stabilize librational dynamics of a satellite with a desired degree of accuracy. Optimal solar pressure controller design has been considered in Refs.[15-18]. In Ref. [18], open-loop optimal control using gradient technique is derived. However, linear controllers [13-19] are effective only for small attitude angle excursions. Using feedback linearization technique (FL), a nonlinear controller has been designed by Singh and Yim [20] for satellite pitch control.

Elliptic Orbit

Most of the research is focused on the application of SRP for stabilizing satellite attitude in circular orbits. Only few papers deal with the problem of controlling satellite attitude in elliptic orbits. When satellites are in elliptic orbits, the amplitude of satellite attitude increases with an increase in eccentricity and the satellite attitude may become unstable even though there are no initial attitude disturbances. To overcome the adverse effect of eccentricity, Joshi and Kumar [23] applied the SRP to control the attitude of earth-oriented axisymmetric satellites by regulating translatory motions of the control surfaces relative to the satellite body. They have developed open loop control law based on canceling out the attitude disturbance torque due to eccentricity with the SRP torque. They were able to show marginal stable response of the satellite pitch for eccentricity as high as $e=0.1$. Instead of translatory motions of the control surfaces, Kumar et al. [27] have utilized rotating control surfaces to produce SRP torque and to overcome adverse effect of eccentricity for earth-oriented axisymmetric satellites. They have designed open-loop control laws for rotating control surfaces to counteract attitude disturbances caused by eccentricity of the order $e=0.1$. The extension of this problem to feedback control has not been yet studied.

1.2.2 Aerodynamic Torques

For satellites orbiting in Low Earth orbits (LEO), aerodynamic torques are significant and thus, can be utilized for satellite attitude stabilization. Several investigations were carried out on this subject [28-37]. Modi and Shrivastava [28] assumed a system of flaps, and flap rotation to damp the attitude motion of a satellite. The flap rotation was regulated based on

linear feedback control with saturation constraints as well as bang-bang control with linear switching criteria. Using similar flaps, Ravindran and Hughes [29] considered performance optimization of an aerodynamic controller by minimizing a performance index weighted equally with respect to the attitude errors and control surface movements. An optimal aerodynamic stabilization of Near-Earth satellites is investigated by Pande and Venkatachalam in reference [30]. Successful application of aerodynamic forces for pitch control of COSMOS-149 was reported by Sarychev [31].

1.2.3 Combination of Environmental Torques

Propellant-less methods have their own limitations and to overcome these limitations, methods using combinations of various environmental forces have been envisaged, such as aerodynamic and gravity (aero-gravity assist), aerodynamic and SRP, aerodynamic and magnetic. Kumar et al. [32] examined passive aerodynamic stabilization and passive magnetic hysteresis damping of attitude rates while Chen et al. [33] considered aerodynamic torque for yaw stabilization and the gravity gradient torque to stabilize pitch and roll attitudes. Magnetic torquers with a gravity-gradient boom have been applied by Wisniewski [34]. Psiaki [35] applied passive aerodynamic drag torques for stabilization of pitch and yaw motions; and roll motion was controlled by active magnetic torquer of a shuttle-cock type satellite. The combination of SRP and aerodynamic forces was applied by Modi and Pande [36] for a low-Earth orbit satellite. Kumar et al [37] proposed the combination of SRP torques with magnetic torquers for three-dimensional attitude control for a geostationary satellite. The satellite pitch and roll controls are based on SRP torques while the yaw attitude is controlled by a magnetic torquer. This research overcomes the limitations of using SRP torques (multiple control surfaces) and magnetic torquers (inability to provide torque about the local magnetic field direction, i.e., pitch axis). The proposed controllers were successful in stabilizing the satellite attitude in the presence attitude disturbances and orbital eccentricity. The control inputs were within the limits of the maximum control surfaces rotation of 40 deg and with the magnetic torquers' maximum moment of 12 Am².

1.3 Motivation

In the design of any control system there are discrepancies between the actual plants and the mathematical model developed for controller design. This mismatch may be due to unmodeled dynamics, variation in system parameters, or the approximation of complex plant. In such situation the design of controller must ensure that the resulting controller has the ability to produce the required performance levels in practice despite such parameter uncertainties. Moreover, the system may experience disturbances due to several factors including modeling error, flap misalignments, and other environmental forces. These disturbances have to be considered during design of control system. This has led me to an intense interest in the development of robust control methods which seek to solve this problem.

Satellite attitude control using environmental forces have their own limitation and to overcome these limitations combinations of various environmental forces have been investigated. However, using only one environmental force for large attitude angle maneuver of the satellite has not been investigated. In the present study, satellite attitude control will be examined based on either SRP or aerodynamic forces.

1.4 Research Objectives

The objectives of this thesis can be summarized as:

- 1) Develop a system model and its equations of motion to study dynamics and control for specific satellite geometry.
- 2) Design robust nonlinear variable structure controller which utilize environmental torques to stabilize satellite attitude.
- 3) Verify the robustness of the proposed controllers by numerical simulations.

1.5 Contributions of Thesis

The present study makes several contributions to the environmental forces stabilized satellites. The major contributions of thesis are:

- 1) Derivation of closed-loop robust nonlinear VSC for satellite attitude control using environmental forces.
- 2) Large angle attitude maneuver using solar radiation pressure torque and aerodynamic torque.
- 3) Derivation of robust feedback control laws for satellite orbiting in elliptic orbits using solar radiation pressure.
- 4) Examination of the system parameter needed for satellite design which utilizes environmental forces for attitude control of a satellite.
- 5) Three-axis satellite attitude control using only aerodynamic torques.
- 6) The current research investigates non-propulsive method for satellite attitude control by utilizing environmental forces. This research provides strong bases for future real-world applications as controlling satellite attitude using environmental forces.

1.6 Thesis Organization

This thesis is organized in the following manner:

In Chapter 2, a brief introduction to the concepts of variable structure control (VSC) is given. This chapter explains the design of sliding surfaces, design of sliding mode control laws using Lyapunov function, and design of reaching laws. Chapter also gives advantages of using variable structure control in control design. Analytical proofs of disturbance rejection and parameter uncertainties are given for VSC.

Chapter 3 deals with satellite attitude control using SRP based on robust variable structure control. The system model and its equation of motion are presented in this chapter. The closed-loop nonlinear controllers are derived for satellite orbiting in circular orbit and elliptic orbits. Also this chapter would give analytical solution for tracking error for Hurwitz polynomial trajectory. The effects of various system parameters on the performance of the control input are examined and the effectiveness of the VSC in presence of parameter uncertainties and the external disturbances is discussed. Finally, the findings of the present investigation are summarized in this chapter.

Chapter 4 presents the application of aerodynamic torques for satellite attitude control based on variable structure control. The system models and their equations of motion are presented for planar and three dimensional cases. Two type of aerodynamic torque model is presented in this chapter, simplified aerodynamic torque model and free molecular flow aerodynamic torque model. The closed-loop nonlinear controllers are derived for satellite orbiting in circular orbit for both planar and three dimensional cases using simplified aerodynamic torque model. The effects of various system parameters on the performance of the control input are examined and the effectiveness of the VSC in presence of parameter uncertainties and the external disturbances are discussed. Finally, the important results are summarized in Summary Section.

Chapter 5 presents the various conclusions drawn from this research work and future works.

Chapter 2

Background on Variable Structure Control

In this chapter, a brief introduction about the concepts of variable structure control (VSC) is given. Different aspects of VSC are discussed; these include design of sliding surfaces, design of sliding mode control laws using Lyapunov function, design of reaching laws, and properties of VSC.

2.1 Introduction

Variable Structure Control (VSC) technique is characterized by surfaces which guarantee asymptotic stability if the state trajectories move along them. These surfaces are called the sliding surfaces or sliding regimes. The motion along them is referred to as a “sliding mode”. A system at the initial state is moved to the final desired state in two phases: reaching phase and sliding phase. In the reaching phase, the control inputs steers the state of the system towards a sliding surface from a given initial state. The reaching phase is followed by the sliding phase wherein the control inputs are designed to make the system stay on the sliding surface and slide towards the desired state thus ensuring asymptotic stability.

The basics of VSC theory can be explained using an example. Consider a time invariant systems with scalar control

$$\begin{aligned}\dot{x}_1 &= x_2 \\ \dot{x}_2 &= U\end{aligned}\tag{2.1}$$

where, x_1 and x_2 are state variables, U is a scalar control input. The derivative is with respect to time.

Let S be the sliding surface (Figure 2.1)

$$S = x_2 + p x_1, \quad p > 0 \quad (2.2)$$

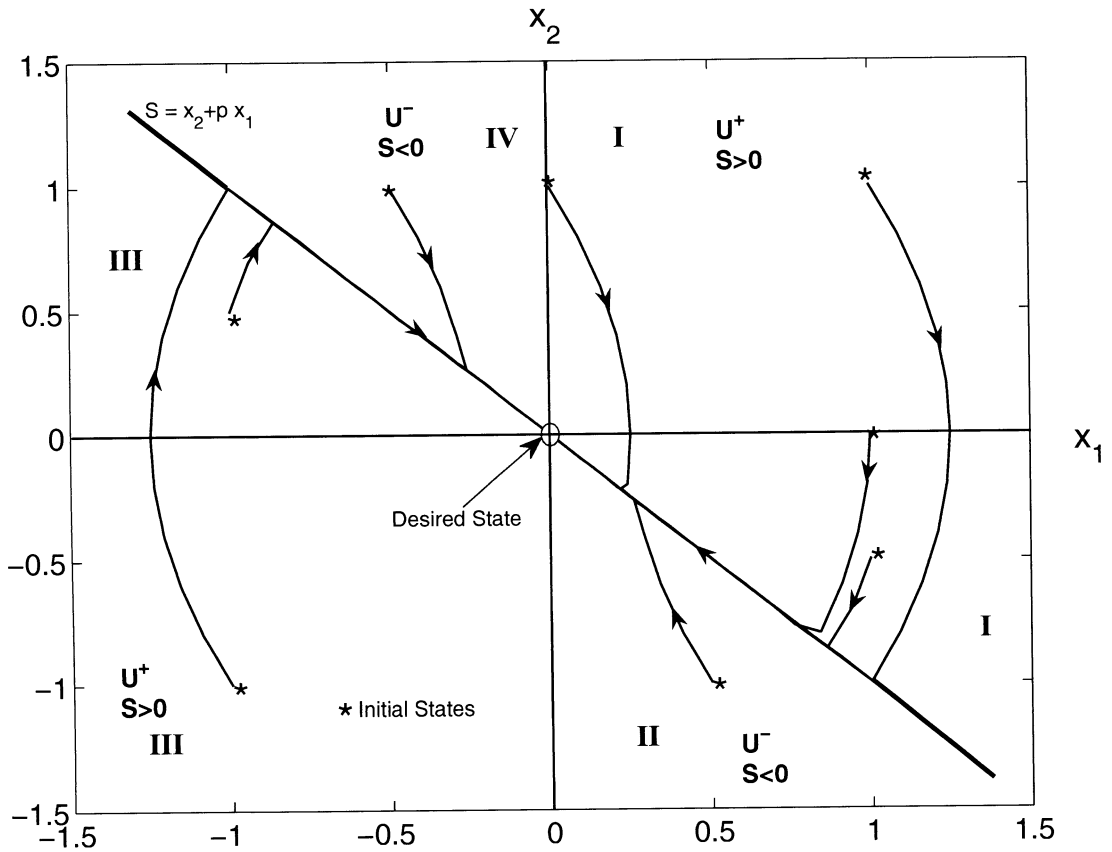


Figure 2.1: Variable structure control trajectories

In Figure 2.1 the x_2 axis and the straight line $S = x_2 + p x_1$ divide the phase plane to four regions.

$$\begin{aligned}
 \text{region I} & : x_1 > 0, s > 0 \\
 \text{region II} & : x_1 > 0, s < 0 \\
 \text{region III} & : x_1 < 0, s < 0 \\
 \text{region IV} & : x_1 < 0, s > 0
 \end{aligned} \tag{2.3}$$

The control input is chosen as

$$U = -2\text{sgn}(S) \quad \text{or} \quad \begin{aligned} U^+ &= -2 & S > 0 \\ U^- &= 2 & S < 0 \end{aligned} \tag{2.4}$$

In this case, S in Eq. (2.2) describes a one dimensional sliding surface and p is a sliding surface coefficient which is selected so as to guarantee a desirable sliding motion. For this example, $p = 1$ is assumed.

For a given initial state, an appropriate U is applied which moves the system trajectory toward $S = 0$ (i.e. reaching phase). Once the trajectory crosses the line $S = 0$ the control switches it direction thus forcing the trajectory towards $S = 0$ again (Figure 2.1).

Let the initial state lie in region I ($x_1 S > 0$), so according to Eq. (2.3) U^+ will be applied and the state will move towards the line S . At some time $t_1 > t_0$ the state will reach the line S and enters region II. In region II ($x_1 S < 0$) and according to Eq. (2.3) U^- will be applied and the state will move along an arc of a hyperbola towards the line S . After some time the state will leave region II and enter region I where the control is switched to U^+ again, thus forcing the state to region II again. It is seen that the state trajectory neither belongs to region I nor to region II and it has to move on the common border between the regions, in this case the straight line $S = x_2 + px_1 = 0$. It is seen that the trajectory cannot lie outside the line $S = 0$ and the only possible motion for the system trajectory is to stay on the surface $S = 0$ and move on it. This motion is called the sliding motion and the line $S = 0$ is called the sliding surface or the switching surface. The initial states that lie in region III and IV will follow the similar trend as of region I and II.

From the above example it is understood that the behavior of the VSC system depends completely upon the design of the switching surface and reaching control laws. Thus, VSC can be designed in three stages as:

- 1) design of the sliding mode dynamics by choice of switching surfaces,
- 2) design of Lyapunov function,
- 3) design of the reaching dynamics by the specification of the reaching laws.

Before explaining all these steps, let us consider the nth order nonlinear system of the form

$$\begin{aligned}
 \dot{x}_1 &= x_2 \\
 \dot{x}_2 &= x_3 \\
 &\vdots \\
 &\vdots \\
 \dot{x}_n &= f(x) + g(x)u
 \end{aligned} \tag{2.5}$$

where it is assumed that f and g are nonlinear function which depends on state x . The control objective is for $y(t) = x_1(t)$ to track a desired signal $y_d(t)$. Let $e = y - y_d$ be the tracking error.

2.2 Sliding Surface Design

First step is to determine a set of hyperplanes providing suitable behavior in the sliding mode.

Linear Hypersurfaces

The sliding mode surface S is defined as

$$S = e^{n-1} + p_{n-1}e^{n-2} + \dots + p_2\dot{e} + p_1e \tag{2.6}$$

where the coefficients $\{p_1, p_2, \dots, p_{n-1}\}$ are selected such that the characteristic equation

$$(s + \lambda_s)^{n-1} = s^{n-1} + \frac{(n-1)}{1!} \lambda_s s^{n-1} + \frac{(n-1)(n-2)}{2!} \lambda_s^2 s^{n-2} + \dots + (n-1) \lambda_s^{n-1} s + \lambda_s^{n-1} = 0 \tag{2.7}$$

is Hurwitz (i.e., all the roots of the polynomial are in the left-half complex plane). Here s is known as Laplace operator and λ_s is desired pole of the closed loop system. In general, the following relation can be used to find the coefficient p_i

$$\begin{aligned}
p_{n-1} &= \frac{(n-1)}{1!} \lambda_s \\
p_{n-2} &= \frac{(n-1)(n-2)}{2!} \lambda_s^2 \\
p_{n-3} &= \frac{(n-1)(n-2)(n-3)}{3!} \lambda_s^3 \\
&\cdot \\
&\cdot \\
&\cdot \\
p_2 &= (n-1) \lambda_s^{n-2} \\
p_1 &= \lambda_s^{n-1}
\end{aligned} \tag{2.8}$$

For example, $n = 3$, coefficients p_1 and p_2 can be obtained as

$$\begin{aligned}
p_2 &= 2\lambda_s \\
p_1 &= \lambda_s^2
\end{aligned} \tag{2.9}$$

and for $n = 4$, coefficients p_1 , p_2 , and p_3 can be obtained as

$$\begin{aligned}
p_1 &= \lambda_s^3 \\
p_2 &= 3\lambda_s^2 \\
p_3 &= 3\lambda_s
\end{aligned} \tag{2.10}$$

The manifold described by $S = 0$ is referred to as the sliding manifold or sliding surface and has dimension $(n-1)$. The objective of sliding mode control is to steer the trajectory onto this sliding manifold. This is achieved by forcing the variable S to zero in finite time. The variable structure control designed based on above linear hypersurfaces is called the Sliding Mode Control (SMC).

Nonlinear Hypersurfaces

Similar to linear hypersurfaces one can also choose nonlinear hyper surfaces [41-46] as sliding surface

$$S = \dot{e} + p_1 e^{q_i/h_i} \tag{2.11}$$

where $p_1 > 0$ is design constant, and q_i and h_i are positive odd integers satisfying $h_i > q_i$. The variable structure control designed based on above non-linear hypersurfaces is called the Terminal Sliding Mode Control (TSMC).

2.3 Lyapunov Design

In previous section, the sliding surface design is given by choosing linear and nonlinear hypersurfaces. Now next step is to design Lyapunov function such that the state trajectories reach the sliding surfaces and remain there. In order to do that the following Lyapunov function candidate is assumed

$$V = \frac{1}{2} S^T S \quad (2.12)$$

where V is a positive definite function for all S except at the origin $S = 0$. Next evaluate the time derivative of V along the trajectory e .

$$\dot{V} = S^T \dot{S} \quad (2.13)$$

The well known Lyapunov stability theory states that [40] if a positive definite function $V(x)$ can be found such that $\dot{V}(x)$ is negative definite, then the origin is asymptotically stable. It can be seen that in order to make the origin asymptotically stable one must have

$$\dot{V} = S^T \dot{S} < 0 \quad (2.14)$$

The above inequality is known as the reaching condition [40]. This inequality imposes that the trajectory e will converge to the origin $S = 0$, i.e., reaching the sliding surface.

2.4 Design of Reaching Laws

The final stage of the VSC design procedure involves the selection of the reaching control which will ensure that the chosen sliding mode is attained. For this reason, the problem of determining a control structure and associated gains, which ensure the reaching or hitting of the sliding mode, is sometimes called the reachability problem. The condition under which the state will move towards and reach a sliding surface is called a reaching condition. The system trajectory under the reaching condition is said to be in the reaching mode, or reaching phase. Reaching control laws are directly specifies the dynamics of the switching function. In the literature [38-46] the following reaching laws are available

(a) The constant rate reaching law

$$\dot{S} = -\eta \operatorname{sgn}(S) \quad (2.15)$$

where η are diagonal matrices with positive elements and

$$\text{sgn}(S) = [\text{sgn}(S_1) \text{sgn}(S_2) \dots \text{sgn}(S_n)]^T \quad (2.16)$$

(b) **The constant plus proportional rate reaching law**

$$\dot{S} = -\eta \text{sgn}(S) - kS \quad (2.17)$$

where η and k are diagonal matrices with positive elements.

(c) **The power rate reaching law**

$$\dot{S} = -\eta |S|^\sigma \text{sgn}(S) \quad (2.18)$$

where $0 < \sigma < 1$.

Now following above three steps, the following VSC law is obtained for system Eq. (2.5) by considering linear hyper surfaces (2.6) and constant rate reaching laws (2.15) as follows:

$$u = \frac{1}{g(x)} [-f(x) + y_d^{(n)} - p_{n-1}e^{n-1} - \dots - p_2\ddot{e} - p_1\dot{e} - \eta \text{sgn}(S)] \quad (2.19)$$

where $\text{sgn}(\cdot)$ denote the signum function as

$$\text{sgn}(S) = \begin{cases} 1 & \text{if } S > 0 \\ 0 & \text{if } S = 0 \\ -1 & \text{if } S < 0 \end{cases} \quad (2.20)$$

2.5 Properties of VSC

The VSC has advantages of robustness to parameter uncertainties, neglected model dynamics and external disturbances. The VSC have the following properties:

- 1) The system response is insensitive to system nonlinearities since the closed-loop system is governed by the sliding plane.
- 2) The system response depends only on the sliding surface coefficients p_i (for $i = 1, 2, \dots, n$) which are chosen by the designer.

Once the system trajectory reaches on the sliding surface $S=0$, then the closed loop system after substituting VSC law (2.19) in system (2.5) becomes

$$e^n + p_{n-1}e^{n-1} + \dots + p_2\ddot{e} + p_1\dot{e} + \eta \operatorname{sgn}(S) = 0 \quad (2.21)$$

Since the characteristic equation given by (2.7) is Hurwitz, the tracking error will go to zero with the selected coefficients $\{p_1, p_2, \dots, p_{n-1}\}$. Then after whole system is governed by above equation and it is insensitive to nonlinearities.

- 3) The system response is insensitive to variation in system parameters and modeling errors.
- 4) The system response is insensitive to external disturbances.

The preceding Eq. (2.21) is the ordinary linear differential equation of error dynamics and it does not contain any external disturbance term or uncertain parameter once reaches on sliding surface. This error equation is asymptotically stable as $t \rightarrow \infty$, tracking error $e \rightarrow 0$. Furthermore, the term $\eta \operatorname{sgn}(S)$ forces the error dynamics to stay onto the sliding plane which makes the system insensitive to system parameter uncertainty and external disturbances.

2.6 Analytical Proofs for Disturbance Rejection and Parameter Uncertainties

The proposed VSC laws are robust against parameter uncertainties and external disturbances. The proofs are as follows:

Disturbance Rejection

The class of nonlinear systems under this study can be described in the state space form with external disturbance w as

$$\begin{aligned} \dot{x} &= f(x) + g(x)u + p(x)w \\ y &= h(x) \end{aligned} \quad (2.22)$$

where x is a state vector, y is an output, and $p(x)$ is a smooth disturbance vector field. The objective is to find a VSC law u such that w has no effect on the output.

Theorem 1: The disturbance rejection problem for the system (2.22) is solvable *iff* the Lie derivatives of $h(x)$ with respect to vector field $p(x)$ and $f(x)$ is

$$L_p L_f^k h(x) = 0 \quad \text{for} \quad k \leq n-1. \quad (2.23)$$

where n is the relative degree of the unperturbed system.

Proof: Equation (2.22) is written in the normal form using Lie derivatives as follows.

$$\begin{aligned} \dot{x}_1 &= x_2 + L_p h(x) w, \\ \dot{x}_2 &= x_3 + L_p L_f h(x) w, \\ &\cdot \quad \cdot \\ &\cdot \quad \cdot \\ \dot{x}_n &= f(x) + g(x)u + L_p L_f^{n-1} h(x) w \end{aligned} \quad (2.24)$$

Using the condition (2.23) yields that the first n equations (2.24) do not contain w . Thus the VSC law

$$u = \frac{1}{g(x)} [-f(x) + v] \quad (2.25)$$

isolate output y from w . Here v is the desired system trajectory. This complete the “if” part of the proof. For “only if” part of the proof, we assume that there exist a VSC law Eq.(2.19) of the form

$$u = f_1(x) + g_1(x)v \quad (2.26)$$

that results in disturbance rejection.

Using this law yields a closed loop system given by

$$\begin{aligned} \dot{x} &= f(x) + g(x)f_1(x) + g(x)g_1(x)v + p(x)w \\ y &= h(x) \end{aligned} \quad (2.27)$$

with $v = 0$ the output needs to be independent of w .

Thus

$$\dot{y} = L_{f+gg_1} h + L_p h w \quad (2.28)$$

needs to be independent of w . Thus $L_p h = 0$. Differentiating above Eq. (2.28) further we get that

$$L_p L_{f+g_1}^i h(x) \equiv 0, \quad 0 \leq i \leq n-1 \quad (2.29)$$

Now note that

$$L_{f+g_1} h = L_f h + f_1 L_g h \quad (2.30)$$

Hence

$$L_g h \equiv 0 \Rightarrow L_{f+g_1} h = L_f h \quad (2.31)$$

We see that the condition (2.29) are equivalent to (2.23). Thus, the Theorem 1 proves that the VSC law result in disturbance rejection and thereby isolate output (y) from disturbance (w).

Parameter Uncertainties

Parameter uncertainties can be modeled as perturbation to $f(x)$, $\Delta f(x)$. The resulting equation is described as

$$\begin{aligned} \dot{x} &= f(x) + \Delta f(x) + g(x)u \\ y &= h(x). \end{aligned} \quad (2.32)$$

The objective is to find a VSC law u such that $\Delta f(x)$ has no effect on the output.

Theorem 2: The parameter uncertainties rejection problem for the system (2.32) is solvable iff the Lie derivatives of $h(x)$ with respect to vector field $\Delta f(x)$ and $f(x)$ is

$$L_{\Delta f} L_f^m h(x) = 0 \quad \text{for} \quad 0 \leq m \leq n-1. \quad (2.33)$$

where n is the relative degree of the unperturbed system (2.32).

Proof: Equation (2.32) is written in the normal form using Lie derivatives as follows.

$$\begin{aligned} \dot{x}_1 &= x_2 + L_{\Delta f(x)} h(x) \Delta f(x), \\ \dot{x}_2 &= x_3 + L_{\Delta f(x)} L_f h(x) \Delta f(x), \\ &\cdot \quad \cdot \\ &\cdot \quad \cdot \\ \dot{x}_n &= f(x) + g(x)u + L_{\Delta f(x)} L_f^{n-1} h(x) \Delta f(x) \end{aligned} \quad (2.34)$$

Using the condition (2.33) yields that the first n equations (2.34) do not contain $\Delta f(x)$. Thus the VSC law

$$u = \frac{1}{g(x)} [-f(x) + v] \quad (2.35)$$

isolate output y from $\Delta f(x)$. Here v represents the desired state inputs. This complete the “if” part of the proof. For “only if” part of the proof, we assume that there exist a VSC law Eq.(2.19) of the form

$$u = f_1(x) + g_1(x)v \quad (2.36)$$

that results in rejection of parameter uncertainties.

Using this law yields a closed loop system given by

$$\begin{aligned} \dot{x} &= f(x) + g(x)f_1(x) + g(x)g_1(x)v + \Delta f(x) \\ y &= h(x) \end{aligned} \quad (2.37)$$

with $v = 0$ the output needs to be independent of $\Delta f(x)$.

Thus

$$\dot{y} = L_{f+g_1} h + L_{\Delta f(x)} h \Delta f(x) \quad (2.38)$$

needs to be independent of $\Delta f(x)$. Thus $L_{\Delta f(x)} h \equiv 0$. Differentiating above Eq. (2.38) further we get that

$$L_{\Delta f(x)} L_{f+g_1}^j h(x) \equiv 0, \quad 0 \leq j \leq n-1 \quad (2.39)$$

Now note that

$$L_{f+g_1} h = L_f h + f_1 L_g h \quad (2.40)$$

Hence

$$L_g h \equiv 0 \Rightarrow L_{f+g_1} h = L_f h \quad (2.41)$$

We see that the condition (2.39) are equivalent to (2.33). Thus, the Theorem 2 proves that the VSC law result in parameter uncertainties rejection and thereby isolate output (y) from parameter uncertainties $\Delta f(x)$. Theorem 1 and Theorem 2 will be further verified in this thesis for a particular system model using theory as well as numerical simulation.

2.7 Chattering Phenomenon

The main disadvantage of VSC arises from the fact that the controls are discontinuous which makes them vulnerable to nonidealities in switching and time delays. This disadvantage causes what is known as the chatter phenomenon [40]. The chatter phenomenon causes the controls to switch directions with a very high frequency. In order to remove chattering there are few solutions available in literature. One is smoothing out the control discontinuity in a thin boundary layer neighboring the switching surface sometimes it is called “boundary layer”. By replacing signum function with saturation function as follow

$$\operatorname{sgn}(S) = \operatorname{sat}\left(\frac{S}{\varphi}\right) = \begin{cases} \operatorname{sgn}(S) & S > \varphi \\ \frac{S}{\varphi} & S \leq \varphi \end{cases} \quad (2.42)$$

where, $\varphi > 0$ or hyperbolic tangent as

$$\operatorname{sgn}(S) = \tanh(k_1 S) \quad (2.43)$$

where, $k_1 > 0$.

Chapter 3

Application of Solar Radiation Pressure for Satellite Attitude Control

3.1 Introduction

This chapter examines the use of SRP for satellite attitude control using nonlinear variable structure control. The system model and its equations of motion are presented in Section 3.2. The closed-loop nonlinear control laws based on VSC are derived in Section 3.3 for circular orbits and elliptic orbits. In Section 3.4, an analytical solution for tracking error is obtained. Theoretical proof of parameter uncertainties and disturbance rejection for the proposed control laws are provided in Section 3.5. In Section 3.6 and Section 3.7, the numerical simulation is carried out for a detailed assessment of the proposed attitude control strategy for circular orbits and elliptic orbits, respectively. The effects of various system parameters on the performance of the controller are examined and the effectiveness of the proposed controller in the presence of parameter uncertainties and external disturbances is given in both Sections. Finally, the findings of the present study are summarized in Section 3.8.

3.2 Proposed System Model

3.2.1 System Description

A system model comprises of a satellite with two-oppositely placed light-weight solar flaps along the satellite Y-axis is considered. System center of mass O moving in an elliptic orbit about the Earth's center E (Figure 3.1 – Figure 3.2) is assumed. The system center of mass O

lies on the center of mass of the satellite. The mass of the solar flaps and other accessories are rather small than the satellite mass and therefore, they are assumed to be negligible. For the system under consideration, an orbital reference frame $O-X_0Y_0Z_0$ is selected such that the Y_0 -axis always points along the local vertical, the X_0 -axis lies normal to the orbital plane, and the Z_0 -axis represents the third axis of this right handed frame taken. The body-fixed coordinate frame is represented by $O-XYZ$. For solar flap- j , its axis n_j initially aligned with the Z -axis is rotated by an angle β_j about the X -axis (normal to the orbit plane $Y-Z$) is considered. The solar flaps are considered to be made of a highly reflective surface (i.e., $\rho_d = 0$; no absorption, specular reflection only) [27]. The distances between the system center of mass O and the center of pressure for both the solar flaps are assumed to be the same and their cross-sectional areas facing the Sun are equal.

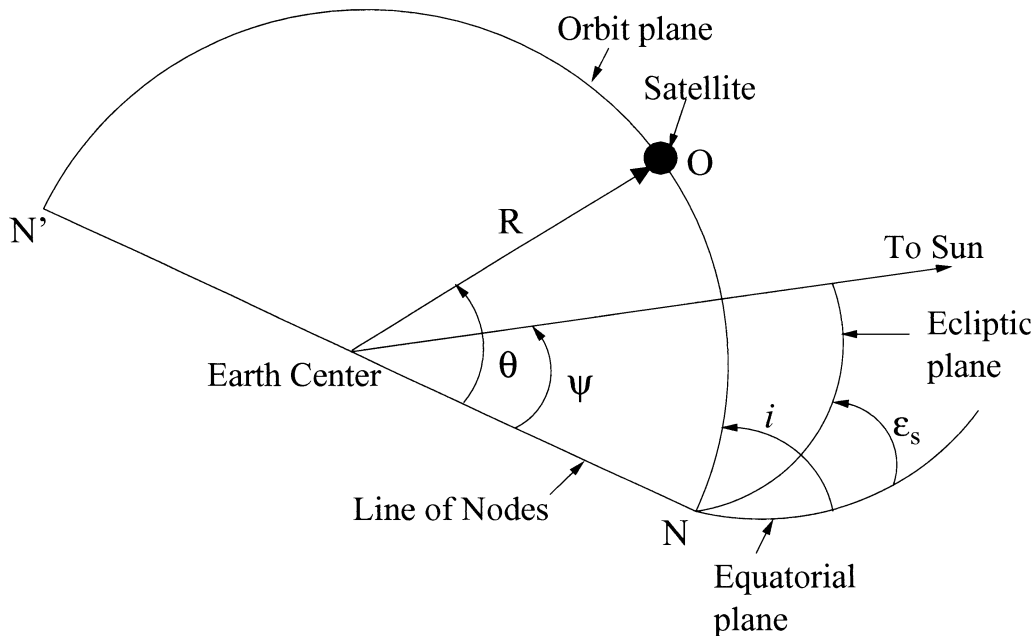


Figure 3.1: Geometry of orbit motion for solar radiation pressure torques stabilized satellite

and T_s denotes torque due to SRP and it is derived as follows.

The force acting on the plate- j due to SRP is given by [2]

$$\vec{F}_{s_j} = pA_j |\vec{s}_j \cdot \vec{n}_j| \left\{ (1 - \rho_s - \rho_t) \vec{s}_j + \left[2\rho_s (\vec{s}_j \cdot \vec{n}_j) + \frac{2}{3} \rho_d \right] \vec{n}_j \right\}, j = 1, 2 \quad (3.3)$$

where ρ_d , ρ_s , and ρ_t are fraction of impinging photons diffusely reflected, specularly reflected, and transmitted, respectively.

Considering a highly reflective surface (i.e., $\rho_d = 0$; no absorption, specular reflection only), the preceding expression (3.3) simplifies to

$$\vec{F}_{s_j} = 2\rho_s pA_j |\vec{s}_j \cdot \vec{n}_j| (\vec{s}_j \cdot \vec{n}_j) \vec{n}_j, j = 1, 2 \quad (3.4)$$

Here \vec{s}_j is the unit vector of the incoming light from the Sun on the solar panel- j and is expressed in the satellite body-fixed reference frame as

$$\begin{aligned} \vec{s}_j = & \left[\sin \psi \sin (i - \varepsilon_s) \right] \hat{i} + \left[-\cos \psi \cos (\theta + \alpha_L) - \sin \psi \cos (i - \varepsilon_s) \sin (\theta + \alpha_L) \right] \hat{j} \\ & + \left[\cos \psi \sin (\theta + \alpha_L) - \sin \psi \cos (i - \varepsilon_s) \cos (\theta + \alpha_L) \right] \hat{k} \end{aligned} \quad (3.5)$$

The vector normal to the solar panel- j , \vec{n}_j is given by

$$\vec{n}_j = \left[-\sin \beta_j \right] \hat{j} + \left[\cos \beta_j \right] \hat{k}, \quad j = 1, 2 \quad (3.6)$$

Thus, the torque exerted by the solar panel- j on the satellite is obtained as

$$\vec{T}_{s_j} = \vec{r}_j \times \vec{F}_{s_j} = (-1)^{j+1} 2\rho_s pA_j r_j |\vec{s}_j \cdot \vec{n}_j| (\vec{s}_j \cdot \vec{n}_j) \left[\cos \beta_j \right] \hat{i}, \quad j = 1, 2 \quad (3.7)$$

Assuming the cross-sectional area of the panel and the distance between the system center of mass O and the center of pressure for both the solar panels being the same (i.e., $A_j=A$, $r_j=r$), the components of the total solar torque about the satellite body axes can be written as

$$T_s = T_{s_1} + T_{s_2} = 2\rho_s pAr \left[|\vec{s}_1 \cdot \vec{n}_1| (\vec{s}_1 \cdot \vec{n}_1) \cos \beta_1 - |\vec{s}_2 \cdot \vec{n}_2| (\vec{s}_2 \cdot \vec{n}_2) \cos \beta_2 \right] \quad (3.8)$$

Let α be the orientation of the satellite with respect to the inertially fixed axis Y_l (Figure 3.1). It follows

$$\alpha = \alpha_L + \theta, \quad \dot{\alpha} = \dot{\alpha}_L + \dot{\theta}, \quad \ddot{\alpha} = \ddot{\alpha}_L + \ddot{\theta} \quad (3.9)$$

where $\theta = \Omega t$ is the orbital angle, and $\Omega = \sqrt{\mu/a^3}$ is the orbital rate.

Substituting, $\alpha_L = \alpha - \theta$, in T_g and T_s [Eq.(3.2) and Eq.(3.8)], and expressing the derivatives with respect to true anomaly θ , and applying the following relations

$$\dot{\alpha} = \dot{\theta}\alpha', \ddot{\alpha} = \dot{\theta}^2\alpha'' + \ddot{\theta}\alpha' \quad (3.10)$$

$$\dot{\theta} = \frac{\sqrt{\mu a(1-e^2)}}{R^2}, \dot{\theta}^2 = \frac{\mu}{R^3}(1+e\cos\theta), \ddot{\theta} = -\frac{2\mu}{R^3}e\sin\theta \quad (3.11)$$

and further replacing R by semi-major axis a , and eccentricity e , using the relation

$$R = \frac{a(1-e^2)}{(1+e\cos\theta)} = \frac{\mu^{1/3}(1-e^2)}{\Omega^{2/3}(1+e\cos\theta)} \quad (3.12)$$

the resulting governing equation of motion of the system are obtained as

$$(1+e\cos\theta)\alpha'' = T_g + T_s + 2e\sin\theta\alpha' \quad (3.13)$$

where

$$\begin{aligned} T_g &= -\frac{3}{2}K\sin 2(\alpha - \theta) \\ T_s &= C\left(\frac{1-e^2}{1+e\cos\theta}\right)^3 \sigma \left\{ \sin^2(\alpha + \gamma + \beta_1)\Delta_1 \cos\beta_1 \right. \\ &\quad \left. - \sin^2(\alpha + \gamma + \beta_2)\Delta_2 \cos\beta_2 \right\} \\ \sigma &= 1 - \sin^2\psi \sin^2(i - \varepsilon_s) \\ \gamma &= -\tan^{-1}(\tan\psi \cos(i - \varepsilon_s)) \\ \Delta_j &= \text{sgn}(\sin(\alpha + \gamma + \beta_j)), j = 1, 2 \\ K &= \frac{I_y - I_z}{I_x}, C = \frac{2\rho_s p A r}{I_x \Omega^2}, \Omega = \frac{\mu}{a^3} \end{aligned} \quad (3.14)$$

and the function sig() denotes signum function. Note that in Eq. (3.14) the solar aspect angle ψ is a function of θ and varies from 0 to 2π radian in a year.

The nonlinear and nonautonomous system equation of motion, Eq. (3.13) is represented in state space form. The following state vector is defined

$$\mathbf{x} = [\alpha \quad \alpha' \quad \beta_1 \quad \beta_2]^T \quad (3.15)$$

A state variable representation of the system (3.13) with a selected controlled output

t variable $y = \alpha$, is given by

$$\begin{aligned}\dot{\mathbf{x}} &= \mathbf{f}(\mathbf{x}) + \mathbf{g} \mathbf{u} \\ y &= \alpha\end{aligned}\tag{3.16}$$

where,

$$\begin{aligned}\mathbf{f}(\mathbf{x}) &= [\alpha' \quad T_{gs} \quad 0 \quad 0]^T \\ \mathbf{u} &= [\beta_1' \quad \beta_2']^T\end{aligned}\tag{3.17}$$

$$\begin{aligned}\mathbf{g} &= [\mathbf{g}_1 \quad \mathbf{g}_2] \\ \mathbf{g}_1 &= [0 \quad 0 \quad 1 \quad 0]^T \\ \mathbf{g}_2 &= [0 \quad 0 \quad 0 \quad 1]^T\end{aligned}\tag{3.18}$$

In Eq.(3.17), $T_{gs} = T_g + T_s$.

Note that the flap deflection (β_j) in Eq. (3.14) involves complex trigonometric relations and therefore it can not be assumed as a control input. However, this problem can be solved by taking the derivative of the flap deflection as the control input, i.e. $\mathbf{u} = [\beta_1' \quad \beta_2']^T$.

3.3 Control Laws

In this section closed loop nonlinear variable structure control is derived for circular orbits and elliptic orbits.

3.3.1 Circular Orbit

3.3.1.1 Sliding Mode Control

Equation of motion Eq. (3.13) is valid for a satellite orbiting in an elliptic orbit. In order to design controller for a circular orbit case, the first task is to obtain an equation of motion of the satellite in the circular orbit. This can be obtained by simply assuming eccentricity ($e = 0$) in equation of motion Eq. (3.13).

Next, for design of control system the followings objectives are considered: 1) drive the system error to zero without oscillations or overshoots, 2) compensate external disturbances

from beginning. To satisfy these objectives, the sliding plane in two phases is considered. In the first phase, a orbit time-varying sliding plane is considered with the constant angle of inclination. Initially the plane moves uniformly in the state space and then it stops at the orbit time θ_f , mathematically expressed as

$$S = \tilde{x}_3 + p_2\tilde{x}_2 + p_1\tilde{x}_1 + a_1 + b_1\theta \quad \theta \leq \theta_f \quad (3.19)$$

where p_1 , p_2 , a_1 and b_1 are constants.

For second phase, the plane stops at the orbit time θ_f , for any $\theta \geq \theta_f$, mathematically stated as

$$S = \tilde{x}_3 + p_2\tilde{x}_2 + p_1\tilde{x}_1 \quad \theta \geq \theta_f \quad (3.20)$$

where

$$\tilde{x}_1 = \alpha - \alpha_d, \tilde{x}_2 = \alpha' - \alpha'_d, \tilde{x}_3 = \alpha'' - \alpha''_d \quad (3.21)$$

The following Lyapunov function candidate is assumed

$$V = \frac{1}{2}S^2 \quad (3.22)$$

Taking the derivative of Eq. (3.22) with respect to θ , one obtains

$$V' = SS' \quad (3.23)$$

In the preceding Eq. (3.23), S' is obtained by taking derivative of Eqs. (3.19)-(3.20) with respect to θ :

$$\begin{aligned} S' &= \tilde{x}_1^{(3)} + p_2\tilde{x}_3 + p_1\tilde{x}_2 + b_1, & \theta \leq \theta_f \\ S' &= \tilde{x}_1^{(3)} + p_2\tilde{x}_3 + p_1\tilde{x}_2 & \theta \geq \theta_f \end{aligned} \quad (3.24)$$

Eq. (3.24) can be rewritten into the following form,

$$\begin{aligned} S' &= \alpha^{(3)} - \alpha_d^{(3)} + p_2(\alpha'' - \alpha''_d) + p_1\tilde{x}_2 + b_1 & \theta \leq \theta_f \\ S' &= \alpha^{(3)} - \alpha_d^{(3)} + p_2(\alpha'' - \alpha''_d) + p_1\tilde{x}_2 & \theta \geq \theta_f \end{aligned} \quad (3.25)$$

From Eq. (3.25) third order derivative of the pitch angle with respect to θ is required, which can obtained as

$$\alpha^{(3)} = \frac{\partial T_{gs}}{\partial \alpha} \alpha' + \frac{\partial T_{gs}}{\partial \theta} \theta' + \frac{\partial T_s}{\partial \beta_1} \beta_1' + \frac{\partial T_s}{\partial \beta_2} \beta_2' \quad (3.26)$$

Since the partial derivative $\partial T_{gs} / \partial \alpha$ is summation of partial derivative of T_g and T_s with respect to α

$$\frac{\partial T_{gs}}{\partial \alpha} = \frac{\partial T_g}{\partial \alpha} + \frac{\partial T_s}{\partial \alpha} \quad (3.27)$$

Taking partial derivative of T_g and T_s given by Eq. (3.14) with respect to α considering $e=0$, the following equations are obtained

$$\frac{\partial T_g}{\partial \alpha} = -3K \cos[2(\alpha - \theta)] \quad (3.28)$$

$$\frac{\partial T_s}{\partial \alpha} = C\sigma \left[\sin(2(\alpha + \gamma + \beta_1)) \Delta_1 \cos \beta_1 - \sin(2(\alpha + \gamma + \beta_2)) \Delta_2 \cos \beta_2 \right] \quad (3.29)$$

Substituting Eq. (3.28) and Eq. (3.29) into Eq. (3.27)

$$\begin{aligned} \frac{\partial T_{gs}}{\partial \alpha} = & -3K \cos[2(\alpha - \theta)] \\ & + C\sigma \left[\sin(2(\alpha + \gamma + \beta_1)) \Delta_1 \cos \beta_1 - \sin(2(\alpha + \gamma + \beta_2)) \Delta_2 \cos \beta_2 \right] \end{aligned} \quad (3.30)$$

Now taking partial derivative of T_g and T_s with respect to θ and applying chain rules, one obtains

$$\frac{\partial T_{gs}}{\partial \theta} = \frac{\partial T_g}{\partial \theta} + \left(\frac{\partial T_s}{\partial \gamma} \frac{\partial \gamma}{\partial \psi} \frac{\partial \psi}{\partial \theta} + \frac{\partial T_s}{\partial \sigma} \frac{\partial \sigma}{\partial \psi} \frac{\partial \psi}{\partial \theta} \right) \quad (3.31)$$

The partial derivatives in Eq. (3.31) can be obtained using Eq.(3.14) for circular orbits as follows:

$$\frac{\partial T_g}{\partial \theta} = 3K \cos[2(\alpha - \theta)] \quad (3.32)$$

$$\frac{\partial T_s}{\partial \gamma} = \frac{\partial T_s}{\partial \alpha} \quad (3.33)$$

$$\frac{\partial \gamma}{\partial \psi} = - \left(\frac{\cos(i - \varepsilon_s) \sec^2 \psi}{1 + \tan^2 \psi \cos^2(i - \varepsilon_s)} \right) \quad (3.34)$$

$$\frac{\partial T_s}{\partial \sigma} = \frac{T_s}{\sigma} \quad (3.35)$$

$$\frac{\partial \sigma}{\partial \psi} = -\sin 2\psi \sin^2(i - \varepsilon_s) \quad (3.36)$$

Substituting Eq. (3.32) - (3.36) into Eq. (3.31), we obtain $\partial T_{gs} / \partial \theta$.

Taking the partial derivative of T_s with respect to β_j , the following equations :

$$\frac{\partial T_s}{\partial \beta_1} = C\sigma\Delta_1 \left[\sin(2(\alpha + \gamma + \beta_1)) \cos \beta_1 - \sin^2(\alpha + \gamma + \beta_1) \sin \beta_1 \right] \quad (3.37)$$

$$\frac{\partial T_s}{\partial \beta_2} = C\sigma\Delta_2 \left[-\sin(2(\alpha + \gamma + \beta_2)) \cos \beta_2 + \sin^2(\alpha + \gamma + \beta_2) \sin \beta_2 \right] \quad (3.38)$$

Substituting Eqs. (3.30), (3.31), (3.37), and (3.38) into Eq. (3.26), $\alpha^{(3)}$ is

$$\alpha^{(3)} = f_s + [B_1 \quad B_2] \begin{bmatrix} u_1 \\ u_2 \end{bmatrix} \quad (3.39)$$

where,

$$\begin{aligned} f_s &= \frac{\partial T_{gs}}{\partial \alpha} \alpha' + \frac{\partial T_{gs}}{\partial \theta} \theta' \\ B_1 &= \frac{\partial T_s}{\partial \beta_1} \\ B_2 &= \frac{\partial T_s}{\partial \beta_2} \end{aligned} \quad (3.40)$$

Now taking $S' = -\eta \operatorname{sgn}(S)$ in Eq. (3.23) yields $V' = -\eta|S|$, which is negative semi-definite of S for positive value of η . So, the proposed control laws are globally stable for assumed Lyapunov Function (3.22). Using Eq. (3.25), Eq. (3.39), and $S' = -\eta \operatorname{sgn}(S)$, one obtains following relations

$$\begin{aligned} f_s + [B][u] - \alpha_d^{(3)} + p_2 \tilde{x}'_2 + p_1 \tilde{x}_2 &= -b_1 - \eta \operatorname{sgn}(S) & \theta \leq \theta_f \\ f_s + [B][u] - \alpha_d^{(3)} + p_2 \tilde{x}'_2 + p_1 \tilde{x}_2 &= -\eta \operatorname{sgn}(S) & \theta \geq \theta_f \end{aligned} \quad (3.41)$$

where $[B] = [B_1 \quad B_2]$ and $[u] = [u_1 \quad u_2]^T$.

Rearranging above Eq. (3.41), the control laws can be written as

$$\begin{aligned} [u] &= \mathbf{B}^T [\mathbf{B}\mathbf{B}^T]^{-1} \left\{ -f_s + \alpha_d^{(3)} - p_2 \tilde{x}_3 - p_1 \tilde{x}_2 - b_1 - \eta \operatorname{sgn}(S) \right\} & \theta \leq \theta_f \\ [u] &= \mathbf{B}^T [\mathbf{B}\mathbf{B}^T]^{-1} \left\{ -f_s + \alpha_d^{(3)} - p_2 \tilde{x}_3 - p_1 \tilde{x}_2 - \eta \operatorname{sgn}(S) \right\} & \theta \geq \theta_f \end{aligned} \quad (3.42)$$

For the existence of the control law (3.42), $\mathbf{B}\mathbf{B}^T$ must be non-zero in the region of interest:

$$\mathbf{B}\mathbf{B}^T = \left(\frac{\partial T_s}{\partial \beta_1} \right)^2 + \left(\frac{\partial T_s}{\partial \beta_2} \right)^2 \neq 0 \quad (3.43)$$

The region of $\Omega_S (\Omega_{S_1} \cap \Omega_{S_2})$ singularity in which $\mathbf{B}\mathbf{B}^T = 0$ is given by

$$\begin{aligned} \Omega_{S_1} &= \left\{ \left(\frac{\partial T_s}{\partial \beta_1} \right)^2 = 0 \right\} \\ &= \left\{ \left\{ C\sigma\Delta_1 \left[\sin(2(\alpha + \gamma + \beta_1)) \cos \beta_1 - \sin^2(\alpha + \gamma + \beta_1) \sin \beta_1 \right] \right\}^2 = 0 \right\} \\ &= \left\{ \left[2 \sin(\alpha + \gamma + \beta_1) \cos(\alpha + \gamma + \beta_1) \cos \beta_1 - \sin^2(\alpha + \gamma + \beta_1) \sin \beta_1 \right]^2 = 0 \right\} \quad (3.44) \\ &= \left\{ \sin(\alpha + \gamma + \beta_1) \cos(\alpha + \gamma + \beta_1) \cos \beta_1 \left[2 - \tan(\alpha + \gamma + \beta_1) \tan \beta_1 \right] = 0 \right\} \\ &= \left\{ \alpha + \gamma + \beta_1 = 2n\pi, \text{ or } \tan(\alpha + \gamma + \beta_1) \tan \beta_1 = 2 \right\} \\ \Omega_{S_2} &= \left\{ \left(\frac{\partial T_s}{\partial \beta_2} \right)^2 = 0 \right\} \\ &= \left\{ \left\{ C\sigma\Delta_2 \left[-\sin(2(\alpha + \gamma + \beta_2)) \cos \beta_2 + \sin^2(\alpha + \gamma + \beta_2) \sin \beta_2 \right] \right\}^2 = 0 \right\} \\ &= \left\{ \left[-2 \sin(\alpha + \gamma + \beta_2) \cos(\alpha + \gamma + \beta_2) \cos \beta_2 + \sin^2(\alpha + \gamma + \beta_2) \sin \beta_2 \right]^2 = 0 \right\} \\ &= \left\{ \sin(\alpha + \gamma + \beta_2) \cos(\alpha + \gamma + \beta_2) \cos \beta_2 \left[-2 + \tan(\alpha + \gamma + \beta_2) \tan \beta_2 \right] = 0 \right\} \\ &= \left\{ \alpha + \gamma + \beta_2 = 2n\pi, \text{ or } \tan(\alpha + \gamma + \beta_2) \tan \beta_2 = 2 \right\} \end{aligned}$$

The control laws (3.42) are well defined as long as the trajectory of the closed-loop system does not enter the region Ω_S .

3.3.1.2 Feedback Linearization Control Law

The feedback linearization control law as given in reference [20], is as follows:

$$[u] = \mathbf{B}^T [\mathbf{B}\mathbf{B}^T]^{-1} \{-f_s + \alpha_d^{(3)} - p_3\ddot{\alpha} - p_2\dot{\alpha} - p_1\tilde{\alpha} - p_0x_s\} \quad (3.45)$$

where \mathbf{B} , f_s is already mention before in Eq. (3.40). Parameters p_1 , p_2 , p_3 , and p_4 are positive constant, $\tilde{\alpha} = \alpha - \alpha_d$ is the pitch angle tracking error, and x_s is the integral of the tracking error, that is,

$$\dot{x}_s = \tilde{\alpha} \quad (3.46)$$

Here error integral feedback term has been used to obtain robustness in the control system to parameter uncertainty. The feedback parameters are properly chosen from Hurwitz polynomial $(s + \lambda)^4$ as follows,

$$p_3 = 4\lambda, \quad p_2 = 6\lambda^2, \quad p_1 = 4\lambda^3, \quad p_0 = \lambda^4 \quad (3.47)$$

To compare with FL control laws, we derive a sliding mode control. In this modified SMC only sliding plane will be different as compared to the previous sliding mode control. Here we have chosen sliding plane with integral tracking error as follows,

$$S = \tilde{x}_3 + p_3\tilde{x}_2 + p_2\tilde{x}_1 + p_1x_s \quad (3.48)$$

Based on this sliding surface, the modified sliding mode control law is derived as

$$[u] = \mathbf{B}^T [\mathbf{B}\mathbf{B}^T]^{-1} \{-f_s + \alpha_d^{(3)} - p_3\ddot{\alpha} - p_2\dot{\alpha} - p_1\tilde{\alpha} - \eta \operatorname{sgn}(S)\} \quad (3.49)$$

3.3.1.3 Desired pitch trajectories

In this section a specific trajectory is given to the system for the purpose of attitude tracking. Two types of trajectory have been considered; simple polynomial based trajectory to achieve final attitude orientation and sinusoidal trajectory to achieve continuous periodic attitude tracking.

Hurwitz filter trajectory

Since the control laws Eq. (3.42) require third order desired pitch response, the following Hurwitz filter trajectory is considered :

$$\alpha_d^{(4)} + 4\lambda_d\alpha_d^{(3)} + 6\lambda_d^2\alpha_d^{(2)} + 4\lambda_d^3\alpha_d' + 6\lambda_d^4\alpha_d = \lambda_d^4\alpha_f \quad (3.50)$$

Where λ_d is positive real number, and α_f is orientation of the satellite final pitch angle.

The general closed form solution of Eq. (3.50) can be obtained as

$$\alpha_d(\theta) = \alpha_f + k_1 e^{-\lambda_d\theta} + \theta k_2 e^{-\lambda_d\theta} + \theta^2 k_3 e^{-\lambda_d\theta} + \theta^3 k_4 e^{-\lambda_d\theta} \quad (3.51)$$

where, $k_1, k_2, k_3,$ and k_4 are obtained from initial conditions $\alpha_d(0), \alpha_d^{(i)}(0), i = 1, 2, 3$.

Eq. (3.51) can be differentiated with respect to θ to obtained $\alpha_d^{(i)}(\theta), i = 1, 2, 3$ for control law Eq. (3.42).

Sinusoidal trajectory

For periodic tracking we have assumed the following trajectory,

$$\alpha_d(\theta) = 10^\circ \sin(\mathbf{k}_{period}\theta) \quad (3.52)$$

where \mathbf{k}_{period} represent oscillation period for sinusoidal tracking.

3.3.2 Elliptic Orbit

This section presents the derivation of the VSC laws for elliptic orbits. The SMC laws are derived first followed by design of the TSMC laws.

3.3.2.1 Sliding Mode Control

The objectives for the design of control system are: 1) drive the system error to zero without oscillations or overshoots, 2) compensate external disturbances. To satisfy these objectives, the sliding plane is considered as

$$S = \tilde{x}_3 + p_2\tilde{x}_2 + p_1\tilde{x}_1 \quad (3.53)$$

where

$$\tilde{x}_1 = \alpha - \alpha_d, \tilde{x}_2 = \alpha' - \alpha_d', \tilde{x}_3 = \alpha'' - \alpha_d'' \quad (3.54)$$

The following Lyapunov function candidate is assumed

$$V = \frac{1}{2} S^2 \quad (3.55)$$

Now taking the derivative of Eq. (3.55) with respect to θ yields

$$V' = SS' \quad (3.56)$$

In the preceding Eq.(3.56), S' is obtained by taking derivative of Eq. (3.53) with respect to θ :

$$S' = \tilde{x}_1^{(3)} + p_2 \tilde{x}_3 + p_1 \tilde{x}_2 \quad (3.57)$$

Eq. (3.57) can be rewritten into the following form,

$$S' = \alpha^{(3)} - \alpha_d^{(3)} + p_2 (\alpha'' - \alpha_d'') + p_1 \tilde{x}_2 \quad (3.58)$$

Next the third order derivative of the pitch angle with respect to θ is required for Eq.(3.58), which can be obtained as

$$\alpha^{(3)} = \left(\frac{1}{1+e \cos \theta} \right) \left\{ 3e \sin \theta \alpha'' + 2e \cos \theta \alpha' + \frac{\partial T_{gs}}{\partial \alpha} \alpha' + \frac{\partial T_{gs}}{\partial \theta} \theta' + \frac{\partial T_s}{\partial \beta_1} \beta_1' + \frac{\partial T_s}{\partial \beta_2} \beta_2' \right\} \quad (3.59)$$

Since the partial derivative $\partial T_{gs} / \partial \alpha$ is summation of partial derivative of T_g and T_s with respect to α

$$\frac{\partial T_{gs}}{\partial \alpha} = \frac{\partial T_g}{\partial \alpha} + \frac{\partial T_s}{\partial \alpha} \quad (3.60)$$

Taking partial derivative of T_g and T_s given by Eq. (3.14) with respect to α the following equations are obtained,

$$\frac{\partial T_g}{\partial \alpha} = -3K \cos [2(\alpha - \theta)] \quad (3.61)$$

$$\frac{\partial T_s}{\partial \alpha} = C\sigma \left(\frac{1-e^2}{1+e \cos \theta} \right)^3 \left[\sin(2(\alpha + \gamma + \beta_1)) \Delta_1 \cos \beta_1 - \sin(2(\alpha + \gamma + \beta_2)) \Delta_2 \cos \beta_2 \right] \quad (3.62)$$

Replacing Eq. (3.61) and Eq. (3.62) into Eq. (3.60), one obtains

$$\begin{aligned} \frac{\partial T_{gs}}{\partial \alpha} = & -3K \cos [2(\alpha - \theta)] \\ & + C\sigma \left(\frac{1-e^2}{1+e \cos \theta} \right)^3 \left[\sin(2(\alpha + \gamma + \beta_1)) \Delta_1 \cos \beta_1 - \sin(2(\alpha + \gamma + \beta_2)) \Delta_2 \cos \beta_2 \right] \end{aligned} \quad (3.63)$$

The partial derivative of T_g and T_s with respect to θ is obtained as follow

$$\frac{\partial T_{gs}}{\partial \theta} = \frac{\partial T_g}{\partial \theta} + \frac{\partial T_s}{\partial \theta} + \left(\frac{\partial T_s}{\partial \gamma} \frac{\partial \gamma}{\partial \psi} \frac{\partial \psi}{\partial \theta} + \frac{\partial T_s}{\partial \sigma} \frac{\partial \sigma}{\partial \psi} \frac{\partial \psi}{\partial \theta} \right) \quad (3.64)$$

The partial derivatives in Eq. (3.64) can be obtained using Eq. (3.14) as follows:

$$\frac{\partial T_g}{\partial \theta} = 3K \cos[2(\alpha - \theta)] \quad (3.65)$$

$$\begin{aligned} \frac{\partial T_s}{\partial \theta} = C\sigma \left(\frac{3e \sin \theta (1-e^2)^3}{(1+e \cos \theta)^4} \right) \\ \times \left[\sin^2(\alpha + \gamma + \beta_1) \Delta_1 \cos \beta_1 - \sin^2(\alpha + \gamma + \beta_1) \Delta_2 \cos \beta_2 \right] \end{aligned} \quad (3.66)$$

$$\frac{\partial T_s}{\partial \gamma} = \frac{\partial T_s}{\partial \alpha} \quad (3.67)$$

$$\frac{\partial \gamma}{\partial \psi} = - \left(\frac{\cos(i - \varepsilon_s) \sec^2 \psi}{1 + \tan^2 \psi \cos^2(i - \varepsilon_s)} \right) \quad (3.68)$$

$$\frac{\partial T_s}{\partial \sigma} = \frac{T_s}{\sigma} \quad (3.69)$$

$$\frac{\partial \sigma}{\partial \psi} = -\sin 2\psi \sin^2(i - \varepsilon_s) \quad (3.70)$$

Using Eq. (3.65)-(3.70), one obtains $\partial T_{gs}/\partial \theta$.

The partial derivative of T_s with respect to β_j is obtained as

$$\frac{\partial T_s}{\partial \beta_1} = C\sigma \Delta_1 \left(\frac{1-e^2}{1+e \cos \theta} \right)^3 \left[\sin(2(\alpha + \gamma + \beta_1)) \cos \beta_1 - \sin^2(\alpha + \gamma + \beta_1) \sin \beta_1 \right] \quad (3.71)$$

$$\frac{\partial T_s}{\partial \beta_2} = C\sigma \Delta_2 \left(\frac{1-e^2}{1+e \cos \theta} \right)^3 \left[-\sin(2(\alpha + \gamma + \beta_2)) \cos \beta_2 + \sin^2(\alpha + \gamma + \beta_2) \sin \beta_2 \right] \quad (3.72)$$

Using Eqs.(3.63), (3.64), (3.71), and (3.72) into Eq.(3.59), $\alpha^{(3)}$ is written as

$$\alpha^{(3)} = \left(\frac{1}{1 + e \cos \theta} \right) \left\{ f_s + [B_1 \ B_2] \begin{bmatrix} u_1 \\ u_2 \end{bmatrix} \right\} \quad (3.73)$$

where,

$$f_s = 3e \sin \theta \alpha'' + 2e \cos \theta \alpha' + \frac{\partial T_{gs}}{\partial \alpha} \alpha' + \frac{\partial T_{gs}}{\partial \theta} \theta' + \frac{\partial T_s}{\partial \beta_1} \beta_1' + \frac{\partial T_s}{\partial \beta_2} \beta_2' \quad (3.74)$$

$$B_1 = \frac{\partial T_s}{\partial \beta_1}, \quad B_2 = \frac{\partial T_s}{\partial \beta_2}$$

Now using $S' = -\eta \operatorname{sgn}(S)$ in Eq. (3.56) yields $V' = -\eta |S|$, which is negative semi-definite of S for positive value of η . So, the proposed control laws are globally stable for assumed Lyapunov Function(3.55). Using Eq.(3.58), Eq.(3.73), and $S' = -\eta \operatorname{sgn}(S)$, one obtains the following relations:

$$\left(\frac{1}{1 + e \cos \theta} \right) \{ f_s + [B][u] \} - \alpha_d^{(3)} + p_2 \tilde{x}_2' + p_1 \tilde{x}_2 = -\eta \operatorname{sgn}(S) \quad (3.75)$$

where $[B] = [B_1 \ B_2]$ and $[u] = [u_1 \ u_2]^T$.

From the above Eq.(3.75), the control laws can be written as

$$[u] = \mathbf{B}^T [\mathbf{B}\mathbf{B}^T]^{-1} \left\{ -f_s + (1 + e \cos \theta) [\alpha_d^{(3)} - p_2 \tilde{x}_3 - p_1 \tilde{x}_2 - \eta \operatorname{sgn}(S)] \right\} \quad (3.76)$$

For the existence of the control laws (3.76), $\mathbf{B}\mathbf{B}^T$ must be non-zero in the region of interest :

$$\mathbf{B}\mathbf{B}^T = \left(\frac{\partial T_s}{\partial \beta_1} \right)^2 + \left(\frac{\partial T_s}{\partial \beta_2} \right)^2 \neq 0 \quad (3.77)$$

The region of $\Omega_s (\Omega_{s_1} \cap \Omega_{s_2})$ singularity in which $\mathbf{B}\mathbf{B}^T = 0$ is given by

$$\begin{aligned}
 \Omega_{S_1} &= \left\{ \left(\frac{\partial T_s}{\partial \beta_1} \right)^2 = 0 \right\} \\
 &= \left[\left\{ C\sigma\Delta_1 \left(\frac{1-e^2}{1+e\cos\theta} \right)^3 \right. \right. \\
 &\quad \left. \left. \times \left[\sin(2(\alpha+\gamma+\beta_1))\cos\beta_1 - \sin^2(\alpha+\gamma+\beta_1)\sin\beta_1 \right] \right\}^2 = 0 \right] \\
 &= \left\{ \left[2\sin(\alpha+\gamma+\beta_1)\cos(\alpha+\gamma+\beta_1)\cos\beta_1 - \sin^2(\alpha+\gamma+\beta_1)\sin\beta_1 \right]^2 = 0 \right\} \\
 &= \left\{ \sin(\alpha+\gamma+\beta_1)\cos(\alpha+\gamma+\beta_1)\cos\beta_1 \left[2 - \tan(\alpha+\gamma+\beta_1)\tan\beta_1 \right] = 0 \right\} \\
 &= \left\{ \alpha+\gamma+\beta_1 = 2n\pi, \text{ or } \tan(\alpha+\gamma+\beta_1)\tan\beta_1 = 2 \right\} \\
 \Omega_{S_2} &= \left\{ \left(\frac{\partial T_s}{\partial \beta_2} \right)^2 = 0 \right\} \\
 &= \left[\left\{ C\sigma\Delta_2 \left(\frac{1-e^2}{1+e\cos\theta} \right)^3 \right. \right. \\
 &\quad \left. \left. \times \left[-\sin(2(\alpha+\gamma+\beta_2))\cos\beta_2 + \sin^2(\alpha+\gamma+\beta_2)\sin\beta_2 \right] \right\}^2 = 0 \right] \\
 &= \left\{ \left[-2\sin(\alpha+\gamma+\beta_2)\cos(\alpha+\gamma+\beta_2)\cos\beta_2 + \sin^2(\alpha+\gamma+\beta_2)\sin\beta_2 \right]^2 = 0 \right\} \quad (3.78) \\
 &= \left\{ \sin(\alpha+\gamma+\beta_2)\cos(\alpha+\gamma+\beta_2)\cos\beta_2 \left[-2 + \tan(\alpha+\gamma+\beta_1)\tan\beta_2 \right] = 0 \right\} \\
 &= \left\{ \alpha+\gamma+\beta_2 = 2n\pi, \text{ or } \tan(\alpha+\gamma+\beta_2)\tan\beta_2 = 2 \right\}
 \end{aligned}$$

The control laws (3.76) is well defined as long as the trajectory of the closed-loop system does not enter the region Ω_S .

3.3.2.2 Terminal Sliding Mode Control

In this section, TSMC laws are developed for the proposed system based on [41-46]. The only difference between SMC and TSMC is design of sliding surfaces. For conventional SMC as presented in preceding section sliding surface is time varying function of linear hyperplane of state errors while in TSMC sliding surface is nonlinear exponential function of state errors [41-46].

In order to obtain the terminal convergence of the state variable, the following sliding surface for proposed system have defined as

$$S = \tilde{x}_3 + p_2 \tilde{x}_2^{q_2/h_2} + p_1 \tilde{x}_1^{q_1/h_1} \quad (3.79)$$

where, $p_i > 0, i=1,2$ are design constant, and q_i and h_i are positive odd integers satisfying $h_i > q_i, i=1,2$.

The TSMC can guarantee stability using Lyapunov theorem. However, the differentiation of terminal sliding mode surface S in the stability derivation process will result in the singular condition due to $h_i/q_i < 1, i=1,2$. Therefore, several terminal sliding mode control approaches avoiding singularity were developed [41], [43], [44] and [46]. In order to avoid singularity and by utilizing similar SMC procedure for deriving TSMC laws, the following control laws are obtained:

For $S \neq 0$, and $\tilde{x}_i \neq 0, i=1,2$

$$\begin{aligned} [u] = \mathbf{B}^\top [\mathbf{B}\mathbf{B}^\top]^{-1} \{ & -f_s \\ & + (1 + e \cos \theta) \left[\alpha_d^{(3)} - p_2 \left(\frac{q_2}{h_2} \right) \tilde{x}_2^{(q_2/h_2 - 1)} \tilde{x}_3 - p_1 \left(\frac{q_1}{h_1} \right) \tilde{x}_1^{(q_1/h_1 - 1)} \tilde{x}_2 - \eta \operatorname{sgn}(S) \right] \} \end{aligned} \quad (3.80)$$

For $S \neq 0$, and $\tilde{x}_i = 0, i=1,2$

$$[u] = \mathbf{B}^\top [\mathbf{B}\mathbf{B}^\top]^{-1} \left\{ -f_s + (1 + e \cos \theta) \left[\alpha_d^{(3)} - p_2 \tilde{x}_3 - p_1 \tilde{x}_2 - \eta \operatorname{sgn}(S) \right] \right\} \quad (3.81)$$

3.4 Analytical Solution for Tracking Error

In this section closed form solution for Hurwitz tracking errors for the satellite pitch motion have obtained.

The following initial condition for the tracking error and the error derivatives are assumed:

$$\tilde{x}_1(0) = \tilde{x}_0, \tilde{x}_2(0) = 0, \tilde{x}_3(0) = 0 \quad (3.82)$$

First, the constants p_1 , p_2 , a_1 and b_1 in Eq. (3.19) should be chosen in such a way that the representative point of the system at the initial orbit time $\theta = \theta_0$ belongs to the switching plane. For that purpose, the following condition must be satisfied

$$S(\tilde{x}(\theta_0), \theta_0) = \tilde{x}_1'' + p_2 \tilde{x}_1' + p_1 \tilde{x}_1 + a_1 + b_1 \theta = 0 \quad (3.83)$$

Consequently, for any orbit time $\theta \in [0, \theta_f]$ the system dynamics is described by Eq. (3.19) with the initial conditions (3.82). Therefore, we consider the following equation

$$\tilde{x}_1'' + p_2 \tilde{x}_1' + p_1 \tilde{x}_1 + a_1 + b_1 \theta = 0 \quad (3.84)$$

Eq. (3.84) is non homogeneous ordinary differential equation which has homogeneous and particular solutions. In order to solve Eq. (3.84), we first consider its homogenous equation

$$\tilde{x}_1'' + p_2 \tilde{x}_1' + p_1 \tilde{x}_1 = 0 \quad (3.85)$$

Since the tracking error convergence to zero without oscillations is required, the characteristic polynomial of Eq. (3.85) must be critically damped and it has double real roots. This ensures that oscillations or overshoots will take place neither before nor after the switching plane stops. Hence, we obtain another condition from critically damped second order system

$$p_2 = 2\sqrt{p_1} \quad (3.86)$$

Furthermore, the parameters p_1 and p_2 must be strictly positive to make the system (3.13) stable in the sliding mode. Solving Eq. (3.84) with condition (3.82) and assuming for the sake of clarity that $\theta_0 = 0$ we obtain the tracking error and its derivatives for the orbit time $\theta \in [0, \theta_f]$

$$\tilde{x}_1(\theta) = \left[\tilde{x}_0 + \frac{a_1}{p_1} - \frac{2b_1\sqrt{p_1}}{p_1^2} + \left(\frac{a_1}{\sqrt{p_1}} + \tilde{x}_0\sqrt{p_1} - \frac{b_1}{p_1} \right) \theta \right] e^{-\sqrt{p_1}\theta} - \frac{a_1}{p_1} + \frac{2b_1\sqrt{p_1}}{p_1^2} - \frac{b_1}{p_1} \theta \quad (3.87)$$

$$\tilde{x}_2(\theta) = \left[\frac{b_1}{p_1} - \left(a_1 + p_1 \tilde{x}_0 - \frac{b_1\sqrt{p_1}}{p_1} \right) \theta \right] e^{-\sqrt{p_1}\theta} - \frac{b_1}{p_1} \quad (3.88)$$

$$\tilde{x}_3(\theta) = \left[-a_1 - p_1 \tilde{x}_0 + p_1 \left(\frac{a_1}{\sqrt{p_1}} + \tilde{x}_0 p_1 - \frac{b_1}{p_1} \right) \theta \right] e^{-\sqrt{p_1}\theta} \quad (3.89)$$

Taking into account condition (3.84) and the assumption that $\theta_0 = 0$ we obtain

$$a_1 = -p_1 \tilde{x}_0 \quad (3.90)$$

Then Eqs. (3.87)-(3.89) can be written as

$$\tilde{x}_1(\theta) = \left(-\frac{2b_1\sqrt{p_1}}{p_1^2} - \frac{b_1}{p_1} \theta \right) e^{-\sqrt{p_1}\theta} + \frac{2b_1\sqrt{p_1}}{p_1^2} + \tilde{x}_0 - \frac{b_1}{p_1} \theta \quad (3.91)$$

$$\tilde{x}_2(\theta) = \frac{b_1}{p_1} (1 + \sqrt{p_1}\theta) e^{-\sqrt{p_1}\theta} - \frac{b_1}{p_1} \quad (3.92)$$

$$\tilde{x}_3(\theta) = -b_1 \theta e^{-\sqrt{p_1}\theta} \quad (3.93)$$

Next, the behavior of the system in the second phase of its motion is analyzed, which is when the switching plane does not move. Notice that for the orbit time $\theta \geq \theta_f$, the switching plane is fixed and passes through the origin of the errors. Considering these conditions, one obtains

$$a_1 + b_1 \theta_f = 0 \quad (3.94)$$

From Eq. (3.90) and Eq. (3.94) one obtains

$$\theta_f = \frac{\tilde{x}_0 p_1}{b_1} \quad (3.95)$$

The orbit time-invariant switching plane is described by Eq. (3.20), which is equivalent to Eq. (3.85). The initial conditions which are necessary to solve Eq. (3.85) can be determined from Eqs. (3.91)-(3.93), whose values are evaluated at the orbit time instant θ_f . Using the following notation

$$k = \frac{p_1 \sqrt{p_1} \tilde{x}_0}{b_1} \quad (3.96)$$

the initial conditions for the second phase of the system motion can be written as

$$\tilde{x}_1(\theta_f) = \left(-\frac{2b_1\sqrt{p_1}}{p_1^2} - \tilde{x}_0 \right) e^{-k} + \frac{2b_1\sqrt{p_1}}{p_1^2} \quad (3.97)$$

$$\tilde{x}_2(\theta_f) = \left(\frac{b_1}{p_1} + \tilde{x}_0 \sqrt{p_1} \right) e^{-k} - \frac{b_1}{p_1} \quad (3.98)$$

$$\tilde{x}_3(\theta_f) = -p_1 \tilde{x}_0 e^{-k} \quad (3.99)$$

The parameter k defined by Eq. (3.96) is strictly positive. Solving Eq. (3.85) with initial conditions (3.97)-(3.99) and using relation (3.90) we obtain

$$\tilde{x}_1(\theta) = e^{-\sqrt{p_1}\theta} \left[-\frac{2b_1\sqrt{p_1}}{p_1^2} + \frac{2b_1\sqrt{p_1}}{p_1^2} e^k - \tilde{x}_0 e^k + \left(-\frac{b_1}{p_1} + \frac{b_1}{p_1} e^k \right) \theta \right] \quad (3.100)$$

$$\tilde{x}_2(\theta) = e^{-\sqrt{p_1}\theta} \left[\frac{b_1}{p_1} - \frac{b_1}{p_1} e^k + \tilde{x}_0 e^k \sqrt{p_1} - \left(-\frac{b_1}{\sqrt{p_1}} + \frac{b_1}{\sqrt{p_1}} e^k \right) \theta \right] \quad (3.101)$$

$$\tilde{x}_3(\theta) = e^{-\sqrt{p_1}\theta} \left[-p_1 \tilde{x}_0 e^k + b_1 (e^k - 1) \theta \right] \quad (3.102)$$

The preceding three Eqs. (3.100) – (3.102) describe the tracking error for any orbit time $\theta \geq \theta_f$.

3.5 Analytical Proofs for Disturbance Rejection and Parameter Uncertainties

The proposed SMC control laws are robust against parameter uncertainties and external disturbances. The proofs are as follows:

Disturbance Rejection

The class of nonlinear systems under this study can be described in the state space form with external disturbance w as

$$\begin{aligned} \dot{\mathbf{x}} &= \mathbf{f}(\mathbf{x}) + \mathbf{g}(\mathbf{x}) \mathbf{u} + \mathbf{p}(\mathbf{x}) w \\ y &= \mathbf{h}(\mathbf{x}). \end{aligned} \quad (3.103)$$

Here $\mathbf{p}(\mathbf{x})$ is a smooth disturbance vector field. The objective is to find a SMC law \mathbf{u} such that w has no effect on the output.

Theorem 1: The disturbance rejection problem for the system (3.103) is solvable if the Lie derivatives of $\mathbf{h}(\mathbf{x})$ with respect to vector field $\mathbf{p}(\mathbf{x})$ and $\mathbf{f}(\mathbf{x})$ is

$$L_p L_f^k \mathbf{h}(\mathbf{x}) = 0 \quad \text{for} \quad k \leq \gamma - 1. \quad (3.104)$$

where $\gamma=3$ is the relative degree of the unperturbed system (3.13).

Proof: Equation (3.103) is written in the normal form using Lie derivatives as follows.

$$\begin{aligned}
 y' &= \left(\frac{\partial \alpha}{\partial \mathbf{x}} \right) [\mathbf{f}(\mathbf{x}) + \mathbf{g}(\mathbf{x}) \mathbf{u} + \mathbf{p}(\mathbf{x}) w] \\
 &= L_f \alpha + (L_g \alpha) \mathbf{u} + (L_p \alpha) w \\
 &= L_f \alpha \\
 y'' &= \left(\frac{\partial L_f \alpha}{\partial \mathbf{x}} \right) [\mathbf{f}(\mathbf{x}) + \mathbf{g}(\mathbf{x}) \mathbf{u} + \mathbf{p}(\mathbf{x}) w] \\
 &= L_f^2 \alpha + (L_g L_f \alpha) \mathbf{u} + (L_p L_f \alpha) w \\
 &= L_f^2 \alpha + (L_p L_f \alpha) w \\
 y''' &= \left(\frac{\partial (L_f^2 \alpha + (L_p L_f \alpha) w)}{\partial \mathbf{x}} \right) [\mathbf{f}(\mathbf{x}) + \mathbf{g}(\mathbf{x}) \mathbf{u} + \mathbf{p}(\mathbf{x}) w] \\
 &= \left(\frac{\partial L_f^2 \alpha}{\partial \mathbf{x}} \right) [\mathbf{f}(\mathbf{x}) + \mathbf{g}(\mathbf{x}) \mathbf{u} + \mathbf{p}(\mathbf{x}) w] \\
 &= L_f^3 \alpha + (L_g L_f^2 \alpha) \mathbf{u} + (L_p L_f^2 \alpha) w
 \end{aligned} \tag{3.105}$$

It follows that

$$\begin{aligned}
 L_p L_f^2 \alpha &= \left(\frac{\partial L_f^2 \alpha}{\partial \mathbf{x}} \right) \mathbf{p}(\mathbf{x}) \\
 &= \frac{\partial T_{gs}}{\partial \mathbf{x}} \mathbf{p}(\mathbf{x}) \\
 &= \begin{bmatrix} \frac{\partial T_{gs}}{\partial \alpha} & \frac{\partial T_{gs}}{\partial \alpha'} & \frac{\partial T_{gs}}{\partial \beta_1} & \frac{\partial T_{gs}}{\partial \beta_2} \end{bmatrix} [0 \ 1 \ 0 \ 0]^T \\
 &= \begin{bmatrix} \frac{\partial T_{gs}}{\partial \alpha} & 0 & \frac{\partial T_{gs}}{\partial \beta_1} & \frac{\partial T_{gs}}{\partial \beta_2} \end{bmatrix} [0 \ 1 \ 0 \ 0]^T \\
 &= 0
 \end{aligned} \tag{3.106}$$

for $k = 2$ which proves Theorem 1. Thus, the proposed VSC laws result in disturbance rejection and thereby isolate output (y) from disturbance (w).

Parameter Uncertainties

Parameter uncertainties can be modeled as perturbation to $\mathbf{f}(\mathbf{x})$, $\Delta \mathbf{f}(\mathbf{x})$ in Eq.(3.16). The resulting equation is

$$\begin{aligned}
 \dot{\mathbf{x}} &= \mathbf{f}(\mathbf{x}) + \Delta \mathbf{f}(\mathbf{x}) + \mathbf{g}(\mathbf{x}) \mathbf{u} \\
 y &= \mathbf{h}(\mathbf{x}).
 \end{aligned} \tag{3.107}$$

Theorem 2: The parameter uncertainties rejection problem for the system (3.107) is solvable if the Lie derivatives of $\mathbf{h}(\mathbf{x})$ with respect to vector field $\Delta\mathbf{f}(\mathbf{x})$ and $\mathbf{f}(\mathbf{x})$ is

$$L_{\Delta f} L_f^i \mathbf{h}(\mathbf{x}) = 0 \quad \text{for} \quad 0 \leq i \leq \gamma - 1. \quad (3.108)$$

where $\gamma=3$ is the relative degree of the unperturbed system (13).

Proof: Equation (3.107) is written in the normal form using Lie derivatives as follows.

$$\begin{aligned} y' &= \left(\frac{\partial \alpha}{\partial \mathbf{x}} \right) [\mathbf{f}(\mathbf{x}) + \mathbf{g}(\mathbf{x}) \mathbf{u} + \Delta\mathbf{f}(\mathbf{x})] \\ &= L_f \alpha + (L_g \alpha) \mathbf{u} + (L_{\Delta f} \alpha) \\ &= L_f \alpha \\ y'' &= \left(\frac{\partial L_f \alpha}{\partial \mathbf{x}} \right) [\mathbf{f}(\mathbf{x}) + \mathbf{g}(\mathbf{x}) \mathbf{u} + \Delta\mathbf{f}(\mathbf{x})] \\ &= L_f^2 \alpha + (L_g L_f \alpha) \mathbf{u} + (L_{\Delta f} L_f \alpha) \\ &= L_f^2 \alpha + (L_{\Delta f} L_f \alpha) \\ y''' &= \left(\frac{\partial (L_f^2 \alpha + (L_{\Delta f} L_f \alpha))}{\partial \mathbf{x}} \right) [\mathbf{f}(\mathbf{x}) + \mathbf{g}(\mathbf{x}) \mathbf{u} + \Delta\mathbf{f}(\mathbf{x})] \\ &= \left(\frac{\partial L_f^2 \alpha}{\partial \mathbf{x}} \right) [\mathbf{f}(\mathbf{x}) + \mathbf{g}(\mathbf{x}) \mathbf{u} + \Delta\mathbf{f}(\mathbf{x})] \\ &= L_f^3 \alpha + (L_g L_f^2 \alpha) \mathbf{u} + (L_{\Delta f} L_f^2 \alpha) \end{aligned} \quad (3.109)$$

It follows that

$$\begin{aligned} L_{\Delta f} L_f^2 \alpha &= \left(\frac{\partial L_f^2 \alpha}{\partial \mathbf{x}} \right) \Delta\mathbf{f}(\mathbf{x}) \\ &= \frac{\partial T_{gs}}{\partial \mathbf{x}} \Delta\mathbf{f}(\mathbf{x}) \\ &= \begin{bmatrix} \frac{\partial T_{gs}}{\partial \alpha} & \frac{\partial T_{gs}}{\partial \alpha'} & \frac{\partial T_{gs}}{\partial \beta_1} & \frac{\partial T_{gs}}{\partial \beta_2} \end{bmatrix} [0 \ 1 \ 0 \ 0]^T \\ &= \begin{bmatrix} \frac{\partial T_{gs}}{\partial \alpha} & 0 & \frac{\partial T_{gs}}{\partial \beta_1} & \frac{\partial T_{gs}}{\partial \beta_2} \end{bmatrix} [0 \ 1 \ 0 \ 0]^T \\ &= 0 \end{aligned} \quad (3.110)$$

for $i = 2$, which proves which proves Theorem 2. Thus, proposed VSC law result in parameter uncertainties rejection and thereby isolate output (y) from parameter uncertainties $\Delta f(x)$.

Closed-Loop Error Dynamics

The system given by Eq. (3.13) is rewritten as

$$\alpha'' = T_{gs} + w \quad (3.111)$$

where w represent a constant external disturbance. By differentiating Eq. (3.111) yields

$$\alpha^{(3)} = f_s + [B][u] \quad (3.112)$$

Substituting VSC control laws into Eq. (3.112) gives

$$\tilde{\alpha}^{(3)} + p_3\ddot{\tilde{\alpha}} + p_2\dot{\tilde{\alpha}} + p_1\tilde{\alpha} + \eta \operatorname{sgn}(S) = 0 \quad (3.113)$$

The preceding Eq. (3.113) is the third order linear differential equation of error dynamics and it does not contain any external disturbance term. This error equation is asymptotically stable as $\theta \rightarrow \infty$, tracking error $\tilde{\alpha}(\theta) \rightarrow 0$. Furthermore, the term $\eta \operatorname{sgn}(S)$ forces the error dynamics to stay onto the sliding plane which makes the system insensitive to system parameter uncertainty and disturbances.

3.6 Results and Discussions

3.6.1 Circular Orbit

In order to study the performance of the proposed controller, the system response is numerically simulated using Eq. (3.13), where $e=0$ is assumed for circular orbit, and control laws Eq. (3.42). The numerical simulation is carried out in MATLAB.

The effects of mass distribution parameter K , solar parameter C , solar angle ψ , and orbit inclination i on the controller performance are studied. The satellite attitude response remains almost unaffected with changes in these parameters (Figure 3.3 – Figure 3.9). Here, an attitude maneuver of satellite initially starting from $\alpha_0 = 110^\circ$ to final $\alpha_d = 0^\circ$ is performed with initial attitude tracking error of 10° .

The effect of mass moment of inertia distribution parameters (K) on the controller performance (Figure 3.3) is examined first. As the parameter K varies from $K=-1$ to $K=1$, the satellite attitude response remains virtually unaffected. However, the solar flap deflection rate (u_1, u_2) varies with changes in K . As K is increased from $K=-1$ to $K=1$, $|u_1|_{\max}$ ($|u_2|_{\max}$) increase from 7.5(4) to 26(28), respectively. The increase in $|u_1|_{\max}$ ($|u_2|_{\max}$) are due to the fact that $K=-1$ corresponds to favorable gravity gradient configuration while $K=1$ corresponds to unfavorable gravity gradient configuration. The maximum solar flaps deflection ($|\beta_j|_{\max}$) remains less than 30° and the corresponding period of β_j in the steady state situation remains same (0.5 orbit) for all cases considered here. This time period is directly proportional to the gravity gradient torque time period (2θ) from T_g in Eq. (3.14) in steady state case.

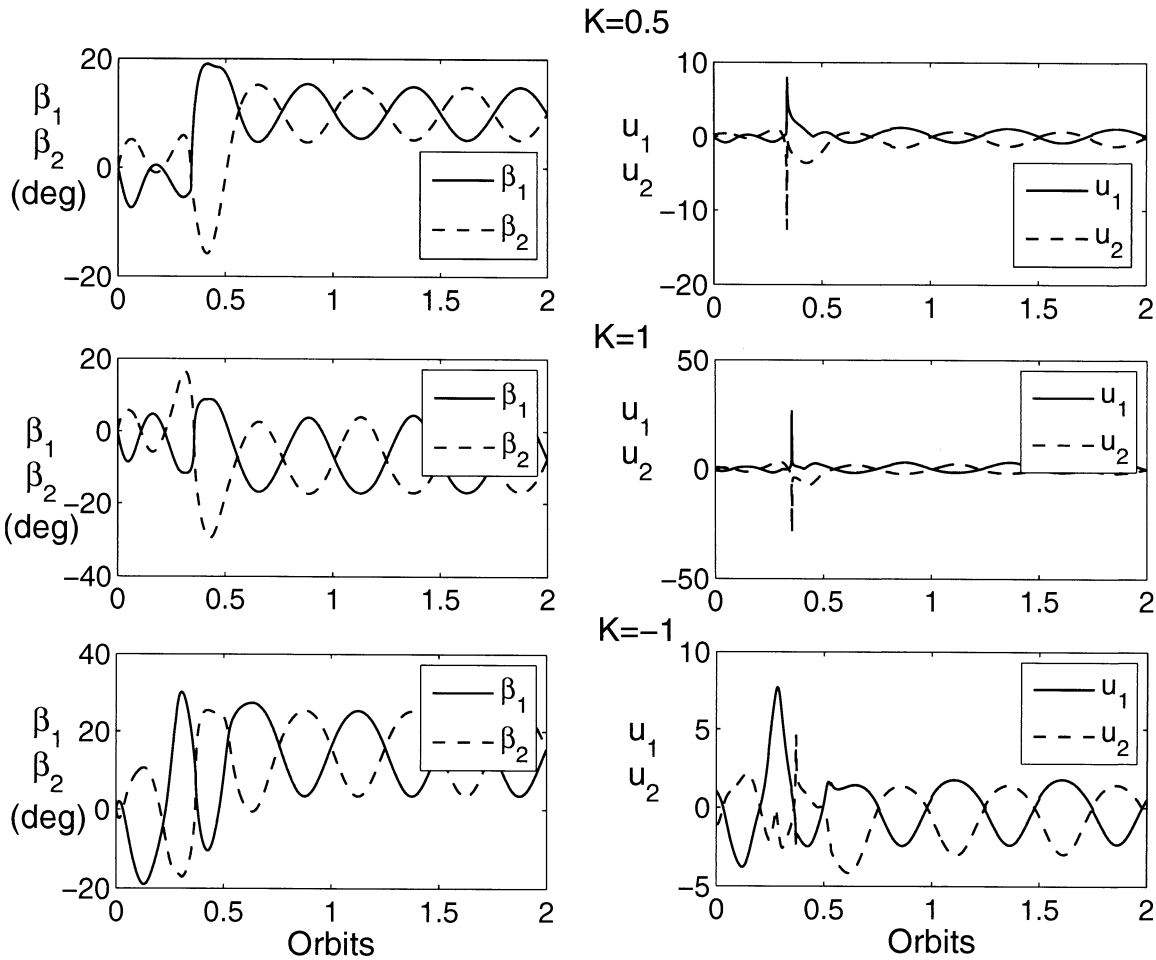


Figure 3.3: Solar flap deflection and solar flap deflection rate response as affected by mass distribution parameter K : $C=5$, $\psi = 45^\circ$, $i = 0^\circ$, $\varepsilon_s = 23.5^\circ$, $\eta = 0.5$, $p_1 = 16$, $p_2 = 8$, $\alpha_0 = 110^\circ$, $\alpha'_0 = 0$.

The solar parameter C has significant effect on the solar flap deflection rate. As the solar parameter C is decreased from 10 to 2, the solar flap deflection rate $((u_1)_{\max}, (u_2)_{\max})$ increases from (2, 3.3) to (123, 42.9) as shown in Figure 3.4. This increase in solar flap deflection rate could be explained from Eq. (3.42) where $|u_1|_{\max}$ is inversely proportion to the solar parameter C (i.e. lower C corresponds to high solar flap deflection rate). With changes in parameter C , however, the satellite attitude response remains unaffected showing robustness of the proposed controller. The maximum solar flap deflection $(\beta_{1\max}, \beta_{2\max})$ is

given in Table 3.1. The maximum-minimum solar flap rotation during steady state situation is given in Table 3.2. It should be noted that for lower solar parameter C it require very large solar flap rotation which may not be practical.

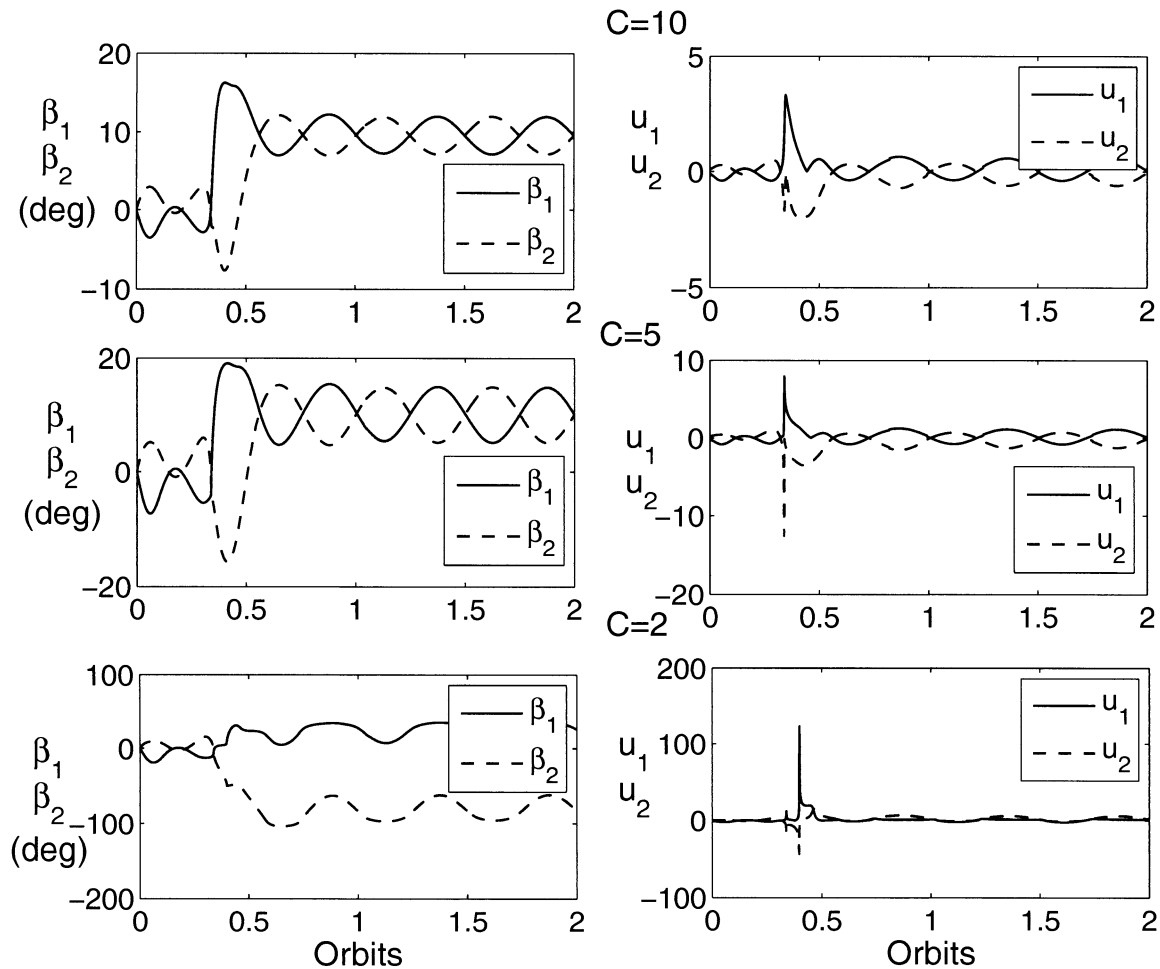


Figure 3.4: Effect of solar parameter C on solar flap deflection and solar flap deflection rate: $K=0.5$, $\psi = 45^\circ$, $i = 0^\circ$, $\varepsilon_s = 23.5^\circ$, $\eta = 0.5$, $p_1 = 16$, $p_2 = 8$, $\alpha_0 = 110^\circ$, $\alpha'_0 = 0$.

Table 3.1: Maximum flap deflection and deflection rate for different solar parameter C for circular orbit (transient condition)

Solar parameter (C)	Flap deflection (deg)	Flap deflection rate Nondimensional
$C = 2$	$ \beta_1 _{\max} = 34$ $ \beta_2 _{\max} = 103$	$ u_1 _{\max} = 123.1$ $ u_2 _{\max} = 42.9$
$C = 5$	$ \beta_1 _{\max} = 19.1$ $ \beta_2 _{\max} = 15.6$	$ u_1 _{\max} = 7.9$ $ u_2 _{\max} = 12.6$
$C = 10$	$ \beta_1 _{\max} = 16.3$ $ \beta_2 _{\max} = 7.5$	$ u_1 _{\max} = 3.3$ $ u_2 _{\max} = 2$

Table 3.2: Min-Max flap deflection for different solar parameter C for circular orbit (steady-state condition)

Solar parameter (C)	Min-Max Flap deflection (deg)
$C = 2$	$(\beta_1)_{\max} = +35.3$ $(\beta_2)_{\max} = -62.4$ $(\beta_1)_{\min} = +6.6$ $(\beta_2)_{\min} = -95.5$
$C = 5$	$(\beta_j)_{\max} = +14.9$ $(\beta_j)_{\min} = +5.2$
$C = 10$	$(\beta_j)_{\max} = +11.9$ $(\beta_j)_{\min} = +7.1$

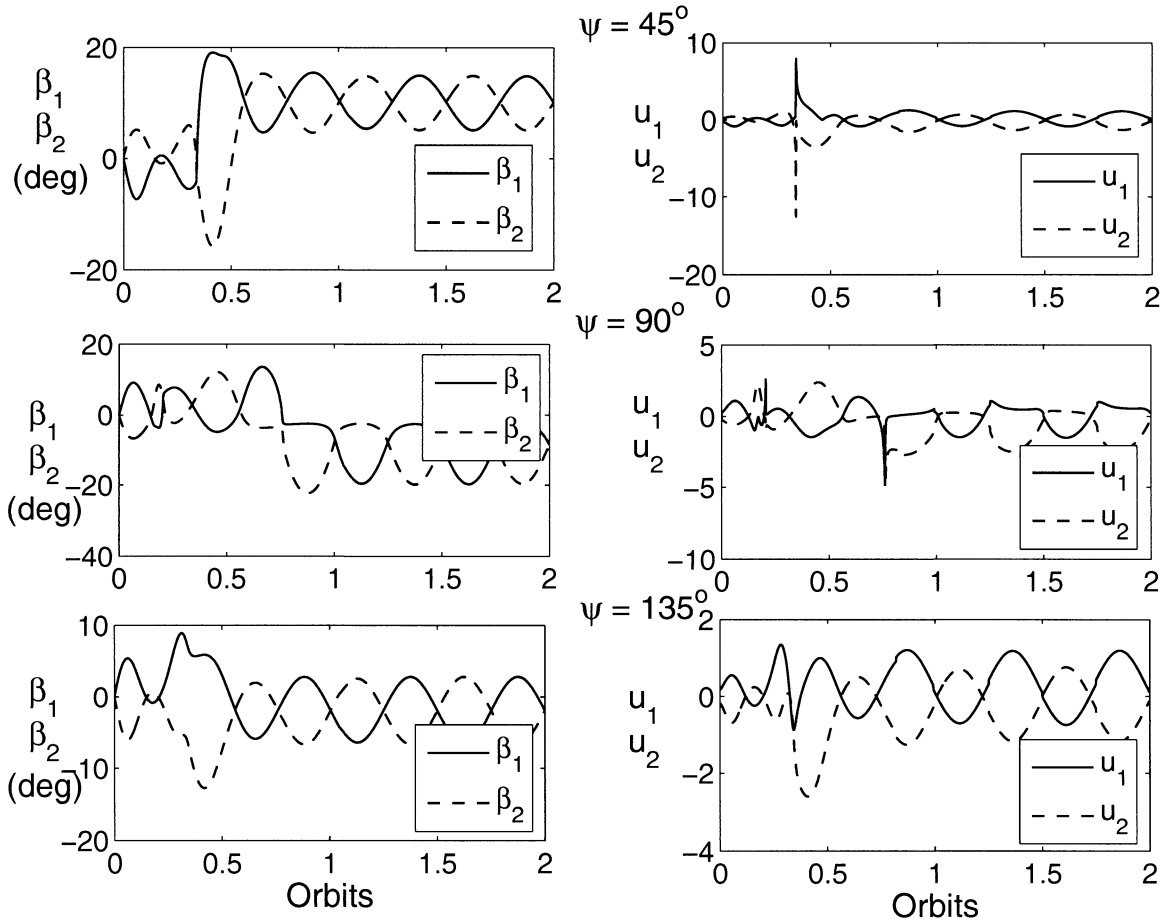


Figure 3.5: Effect of solar aspect angle ψ on solar flap deflection and solar flap deflection rate: $K=0.5, C=5, i=0^\circ, \varepsilon_s = 23.5^\circ, \eta = 0.5, p_1 = 16, p_2 = 8, \alpha_0 = 110^\circ, \alpha'_0 = 0$.

Figure 3.5 shows the effect of the solar angle ψ on the controller performance. As ψ is increased from 45 deg to 225 deg, the satellite attitude angle $|\alpha|$ remains unchanged proving the effectiveness of the proposed controller. However, the flap deflection β_1 and β_2 get changed with solar aspect angle (ψ) as shown in Table 3.3 and Table 3.4. Note that for the case of $\psi=90$ deg, β_1 and β_2 have negative values. This phenomena could be explained from Figure 3.1 when the sun is 90 deg from line of node, flaps have to deflect in clock wise direction from the local vertical (Figure 3.2).

Table 3.3: Maximum flap deflection and deflection rate for different solar aspect angle for circular orbit (transient condition)

Solar Aspect Angle (deg)	Flap deflection (deg)	Flap deflection rate Nondimensional
$\psi = 45^\circ$	$ \beta_1 _{\max} = 18$ $ \beta_2 _{\max} = 16$	$ u_1 _{\max} = 4$ $ u_2 _{\max} = 7$
$\psi = 90^\circ$	$ \beta_1 _{\max} = 14$ $ \beta_2 _{\max} = 22$	$ u_1 _{\max} = 5$ $ u_2 _{\max} = 2.5$
$\psi = 135^\circ$	$ \beta_1 _{\max} = 9$ $ \beta_2 _{\max} = 13$	$ u_1 _{\max} = 0.4$ $ u_2 _{\max} = 0.4$
$\psi = 225^\circ$	$ \beta_1 _{\max} = 18$ $ \beta_2 _{\max} = 16$	$ u_1 _{\max} = 4$ $ u_2 _{\max} = 7$

Table 3.4: Min-Max flap deflection for different solar aspect angle for circular orbit (steady-state condition)

Solar Aspect Angle (deg)	Min-Max Flap deflection (deg)
$\psi = 45^\circ$	$(\beta_j)_{\max} = +15$ $(\beta_j)_{\min} = -15$
$\psi = 90^\circ$	$(\beta_j)_{\max} = -2$ $(\beta_j)_{\min} = -20$
$\psi = 135^\circ$	$(\beta_j)_{\max} = -2.5$ $(\beta_j)_{\min} = -7$
$\psi = 225^\circ$	$(\beta_j)_{\max} = +15$ $(\beta_j)_{\min} = -15$

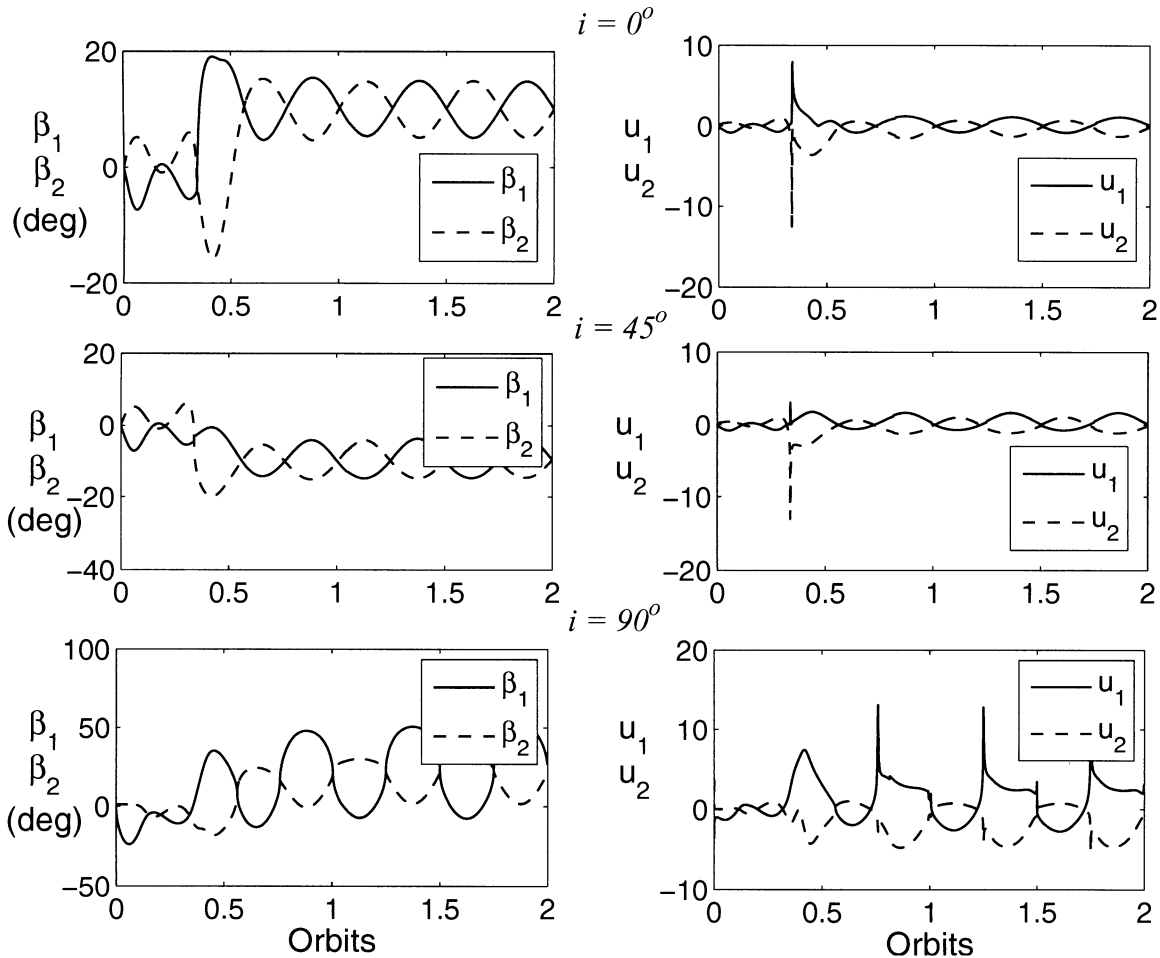


Figure 3.6: Effect of orbit inclination i on solar flap deflection and solar flap deflection rate: $K=0.5$, $C=5$, $\psi = 45^\circ$, $\varepsilon_s = 23.5^\circ$, $\eta = 0.5$, $p_1 = 16$, $p_2 = 8$, $\alpha_0 = 110^\circ$, $\alpha'_0 = 0$.

Next the effect of the orbital inclination on to the controller performances has been presented (Figure 3.6). The attitude response remains unaffected as i is changed from -45 deg to 90 deg. As inclination (i) is increased from 0 deg to 90 deg, the flap deflection β_1 and β_2 changes as shown in Table 3.5. The effect of orbit inclination could be explained as follows, the parameter σ in Eq. (3.14) decreases as inclination increases from 0 deg to 90 deg because value of $\sin(i - \varepsilon_s)$ increases with increase in inclination (i). Moreover, this decrease in the parameter σ is inversely proportional to the $|u_1|_{\max}$ in Eq. (3.42) which results in the increase of flap deflection rate. Hence, increases in flap deflection rate correspond to increase in deflection angle (β_1 , β_2) (Figure 3.6). However, there is an

exception when case $i=0$ deg varies to $i=45$ deg. In the case of $i=0$ deg, the value of $\sin(i - \varepsilon_s)$ in parameter σ (in Eq. (3.14)) is less than the case of $i=45$ deg.

Table 3.5: Maximum flap deflection and deflection rate for different orbit inclination for circular orbit (transient condition)

Orbit Inclination (deg)	Flap deflection (deg)	Flap deflection rate Nondimensional
$i = 0^\circ$	$ \beta_1 _{\max} = 19.1$ $ \beta_2 _{\max} = 15.6$	$ u_1 _{\max} = 8$ $ u_2 _{\max} = 12.6$
$i = 45^\circ$	$ \beta_1 _{\max} = 14.6$ $ \beta_2 _{\max} = 19.9$	$ u_1 _{\max} = 3$ $ u_2 _{\max} = 3$
$i = 90^\circ$	$ \beta_1 _{\max} = 50.5$ $ \beta_2 _{\max} = 31.2$	$ u_1 _{\max} = 15.7$ $ u_2 _{\max} = 5.3$
$i = -45^\circ$	$ \beta_1 _{\max} = 50.1$ $ \beta_2 _{\max} = 29.2$	$ u_1 _{\max} = 15.8$ $ u_2 _{\max} = 5.1$

Table 3.6: Min-Max flap deflection for different orbit inclination for circular orbit (steady-state condition)

Orbit Inclination (deg)	Min-Max Flap deflection (deg)
$i = 0^\circ$	$(\beta_j)_{\max} = +15, (\beta_j)_{\min} = +5$
$i = 45^\circ$	$(\beta_j)_{\max} = -3.7, (\beta_j)_{\min} = -14.8$
$i = 90^\circ$	$(\beta_1)_{\max} = +50 \quad (\beta_2)_{\max} = +31.2$ $(\beta_1)_{\min} = -7 \quad (\beta_2)_{\min} = +2.4$
$i = -45^\circ$	$(\beta_1)_{\max} = +50.1 \quad (\beta_2)_{\max} = +29.2$ $(\beta_1)_{\min} = -9.6 \quad (\beta_2)_{\min} = +0.3$

Figure 3.7 illustrate typical cases wherein the satellite may be required to undergo specified harmonic pitch chase-maneuvers. Here sinusoidal trajectory as mention before in Section 3 as per Eq. (3.52) has been given. For better appreciation of maneuver precision attained in pitch control, the corresponding attitude errors are also given in Figure 3.7. Even for the rapid chase-maneuver shown here, the attitude errors are found to remain well within small fraction of a degree. The larger the period of desired harmonic attitude changes, the smaller would be the associated error levels, as expected. The maximum solar flaps deflection $(|\beta_j|_{\max})$ remains less than 7° and the corresponding period of β_j remains same (0.5 orbit) for both cases considered here. However, as the period of desired harmonic attitude decreases, more control effort is required resulting in increase in solar flap deflection rate.

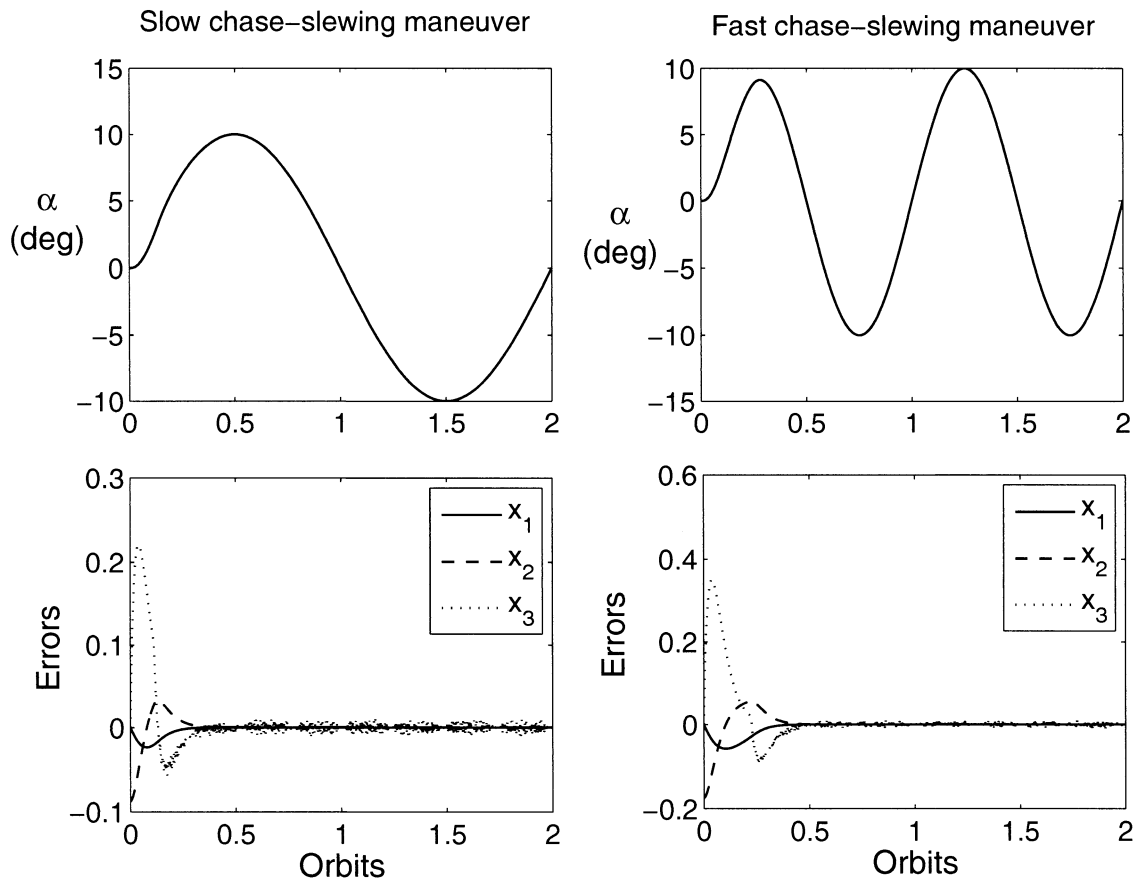


Figure 3.7: Performance of sliding mode control (SMC) under the periodic tracking: $K=0.5, C=5, \psi = 45^\circ, i = 0^\circ, \varepsilon_s = 23.5^\circ, \eta = 1, p_1 = 16, p_2 = 8, \alpha_0 = 110^\circ, \alpha'_0 = 0.$

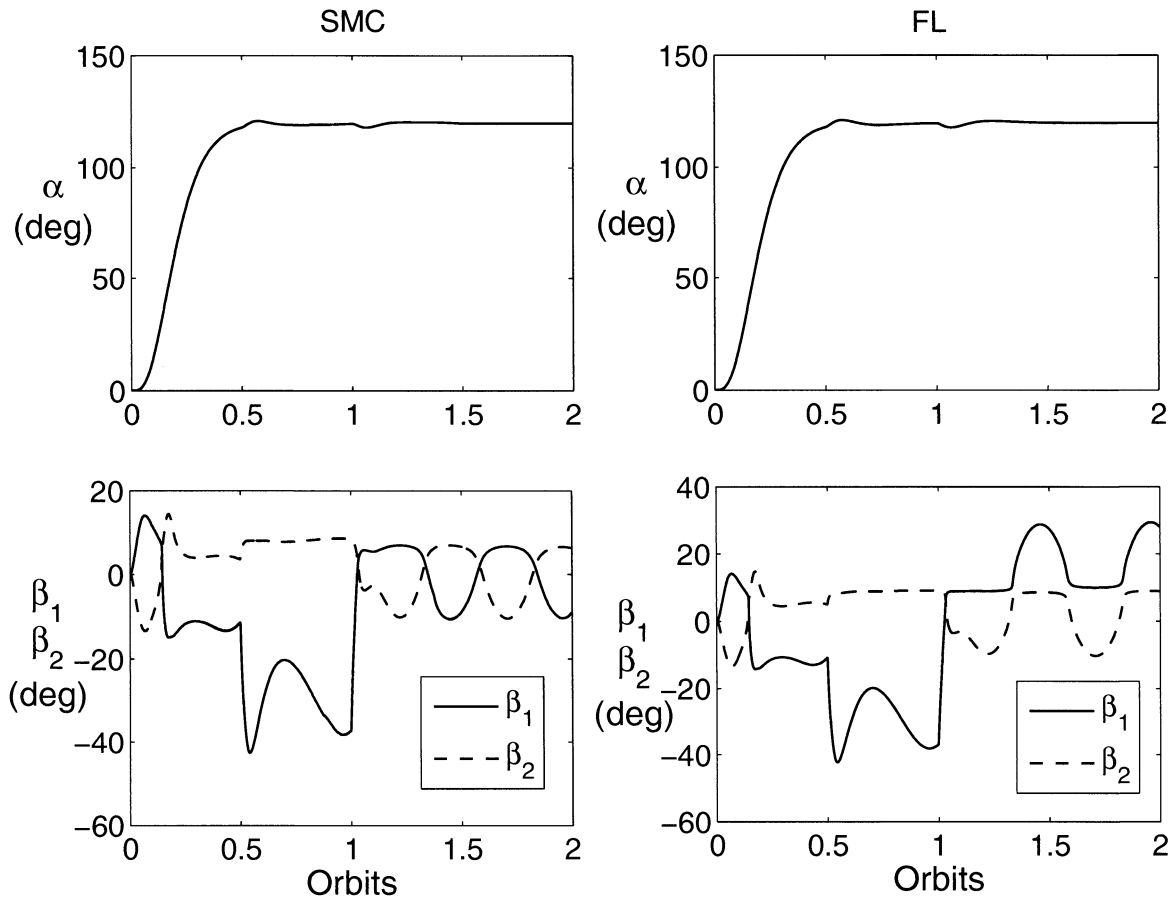


Figure 3.8: Performance of sliding mode control (SMC) and feedback linearization (FL) under the effect of disturbance: $K=0.5$, $C=5$, $\psi = 45^\circ$, $i = 0^\circ$, $\varepsilon_s = 23.5^\circ$, $\eta = 1$, $p_0 = 81$, $p_1 = 108$, $p_2 = 54$, $p_3 = 12$, $\alpha_0 = 0^\circ$, $\alpha'_0 = 0$.

Next, the performance of sliding mode control laws with feedback linearization control laws as developed in Ref. [20] is compared (Figure 3.8). Here for an appreciation about the effectiveness of the proposed control laws, a typical satellite with $I_x=400 \text{ kg}\cdot\text{m}^2$, $I_y=300 \text{ kg}\cdot\text{m}^2$, and $I_z=500 \text{ kg}\cdot\text{m}^2$ is considered. The solar flap has the following specifications: $A=0.25 \text{ m}^2$, $r=3 \text{ m}$. The values of constant parameters are $p=4.563 \times 10^{-6} \text{ N/m}^2$ and $\rho_s=1$. The system may experience disturbance torques due to several factors including SRP modeling errors (i.e., $\rho_s \neq 1$), solar flap misalignment and other environmental forces. The disturbance torques are assumed to be in the order of 10^{-6} . The disturbance torques of $5 \times 10^{-6} [N\cdot m]$ is applied from 0.5 orbits to 1 orbits in simulation. This disturbance torque to the system has been applied when the system almost reaches its desired pitch angle 120 deg in 0.5 orbits. As

shown in Figure 3.8, the desired pitch is successfully attained for both cases in presence of disturbances. In both cases solar flap deflection ($|\beta_1|_{\max}$) reaches to a maximum of 42 deg. In steady state situation, however, FL control laws require solar flap deflection ($|\beta_j|_{\max}$) of 28.7 deg as compared to SMC laws require 10.6 deg. This variation in solar flap deflection can be justified by comparing both control laws. If we compare sliding mode control law Eq. (3.49) with the feedback linearization Eq. (3.45) as given in reference [20] only difference is an addition of selection of sliding plane term $\eta \text{sign}(S)$ which makes SMC more robust against external disturbances and system uncertainties as compared to FL.

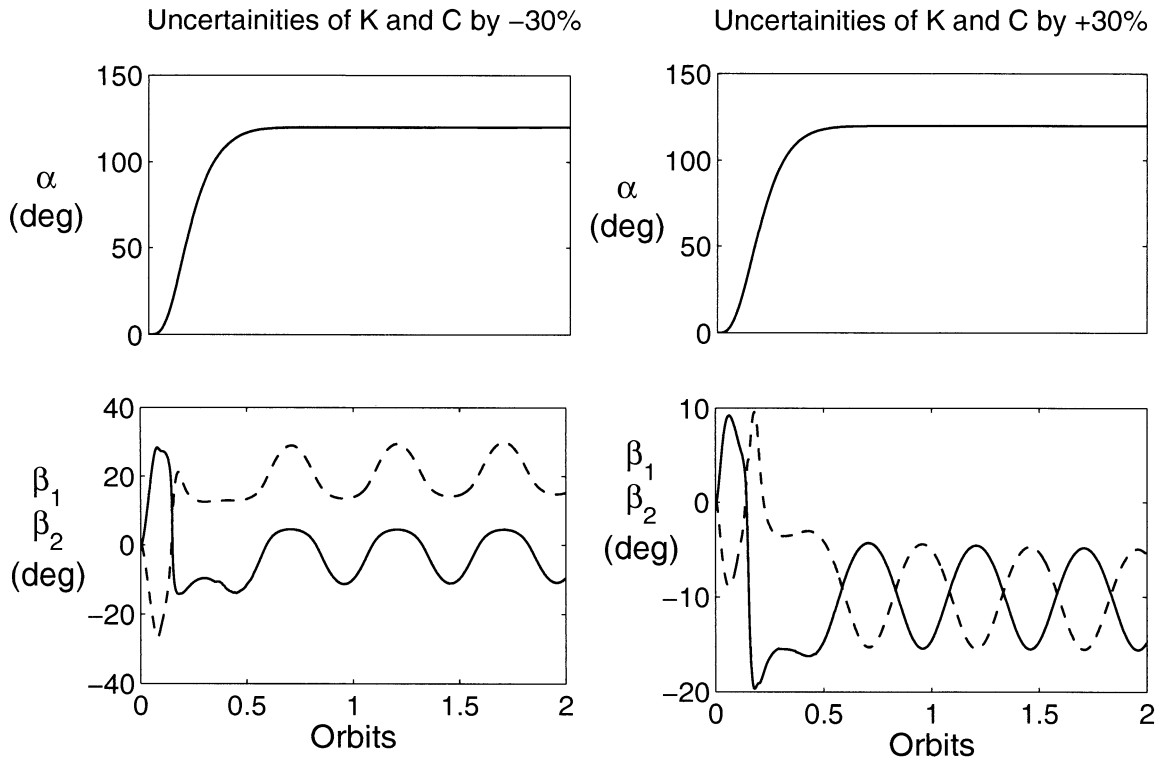


Figure 3.9: Performance of sliding mode control (SMC) in presence of parameter uncertainties into the mass distribution parameter (K) and the solar parameter (C): $K=0.5$, $C=5$, $\psi = 45^\circ$, $i = 0^\circ$, $\varepsilon_s = 23.5^\circ$, $\eta=1$, $p_0 = 81$, $p_1 = 108$, $p_2 = 54$, $p_3 = 12$, $\alpha_0 = 0^\circ$, $\alpha'_0 = 0$.

Finally, In order to study the performance of the proposed SMC in presence of the parameter uncertainties, the numerical simulation was done in the perturbed modes (Figure 3.9). First,

the mass distribution parameter (K) and the solar parameter (C) are decreased by 30% from its nominal values as follows: $K=0.35$ and $C=3.5$, respectively in the plant dynamics. In the second case, the mass distribution parameter (K) and the solar parameter (C) are increased by 30% from its nominal values as follows: $K=0.65$ and $C=6.5$, respectively. The above parameters are remained same as its nominal values as $K=0.5$ and $C=5$ in the SMC controller Eq. (3.49). The results of the numerical simulation are shown in Figure 3.9 for parameter uncertainties into the mass distribution parameter and the solar parameter. The desired pitch orientation of the satellite is achieved smoothly within 0.5 orbits. Also note that the SMC stabilized the pitch motion without any overshoot. Thus, the proposed SMC is robust against the parameter uncertainties and the numerical simulation verifies the theory presented in Section 3.5.

3.6.2 Elliptic Orbit

In order to study the performance of the proposed controller, the system response is numerically simulated using Eq. (3.13) and Eq. (3.76). The numerical simulation is carried out in MATLAB.

The effects of orbital eccentricity e , mass distribution parameter K , solar parameter C , solar angle ψ , and orbit inclination i on the controller performance are studied. The satellite attitude response remains almost unaffected with changes in these parameters (Figure 3.10- Figure 3.14). Here an attitude maneuver of satellite initially starting from $\alpha_0 = 100$ deg to final $\alpha_d = 0$ deg has been performed with initial attitude tracking error of 10 deg.

The effect of orbital eccentricity on the system performance and control solar flap deflection are examined first (Figure 3.10). The control solar flap deflection (β_f) is continuously adjusted as per control laws Eq. (3.76) given in Section 3.3.2. As the orbital eccentricity e increases from $e=0.05$ to $e=0.4$, the satellite attitude response remains virtually unaffected. From Figure 3.10 it can be seen that using the proposed SMC controller attitude tracking error goes to zero within 0.8 orbits in both the cases considered here.

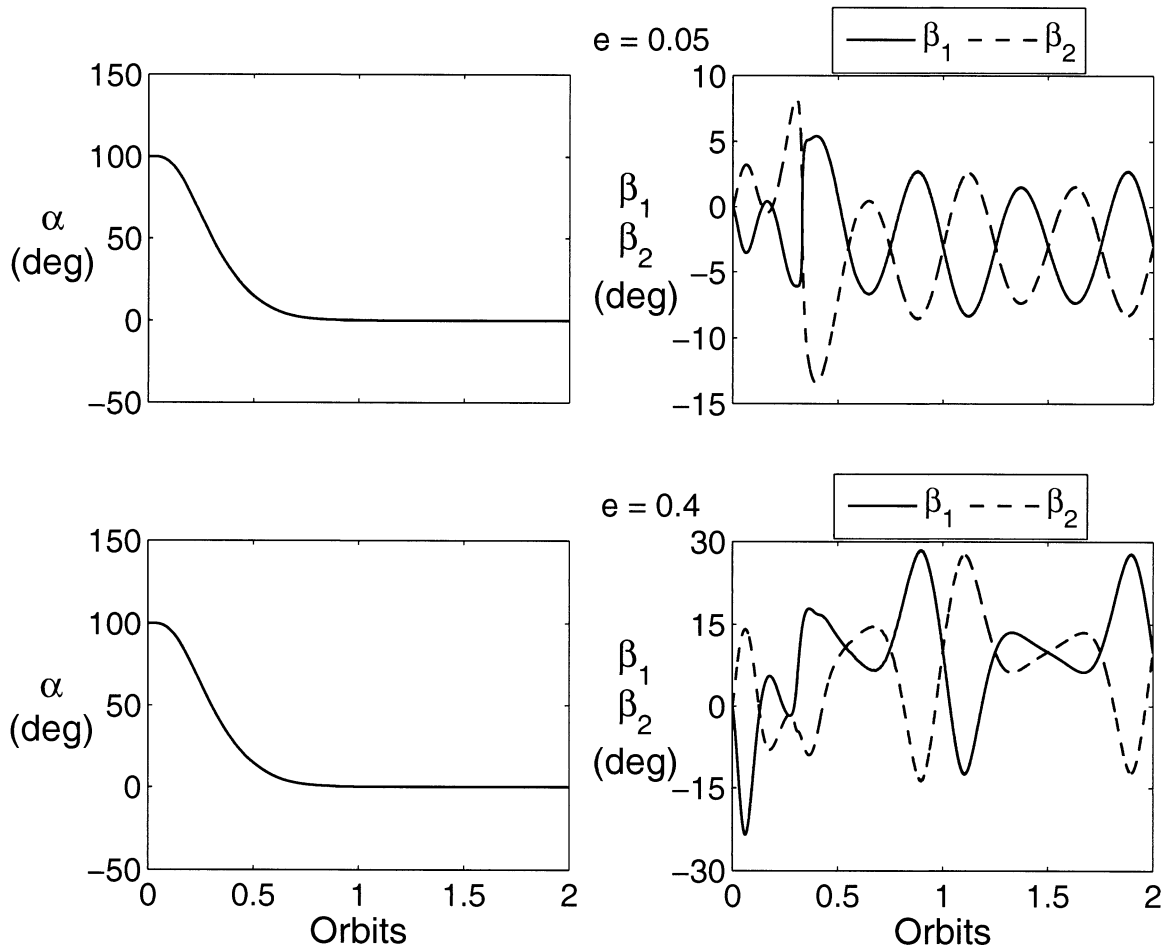


Figure 3.10: Effect of eccentricity on the system performance and control solar flap deflection: $K=0.5$, $C=5$, $\psi = 45^\circ$, $i = 0^\circ$, $\varepsilon_s = 23.5^\circ$, $\eta = 0.5$, $p_1 = 9$, $p_2 = 6$, $\alpha_0 = 100^\circ$, $\alpha'_0 = 0$.

As the orbital eccentricity e increases from $e=0.05$ to $e=0.4$, the control solar flap deflection (β_j) increases with increase in the eccentricity. This phenomenon can be explained by the fact that the orbital eccentricity acts as an external disturbance into the system. In order to counteract the effect of eccentricity, the controller has to produce more SRP torque by rotating large solar flap deflection. Thus, using the proposed SMC controller it is possible to achieve higher satellite attitude tracking performance for orbital eccentricity as high as $e=0.4$.

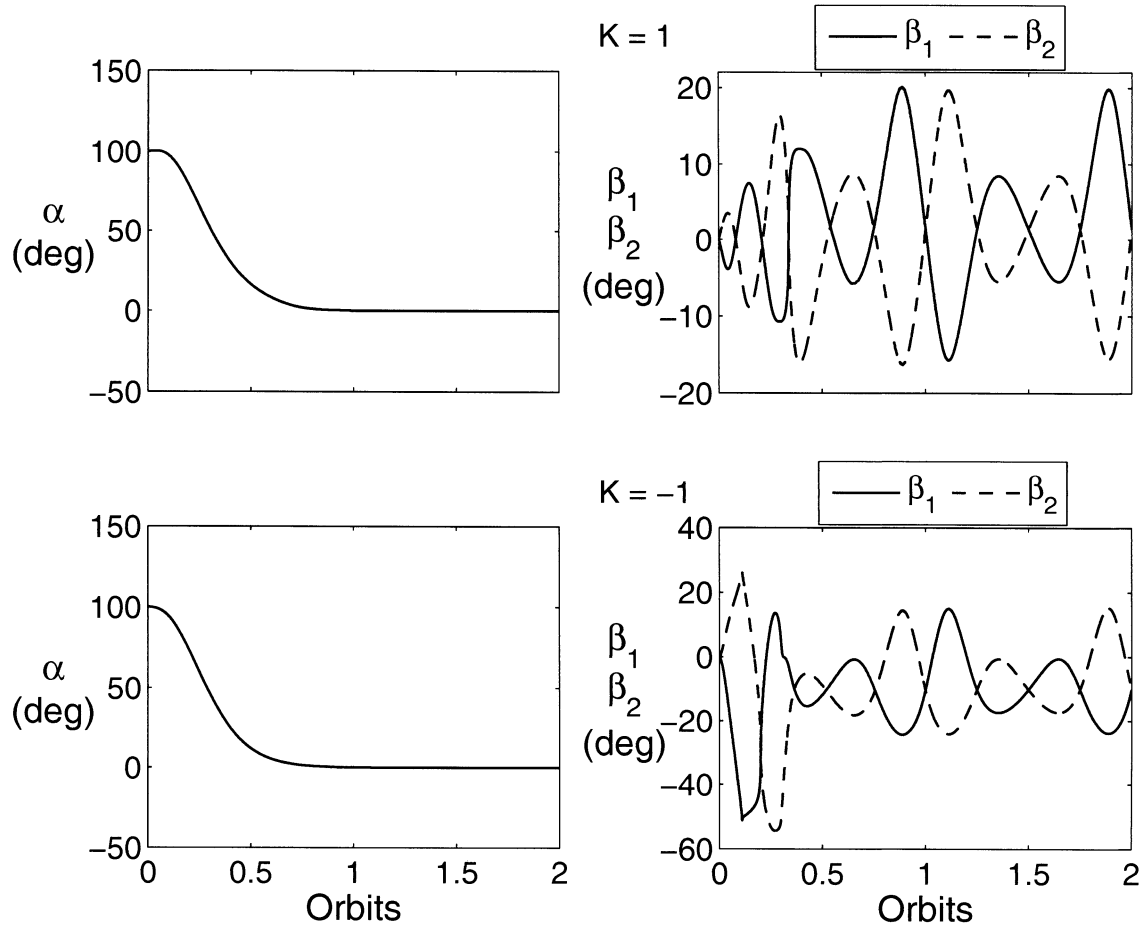


Figure 3.11: The system performance and control solar flap deflection response as affected by mass distribution parameter K : $e=0.2$, $C=5$, $\psi = 45^\circ$, $i = 0^\circ$, $\varepsilon_s = 23.5^\circ$, $\eta = 0.5$, $p_1 = 9$, $p_2 = 6$, $\alpha_0 = 100^\circ$, $\alpha'_0 = 0$.

Next the effect of mass moment of inertia distribution parameters (K) on the controller performance is examined (Figure 3.11). The value of K is varied from -1 to 1. Here $K=-1$ refers to an unstable gravity gradient configuration while $K=1$ signifies a stable gravity gradient configuration. Figure 3.11 shows the satellite attitude and control solar flap deflection responses obtained for $K=1$, and $K=-1$ with orbital eccentricity $e=0.2$. As the parameter K varies from $K=-1$ to $K=1$, the satellite attitude response remains virtually unaffected. However, the control solar flap deflection (β_j) varies with changes in K . As K is increased from $K=-1$ to $K=1$, $|\beta_1|_{\max}$ ($|\beta_2|_{\max}$) decrease from 50.1(54.4) deg to 20(19.5) deg,

respectively. The large control solar flap deflection $|\beta_1|_{\max}$ ($|\beta_2|_{\max}$) for negative value of K are due to the fact that $K=-1$ corresponds to an unfavorable gravity gradient configuration while the small control solar flap deflection $|\beta_1|_{\max}$ ($|\beta_2|_{\max}$) for $K=1$ corresponds to a favorable gravity gradient configuration. The maximum control solar flaps deflection ($|\beta_j|_{\max}$) remains less than 60 deg for both the cases considered here.

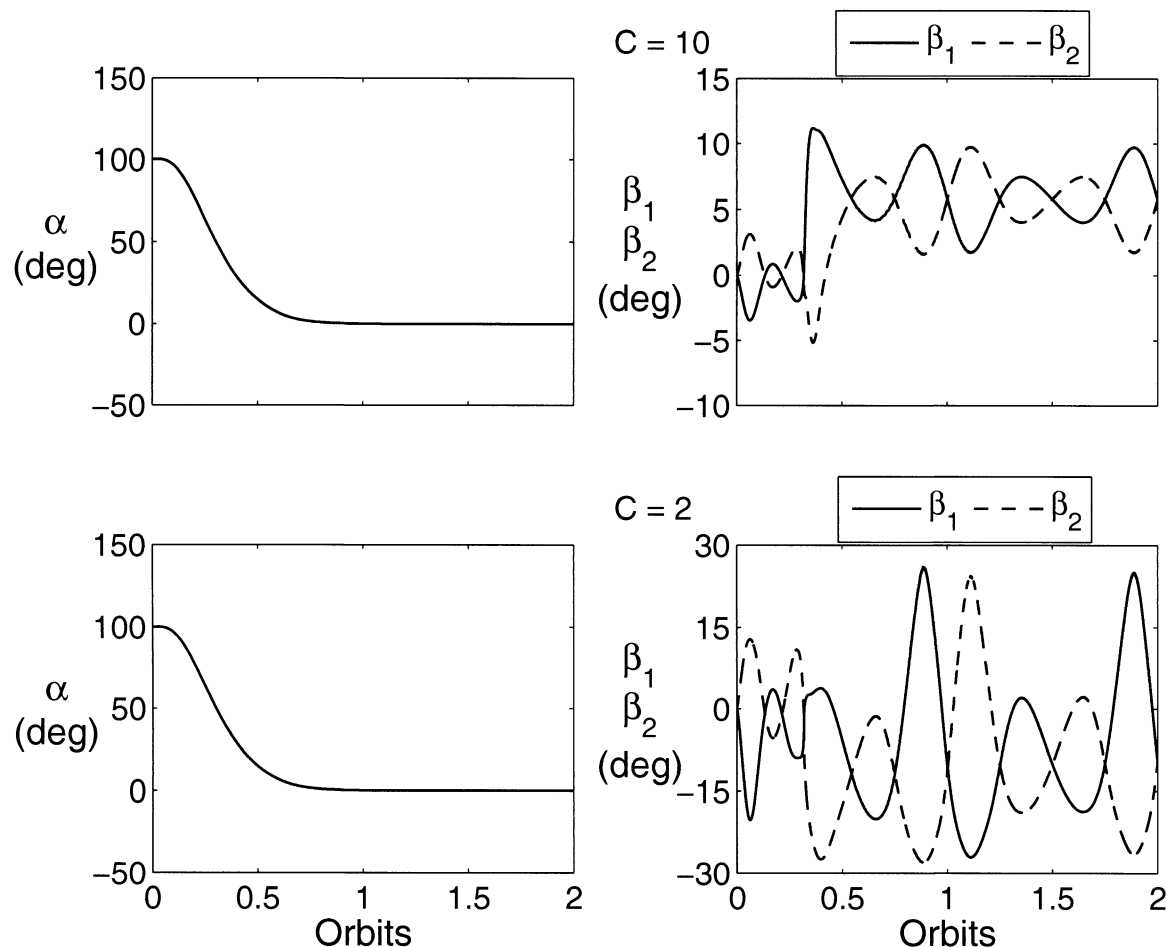


Figure 3.12: Effect of solar parameter C on the system performance and control solar flap deflection: $e=0.2$, $K=0.5$, $\psi = 45^\circ$, $i = 0^\circ$, $\varepsilon_s = 23.5^\circ$, $\eta = 0.5$, $p_1 = 9$, $p_2 = 6$, $\alpha_0 = 100^\circ$, $\alpha'_0 = 0$.

The effect of the solar parameter C is examined next (Figure 3.12). The solar parameter C has significant effect on the control solar flap deflection. As the solar parameter C is decreased from 10 to 2, the control solar flap deflection ($|\beta_1|_{\max}$, $|\beta_2|_{\max}$) increases from

(11.2, 9.7) deg to (27, 27.4) deg. This increase in solar flap deflection rate could be explained from Eq. (3.76) where $|u_j|_{\max}$ is inversely proportional to the solar parameter C (i.e. lower C corresponds to high control solar flap deflection rate). With changes in parameter C, however, the satellite attitude response remains unaffected showing robustness of the proposed controller. The maximum solar flap deflection ($\beta_{1\max}$, $\beta_{2\max}$) is given in Table 3.7. It should be noted that with lower solar parameter C the controller requires very large control solar flap deflection.

Table 3.7: Maximum control solar flap deflection for different solar parameter C

Solar parameter (C)	Control Solar Flap deflection (deg)
$C = 2$	$ \beta_1 _{\max} = 27$ $ \beta_2 _{\max} = 27.4$
$C = 10$	$ \beta_1 _{\max} = 11.2$ $ \beta_2 _{\max} = 9.7$

Next, whether performance of the controller is effective at different times in a year is examined (Figure 3.13). Figure 3.13 shows the effect of the solar angle ψ on the system performance and control solar flap deflection. As ψ is increased from 90 deg to 135 deg, the satellite attitude response remains unchanged proving the effectiveness of the proposed controller. However, the control solar flap deflection β_1 and β_2 get changed with solar aspect angle (ψ). The maximum control solar flap deflections for different solar aspect angles are summarized in Table 3.8. The maximum control solar flap deflection remained less than 30 deg for all cases considered here.

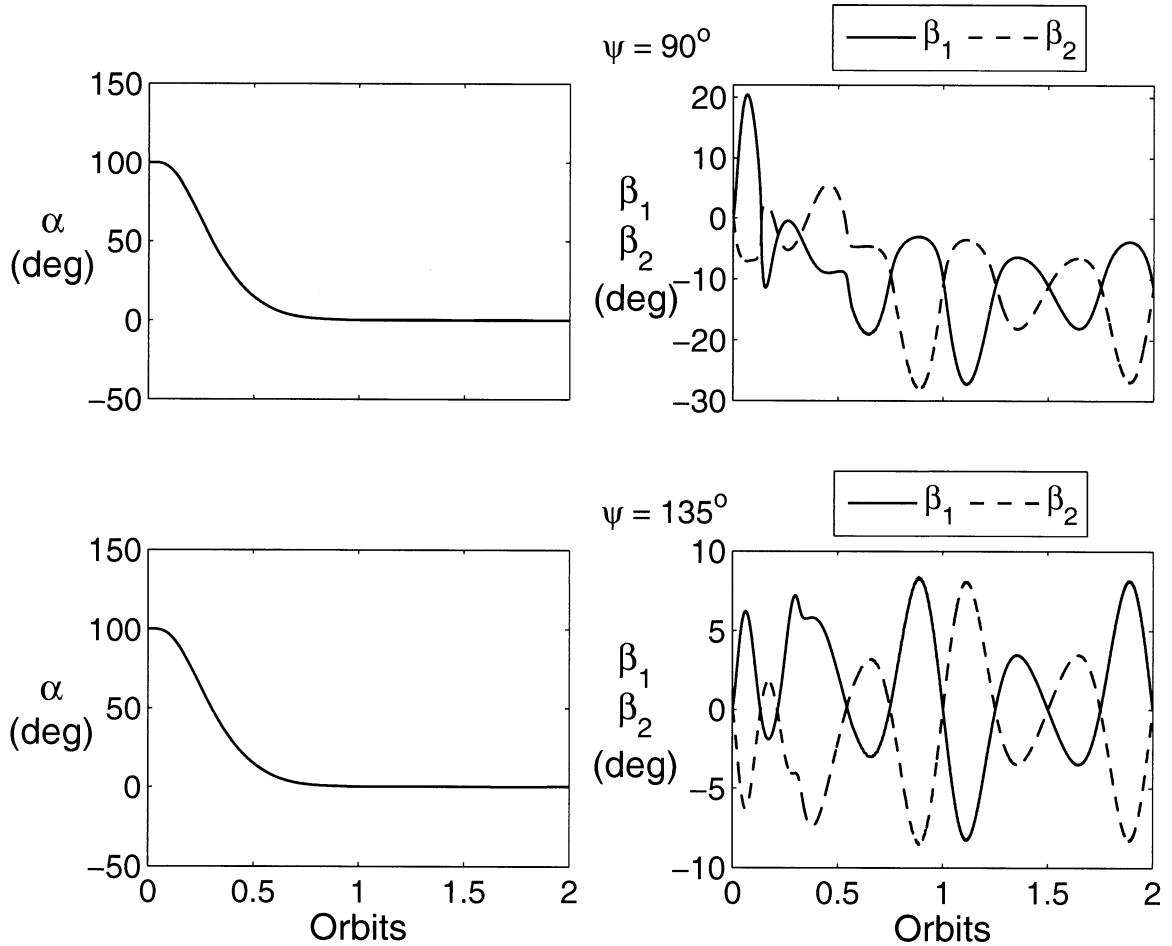


Figure 3.13: Effect of solar aspect angle ψ on the system performance and control solar flap deflection: $e=0.2$, $K=0.5$, $C=5$, $i=0^\circ$, $\varepsilon_s = 23.5^\circ$, $\eta = 0.5$, $p_1 = 9$, $p_2 = 6$, $\alpha_0 = 100^\circ$, $\alpha'_0 = 0$.

Table 3.8: Maximum control solar flap deflection for different solar aspect angle

Solar Aspect Angle (deg)	Flap deflection (deg)
$\psi = 90^\circ$	$ \beta_1 _{\max} = 28.1$ $ \beta_2 _{\max} = 27.3$
$\psi = 135^\circ$	$ \beta_1 _{\max} = 8.3$ $ \beta_2 _{\max} = 8.6$

Next the effect of the orbit inclination on the controller performances is studied (Figure 3.14). The system performance remains unaffected as i is changed from 0 deg to 90 deg.

With increase in inclination (i) from 0 deg to 90 deg, the flap deflections β_1 and β_2 are changed according to inclination change. The effect of orbit inclination could be explained as follows, the parameter σ in Eq. (3.14) decreases as orbit inclination increases from 0 deg to 90 deg because value of $\sin(i - \varepsilon_s)$ increases with increase in orbit inclination (i). Moreover, this decrease in the parameter σ is inversely proportional to the $|u_j|_{\max}$ in Eq. (3.76) which results in the increase of flap deflection rate. Hence, an increase in solar flap deflection rate corresponds to increase in control solar flap deflection (β_1, β_2) (Figure 3.14). The maximum control solar flap deflection for different orbit inclination is given in Table 3.9.

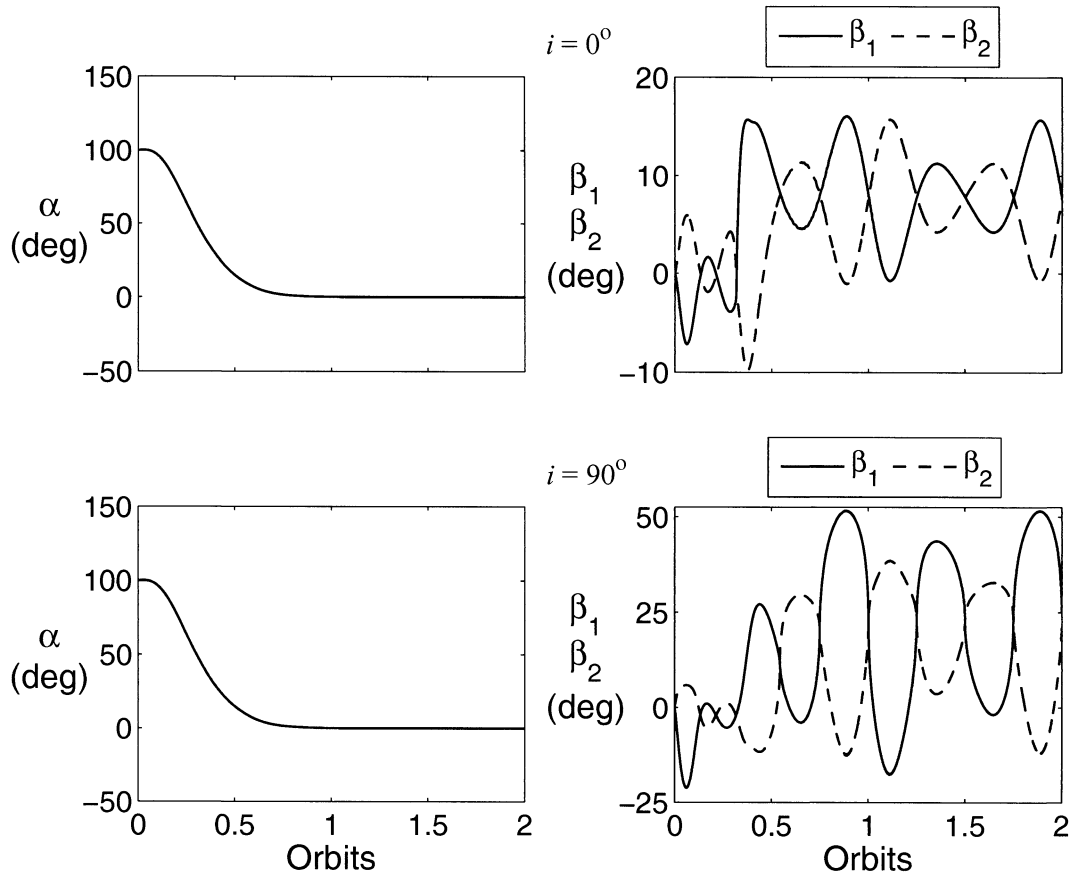


Figure 3.14: Effect of orbit inclination i on the system performance and control solar flap deflection: $e=0.2$, $K=0.5$, $C=5$, $\psi = 45^\circ$, $\varepsilon_s = 23.5^\circ$, $\eta = 0.5$, $p_1 = 9$, $p_2 = 6$, $\alpha_0 = 100^\circ$, $\alpha'_0 = 0$.

Table 3.9: Maximum control solar flap deflection for different orbit inclination

Orbit Inclination (deg)	Flap deflection (deg)
$i = 0^\circ$	$ \beta_1 _{\max} = 16.1$ $ \beta_2 _{\max} = 15.7$
$i = 90^\circ$	$ \beta_1 _{\max} = 51.6$ $ \beta_2 _{\max} = 38.5$

In order to study the performance of the proposed SMC in presence of the parameter uncertainties, the numerical simulation was done in the perturbed modes (Figure 3.15). First, orbital eccentricity (e), mass distribution parameter (K), and solar parameter (C) are decreased by 30% from its nominal values as follows: $e=0.14$, $K=0.35$, and $C=3.5$, respectively in the plant dynamics. In the second case, orbital eccentricity (e), mass distribution parameter (K) and solar parameter (C) are increased by 30% from its nominal values as follows: $e=0.26$, $K=0.65$, and $C=6.5$, respectively. The above parameters are remained same as its nominal values as $e=0.2$, $K=0.5$, and $C=5$ in the SMC controller Eq. (3.76). The results of the numerical simulation are shown in Figure 3.15 for parameter uncertainties in orbital eccentricity, mass distribution parameter, and solar parameter. The desired attitude of the satellite is achieved smoothly within 0.8 orbits. Thus, the proposed SMC is robust against the parameter uncertainties and the numerical simulation verifies the theory presented in Section 3.5.

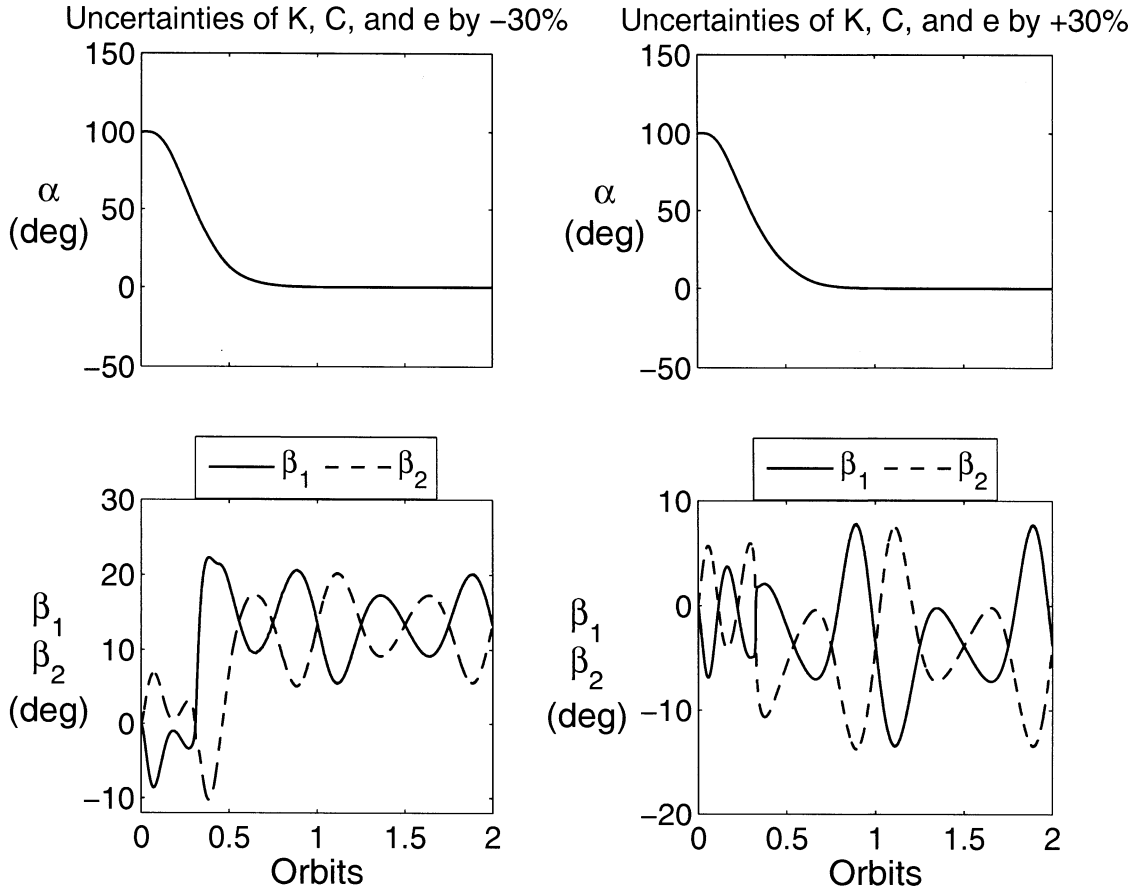


Figure 3.15: Performance of sliding mode control (SMC) in presence of parameter uncertainties into the orbital eccentricity (e), the mass distribution parameter (K) and the solar parameter (C): $e=0.2$, $K=0.5$, $C=5$, $\psi = 45^\circ$, $i = 0^\circ$, $\varepsilon_s = 23.5^\circ$, $\eta = 0.5$, $p_1 = 9$, $p_2 = 6$, $\alpha_0 = 100^\circ$, $\alpha'_0 = 0$.

Next, the performance of SMC laws with TSMC laws as proposed in section 3.3.2 is compared (Figure 3.16). In order to compare the performance of the proposed SMC and TSMC, the satellite attitude tracking is considered for orbit eccentricity $e=0.2$. In this case, all parameters of SMC and TSMC are taken same, e.g., $\eta = 0.5$, $p_1=9$, and $p_2=6$. The other parameters of the proposed TSMC controller are as follows: $h_i=15$ and $q_i=13$, $i=1,2$. In addition, all initial conditions of system parameters are taken same. The maximum control solar flap deflection $|\beta_j|_{\max}$ is 16 deg in the SMC while in the TSMC it increases to 19 deg. Attitude tracking error goes to zero within 0.8 orbit in SMC and TSMC. In both the cases, the control solar flap deflection almost matches during transient condition whereas in the steady

state the control solar flap deflection differs (Figure 3.16). TSMC converges tracking error very precisely to zero and the tracking error remained lower than the SMC response from 1.2 orbits to 2 orbits. Advantage of TSMC is precise attitude tracking error in finite time.

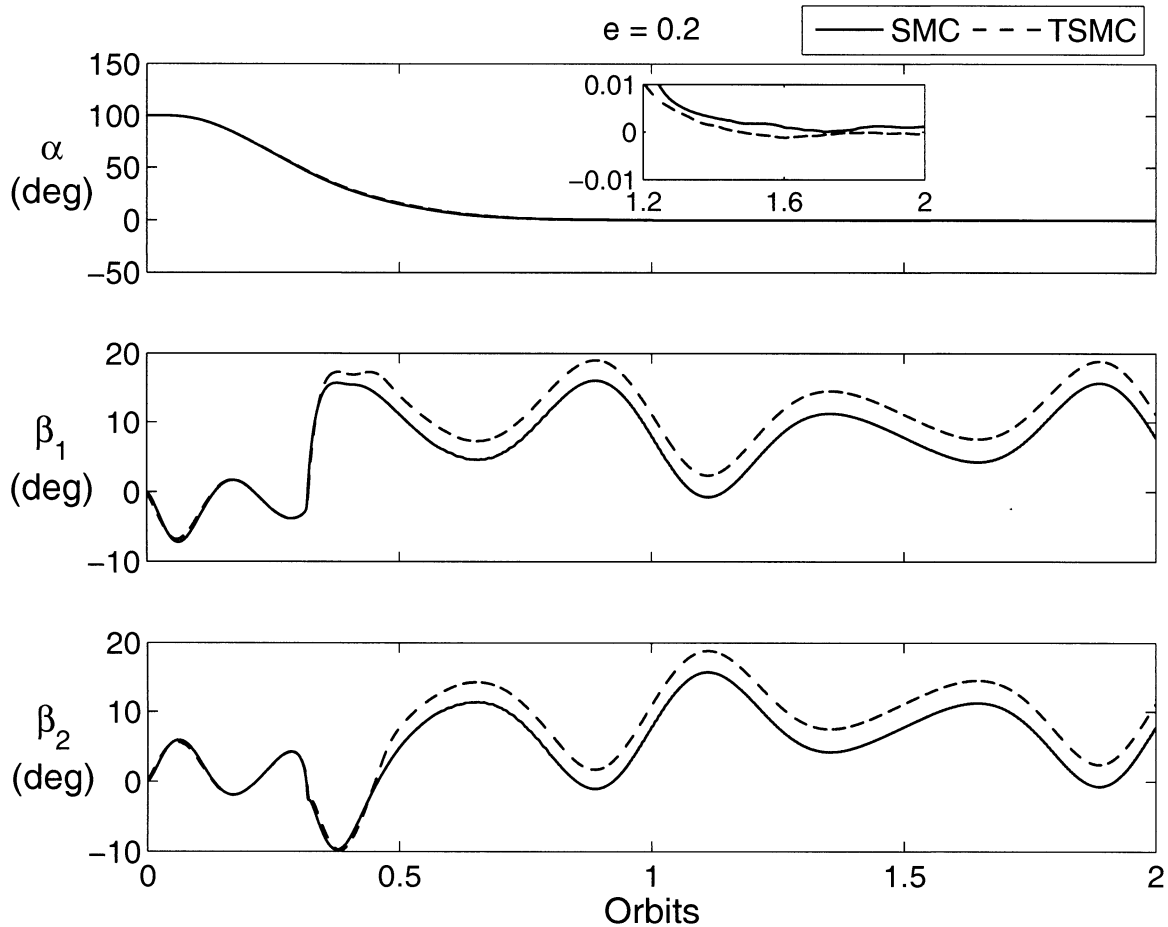


Figure 3.16: Performance comparison of sliding mode control (SMC) and terminal sliding mode control (TSMC): $K=0.5$, $C=5$, $\psi = 45^\circ$, $i = 0^\circ$, $\varepsilon_s = 23.5^\circ$, $\eta = 0.5$, $p_1 = 9$, $p_2 = 6$, $\alpha_0 = 100^\circ$, $\alpha'_0 = 0$.

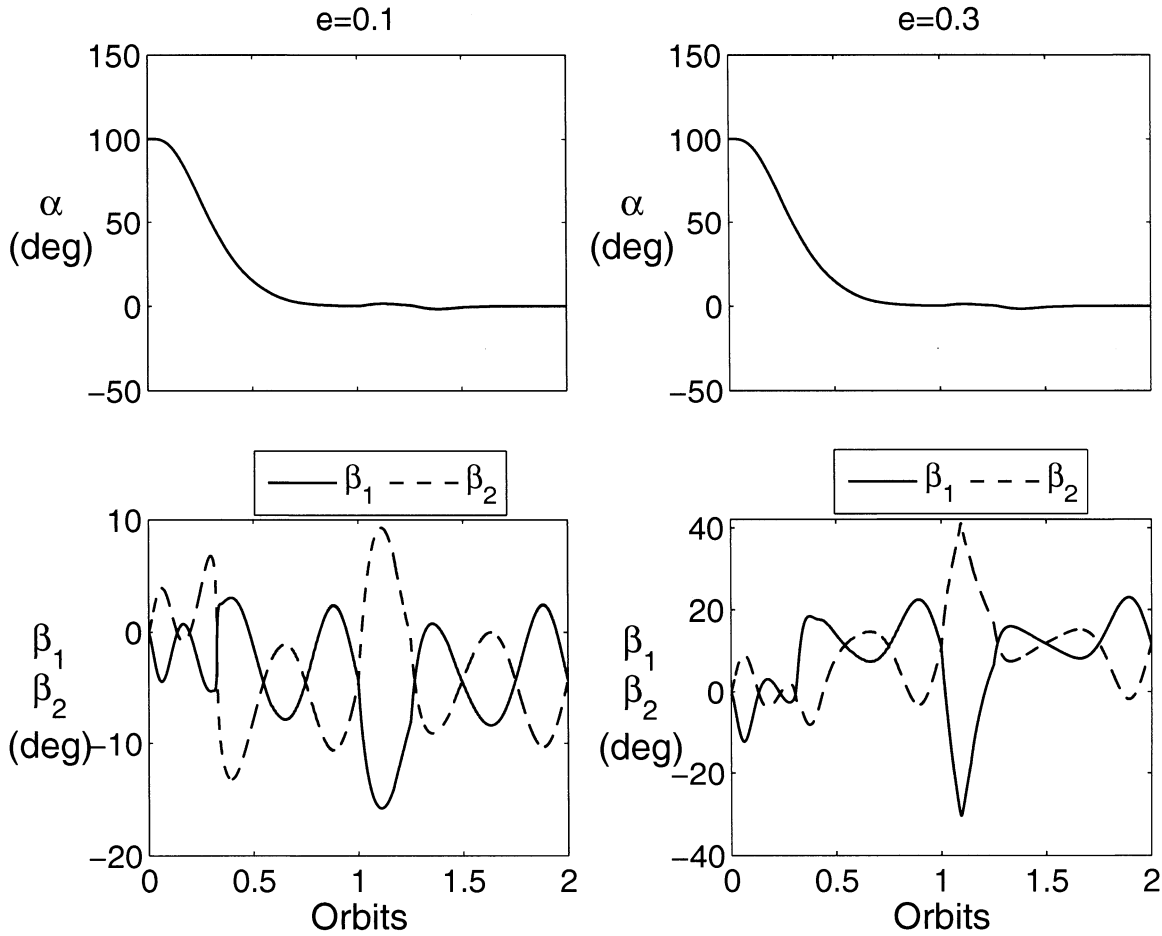


Figure 3.17: Performance of sliding mode control (SMC) in presence of external disturbance: $K=0.5$, $C=5$, $\psi = 45^\circ$, $i = 0^\circ$, $\varepsilon_s = 23.5^\circ$, $\eta = 0.5$, $p_1 = 9$, $p_2 = 6$, $\alpha_0 = 100^\circ$, $\alpha'_0 = 0$.

For an appreciation about the effectiveness of the proposed control laws in presence of external disturbance (Figure 3.17), a typical satellite with $I_x=400 \text{ kg}\cdot\text{m}^2$, $I_y=300 \text{ kg}\cdot\text{m}^2$, and $I_z=500 \text{ kg}\cdot\text{m}^2$ is considered. The solar flap has the following specifications: $A=0.25 \text{ m}^2$, $r=3 \text{ m}$. The values of constant parameters are $p=4.563 \times 10^{-6} \text{ N/m}^2$ and $\rho_s=1$. The semi-major axis is taken as $a=42241 \text{ km}$. The system may experience disturbance torques due to several factors including SRP modeling errors (i.e., $\rho_s \neq 1$), solar flap misalignment and other environmental forces. The disturbance torque is assumed to be in the order of 10^{-6} for the satellite in the geosynchronous orbit. The disturbance torques of $1.2 \times 10^{-6} [N\cdot m]$ is applied from 1.0 orbits to 1.5 orbits. This disturbance torque is in fact applied to the system when the

system almost reaches its desired pitch angle of 0 deg in 0.9 orbits. Two cases have considered: the first case with eccentricity $e=0.1$ and the second case $e=0.3$. As shown in Figure 3.17, the desired pitch is successfully attained for both the cases in presence of disturbances with small errors between 1 orbits to 1.5 orbits. For the first case the maximum control solar flap deflection $|\beta_j|_{\max}$ increases to 15.8 deg while in the second case it increases to 41.1 deg as compared to the case of no disturbance. This increase in $|\beta_j|_{\max}$ is due to the fact that large SRP torque is required to compensate external disturbances, resulting in increase in the control solar flap deflection. Thus, external disturbances rejection property of the proposed SMC verifies the theory presented in Section 3.5.

3.7 Summary

The present chapter examines the attitude control of satellites using SRP. The synthesis of closed-loop control laws for suitably rotating solar flaps is developed using variable structure control for circular and elliptic orbits to utilize proper SRP torque for desired attitude response. The rotation angle β_j of solar flaps is continuously adjusted as per the control laws. The proposed controller is very effective with initial attitude tracking errors. The satellite attitude response remains virtually unaffected with changes in orbital eccentricity e , solar parameter C , solar aspect angle ψ , mass distribution parameter K , and orbital inclination i . However, the control solar flap deflection has significant effect as these parameters change.

For SRP stabilized satellite in circular orbit the following conclusions can be summarized from analysis presented in Section 3.6.1. With an increase in K from $K=-1$ to $K=1$, $(|u_1|_{\max}, |u_2|_{\max})$ increase from 7.5(4) to 26(28), respectively. As the solar parameter C is decreased from 10 to 2, the solar flap deflection rate $((u_1)_{\max}, (u_2)_{\max})$ increases from (2, 3.3) to (123, 42.9). It is noted that for lower solar parameter C , the system requires very large solar flap rotation which may not be practical. Such large solar flap rotation gives certain

limitation on the application of SRP for attitude control of satellites. As orbit inclination increases solar flap deflection increases. In steady state situation period of solar flaps deflection is directly proportional to the gravity gradient torque time period of 2θ for all cases considered here. The SMC is very effective in controlling the satellite harmonic chase-maneuvers. However, as the period of desired harmonic attitude decreases, more control effort is required resulting in increase in solar flaps deflection rates. Furthermore, the SMC is more robust against external disturbances and parameter uncertainties in comparison to FL. In the simulation examined in this paper, SMC laws require solar flap deflection $|\beta_j|_{\max}$ of 10.6 deg while FL laws require 28.7 deg in steady-state condition.

For SRP stabilized satellite in an elliptic orbit the following conclusions can be summarized from analysis presented in Section 3.6.2. As the orbital eccentricity e increases from $e=0.05$ to $e=0.4$, the control solar flap deflection (β_j) increases while K is increased from $K=-1$ to $K=1$, $|\beta_1|_{\max}$ ($|\beta_2|_{\max}$) decreases from 50.1(54.5) deg to 20(19.5) deg, respectively. In the case the solar parameter C is decreased from 10 to 2, the control solar flap deflection $(|\beta_1|_{\max}, |\beta_2|_{\max})$ increases from (11.2, 9.7) deg to (27, 27.4) deg. It is noted that for lower solar parameter C , the system may require large solar flap deflection resulting in limitation on the applicability of SRP based attitude control system. As the orbit inclination increases the solar flap deflection increases. With regard to SMC and TSMC, the control solar flap deflection almost matches during transient whereas in the steady state the control solar flap deflection differs. Advantage of TSMC is its precise tracking error in finite time.

Furthermore, the proposed controller is found to be robust against parameter uncertainties and external disturbances for both circular orbits and elliptic orbits. The proposed control strategy can be augmented with the existing attitude control system of the satellite and may extend the life of the satellite mission experiencing attitude actuator failures.

Chapter 4

Application of Aerodynamic Forces for Satellite Attitude Control

4.1 Introduction

In this chapter, the application of aerodynamic forces for satellite attitude control based on VSC is presented. Two system models are considered in this chapter, (Model – I) and (Model – II). In Section 4.2 detailed system configuration about planar case (Model-I) is explained with system modeling, equations of motion, control design and important findings. In the next Section 4.3, three axis attitude control (Model -II) of the satellite is studied. Also in this section system modeling, kinematics and dynamics of the system, and control design is given. Finally, in the end chapter 4 is summarized in Section 4.4.

4.2 System Model - I

4.2.1 System Description

A system model that comprises of a satellite with two-oppositely placed light-weight aero flaps along the satellite Y-axis and its center of mass O moving in a circular orbit about the Earth's center E is considered (Figure 4.1). The system center of mass O lies on the center of mass of the satellite. For simplicity, the cube satellite is considered with length, width and height given as l_s , w_s , and h_s , respectively. The mass of the aero flaps and other accessories are assumed to be negligible. For the system under consideration, an orbital reference frame $O-X_0Y_0Z_0$ is selected such that the X_0 -axis always points along the local vertical, the Z_0 -axis

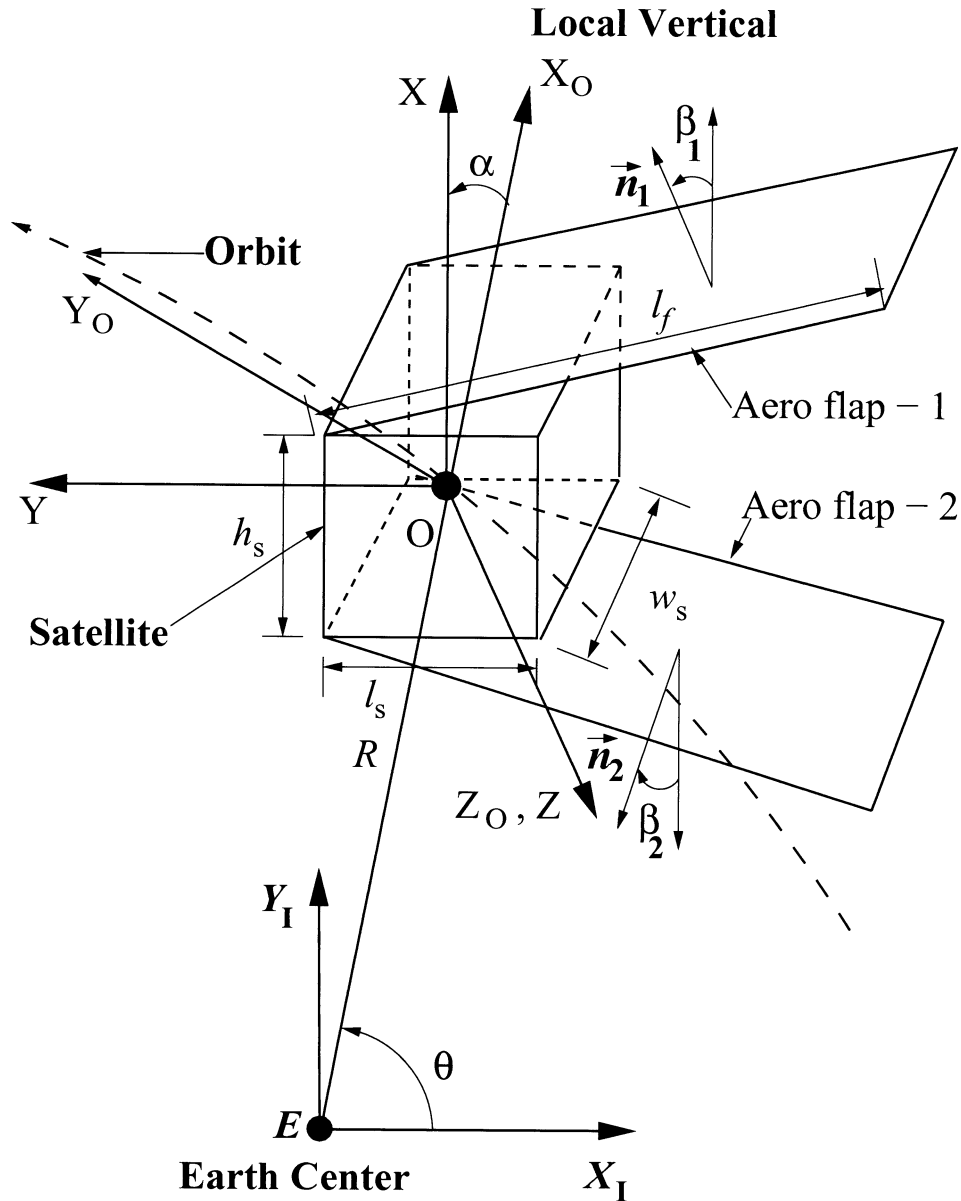


Figure 4.1: Geometry of orbit motion and proposed aerodynamic controller configuration

lies normal to the orbital plane, and the Y_o -axis represents the third axis of this right handed frame taken. The body-fixed coordinate frame is represented by O - XYZ . For aero flap- j , we consider its axis n_j initially aligned with the X -axis is rotated by an angle β_j about the Z -axis (normal to the orbit plane Y - Z). The aero flaps are considered to be made of a light weight material. The distances between the system center of mass O and the center of pressure for

both the aero flaps are assumed to be the same and their cross-sectional areas facing the incoming air velocity are equal.

4.2.2 Equation of Motion

As our focus in this investigation is to derive a nonlinear SMC laws for satellite attitude control using aerodynamic torque by rotating aero flaps, we only consider the control of the satellite pitch motion. Using Euler's attitude equations, the governing equation of motion of the system is written as [2]

$$I_z \dot{\omega}_z - (I_x - I_y) \omega_x \omega_y = T_g + T_a \quad (4.1)$$

where, $\omega_z = \dot{\theta} + \dot{\alpha}$, $\omega_x = 0$, and $\omega_y = 0$.

Here T_g represents gravity gradient torque and T_a represents aerodynamic torque.

4.2.2.1 Gravity gradient torque

The gravity gradient torque is given by following relation for chosen configuration as

$$T_g = -\frac{3\mu}{R^3} (I_y - I_x) \sin \alpha \cos \alpha \quad (4.2)$$

where I_y and I_x are Moment of inertias about respective axis. Next we have obtained non dimensional gravity gradient torque by dividing $I_z \Omega^2$ as follows:

$$\hat{T}_g = -3K \sin \alpha \cos \alpha \quad (4.3)$$

where

$$K = \frac{I_y - I_x}{I_z}, \Omega = \sqrt{\frac{\mu}{R^3}} \quad (4.4)$$

4.2.2.2 Aerodynamic torques

The aerodynamic forces or torques experience by satellites vary with their altitudes. So far in literature researchers have considered two types of model for calculating aerodynamic torques: simplified aerodynamic torque model and more realistic free molecular flow

aerodynamic model. Both aerodynamic torque models will be given in this section for Model – I.

Simplified Aerodynamic Torque Model

Assuming flat flaps and considering only aerodynamic drag, the force acting on the aero flap-j is given by

$$\vec{F}_{a_{smj}} = -\frac{1}{2}\rho\|\vec{V}_R\|^2 C_D A_j |\cos \zeta_j| \hat{V}_R, j = 1, 2 \quad (4.5)$$

where ρ = density of the atmosphere; \vec{V}_R = The relative velocity of the satellite with respect to the atmosphere in the direction of the orbital velocity; C_D = drag coefficient; A_j = total area of the aero flap-j; ζ = angle between the relative velocity \vec{V}_R and the outward unit normal vector \vec{n}_j of the aero flap-j . We assume that the drag force is acting opposite to the local horizontal direction, i.e., $-Y_0$ direction.

In Eq.(4.5), Angle ζ_j is calculated using following relation,

$$\zeta_j = \cos^{-1}(\hat{V}_R \cdot \vec{n}_j) \quad (4.6)$$

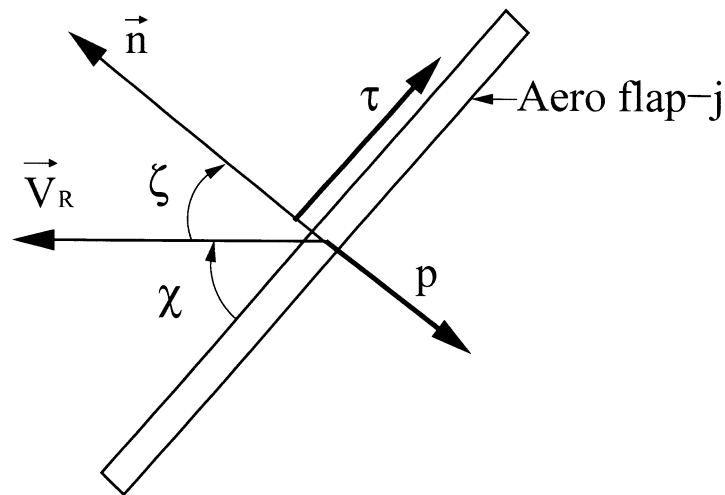


Figure 4.2: Geometry of aerodynamic control surface element

Also it should be noted that using Eq.(4.5) for projected area of aero flap-j ,if $\cos \zeta \geq 0$ then there will be aerodynamic forces otherwise for $\cos \zeta < 0$ there will be no aerodynamic forces produced by aero flap-j.

Here \hat{V}_R is the unit vector of the incoming air velocity from atmosphere on the aero flap-j and is expressed in the satellite body-fixed reference frame as

$$\hat{V}_R = \hat{j}_o = [\sin \alpha] \hat{i} + [\cos \alpha] \hat{j} \quad (4.7)$$

The outward unit normal vector of the aero flap-j, \bar{n}_j is given by

$$\bar{n}_j = (-1)^{1+j} [\cos \beta_j] \hat{i} + [\sin \beta_j] \hat{j}, \quad j=1,2 \quad (4.8)$$

The position vector \bar{r}_j from center of mass O to the center of pressure of the aero flap-j is obtained as

$$\bar{r}_j = (-1)^{1+j} \left(\frac{h_s}{2} + \frac{l_f}{2} \sin \beta_j \right) \hat{i} + \left(\frac{l_s}{2} - \frac{l_f}{2} \cos \beta_j \right) \hat{j}, \quad j=1,2 \quad (4.9)$$

where h_s = height of the satellite; w_s = width of the satellite; l_s = length of the satellite; l_f = length of the aero flap-j.

Thus, the torque exerted by the aero flap-j on the satellite is obtained as

$$\begin{aligned} \bar{T}_{a_{Simj}} &= \bar{r}_j \times \bar{F}_{a_{Simj}} \\ &= -\frac{1}{4} \rho \|\bar{V}_R\|^2 C_D A_j |\cos \zeta_j| \left[(-1)^{1+j} \cos \alpha (h_s + l_f \sin \beta_j) \right. \\ &\quad \left. - \sin \alpha (l_s - l_f \sin \beta_j) \right] \hat{k}, \quad j=1,2 \end{aligned} \quad (4.10)$$

Assuming the cross-sectional area of the aero flaps being the same (i.e., $A_j=A$), the components of the total aerodynamic torque about the satellite body axes can be written as

$$\begin{aligned} T_{a_{Sim}} &= T_{a_1} + T_{a_2} \\ &= \frac{1}{4} \rho \|\bar{V}_R\|^2 C_D A \left\{ |\sin(\alpha + \beta_1)| \left[\cos \alpha (-h_s - l_f \sin \beta_1) + \sin \alpha (l_s - l_f \cos \beta_1) \right] \right. \\ &\quad \left. + |\sin(\alpha - \beta_2)| \left[\cos \alpha (h_s + l_f \sin \beta_2) + \sin \alpha (l_s - l_f \cos \beta_2) \right] \right\} \end{aligned} \quad (4.11)$$

Next, nondimensional aerodynamic torque is obtained by dividing $I_z \Omega^2$ factor to Eq.(4.11) as follows:

$$\begin{aligned} \hat{T}_{a_{sm}} = C_a C_D \left\{ \Delta_1 \left[-\sin(\alpha + \beta_1) (\hat{h}_s \cos \alpha - \hat{l}_s \sin \alpha) - \hat{l}_f \sin^2(\alpha + \beta_1) \right] \right. \\ \left. + \Delta_2 \left[\sin(\alpha - \beta_2) (\hat{h}_s \cos \alpha + \hat{l}_s \sin \alpha) - \hat{l}_f \sin^2(\alpha - \beta_2) \right] \right\} \end{aligned} \quad (4.12)$$

where

$$\begin{aligned} C_a = \frac{\rho \|\vec{V}_R\|^2 A r_s}{4 I_z \Omega^2}, \Omega = \sqrt{\frac{\mu}{R^3}}, \hat{h}_s = \frac{h_s}{r_s}, \hat{l}_s = \frac{l_s}{r_s}, \hat{l}_f = \frac{l_f}{r_s} \\ \Delta_j = \text{sgn}(\sin(\alpha + (-1)^{1+j} \beta_j)) \end{aligned} \quad (4.13)$$

Free Molecular Aerodynamic Torque Model

Based on the free-molecular aerodynamic force model [2], the force on a flap surface with area A in the body fixed frame is

$$\vec{F}_{Mol_j} = A q_\infty \left[-\vec{n}_j \hat{p}_j + (\vec{n}_j \sin \chi_j - \hat{V}_R) \hat{\tau}_j \right] \quad (4.14)$$

where \hat{p}_j is the nondimensional total pressure and $\hat{\tau}_j$ is the nondimensional shearing stress.

For analytical simplicity, all flaps were considered to have the same area. The total pressure \hat{p}_j and shearing stress $\hat{\tau}_j$ are calculated

$$\begin{aligned} \hat{p}_j = \frac{p_j}{q_\infty} = \left[\left(\frac{2 - \sigma_n}{\sqrt{\pi}} \right) \sin \chi_j + \frac{\sigma_n}{2s} \sqrt{\frac{T_s}{T_\infty}} \right] \\ \times \left\{ \frac{1}{s} e^{-s^2 \sin^2 \chi_j} + \sqrt{\pi} \sin \chi_j \left[1 + \text{erf}(s \sin \chi_j) \right] \right\} \\ + \left(\frac{2 - \sigma_n}{2s^2} \right) \left[1 + \text{erf}(s \sin \chi_j) \right] \end{aligned} \quad (4.15)$$

$$\hat{\tau}_j = \frac{\tau_j}{q_\infty} = \sigma_t \cos \chi \left\{ \frac{1}{s\sqrt{\pi}} e^{-s^2 \sin^2 \chi_j} + \sin \chi_j \left[1 + \text{erf}(s \sin \chi_j) \right] \right\} \quad (4.16)$$

where σ_n and σ_t are normal and tangential accommodation coefficients, T_s is the absolute temperature of the spacecraft surface, T_∞ is the atmospheric temperature, q_∞ is the dynamic pressure given by

$$q_\infty = \frac{1}{2} \rho V_R^2 \quad (4.17)$$

$erf()$ is the error function defined by

$$erf = \frac{2}{\sqrt{\pi}} \int_0^x e^{-y^2} dy \quad (4.18)$$

and s is the air speed, non-dimensionalized by the mean molecular speed of the atmosphere

$$s = \sqrt{\frac{M_a V_R^2}{2R^* T_\infty}} \quad (4.19)$$

where M_a is the mean molar mass of the atmosphere and R^* is the universal gas constant.

Above free molecular force model is general equation which consists of lift and drag force. So for comparison purpose it has to be converted into only drag force by knowing following relation

$$\vec{n}_j = \sin \chi_j \hat{V}_R \quad (4.20)$$

Then free molecular force that consist only drag force on aero flap- j can be obtained as

$$\vec{F}_{MD_j} = -A q_\infty [\hat{p}_j \sin \chi_j + \hat{\tau}_j \cos \chi_j] \hat{V}_R \quad (4.21)$$

Thus, the aerodynamic torque exerted by the aero flap- j on the satellite using free molecular aerodynamic flow model is obtained as

$$\vec{T}_{a_{MD_j}} = \vec{r}_j \times \vec{F}_{MD_j}, j = 1, 2 \quad (4.22)$$

Assuming the cross-sectional area of the aero flaps being the same (i.e., $A_j=A$), the components of the total aerodynamic torque about the satellite body axes can be written as

$$\begin{aligned} T_{a_{MD}} &= T_{a_{MD_1}} + T_{a_{MD_2}} \\ &= \frac{1}{4} \rho \|\vec{V}_R\|^2 A \left\{ (\hat{p}_1 \sin \chi_1 + \hat{\tau}_1 \cos \chi_1) [\cos \alpha (-h_s - l_f \sin \beta_1) + \sin \alpha (l_s - l_f \cos \beta_1)] \right. \\ &\quad \left. + (\hat{p}_2 \sin \chi_2 + \hat{\tau}_2 \cos \chi_2) [\cos \alpha (h_s + l_f \sin \beta_2) + \sin \alpha (l_s - l_f \cos \beta_2)] \right\} \end{aligned} \quad (4.23)$$

Then next nondimensional free molecular aerodynamic drag torque is obtained by dividing $I_z \Omega^2$ factor to Eq.(4.23) as follows:

$$\begin{aligned} \hat{T}_{a_{MD}} &= C_a \left\{ (\hat{p}_1 \sin \chi_1 + \hat{\tau}_1 \cos \chi_1) [\cos \alpha (-\hat{h}_s - \hat{l}_f \sin \beta_1) + \sin \alpha (\hat{l}_s - \hat{l}_f \cos \beta_1)] \right. \\ &\quad \left. + (\hat{p}_2 \sin \chi_2 + \hat{\tau}_2 \cos \chi_2) [\cos \alpha (\hat{h}_s + \hat{l}_f \sin \beta_2) + \sin \alpha (\hat{l}_s - \hat{l}_f \cos \beta_2)] \right\} \end{aligned} \quad (4.24)$$

4.2.3 Control Laws

In this subsection, control laws are derived based on simplified aerodynamic torque model as explained in previous section.

Substituting simplified aerodynamic torque in \hat{T}_{aSim} Eq. (4.1) and expressing the derivatives with respect to true anomaly θ , the resulting nondimensional equation of motion of the system are obtained as follows:

$$\alpha'' = \hat{T}_g + \hat{T}_{aSim} \quad (4.25)$$

The nonlinear and nonautonomous system equation of motion, Eq. (4.25) is represented in state space form. The following state vector is defined

$$\mathbf{x} = [\alpha \quad \alpha' \quad \beta_1 \quad \beta_2]^T \quad (4.26)$$

A state space representation of the system (4.25) with a selected controlled output variable $y = \alpha$, is given by

$$\begin{aligned} \dot{\mathbf{x}} &= \mathbf{f}(\mathbf{x}) + \mathbf{g} \mathbf{u} \\ y &= \alpha \end{aligned} \quad (4.27)$$

where,

$$\mathbf{f}(\mathbf{x}) = [\alpha' \quad \hat{T}_{ga} \quad 0 \quad 0] \quad (4.28)$$

$$\mathbf{u} = [\beta_1' \quad \beta_2']^T$$

$$\mathbf{g} = [\mathbf{g}_1 \quad \mathbf{g}_2]$$

$$\mathbf{g}_1 = [0 \quad 0 \quad 1 \quad 0]^T \quad (4.29)$$

$$\mathbf{g}_2 = [0 \quad 0 \quad 0 \quad 1]^T$$

In Eq. (4.28) $\hat{T}_{ga} = \hat{T}_g + \hat{T}_{aSim}$.

Note that the control flap deflection (β_j) in Eq. (4.12) involves complex trigonometric relations and therefore it can not be assumed as a control input. However, this problem can be solved by taking the derivative of the flap deflection as the control input, i.e.

$$\mathbf{u} = [\beta_1' \quad \beta_2']^T.$$

The objectives for the design of control system are: 1) drive the system error to zero without oscillations or overshoots, 2) compensate external disturbances from beginning. To satisfy these objectives, the sliding plane is considered as

$$S = \tilde{x}_3 + p_3\tilde{x}_2 + p_2\tilde{x}_1 + p_1x_s \quad (4.30)$$

where

$$\tilde{x}_1 = \alpha - \alpha_d, \tilde{x}_2 = \alpha' - \alpha'_d, \tilde{x}_3 = \alpha'' - \alpha''_d \quad (4.31)$$

Parameters p_1 , p_2 , and p_3 are positive constant, $\tilde{\alpha} = \alpha - \alpha_d$ is the pitch angle tracking error, and x_s is the integral of the tracking error, that is,

$$\dot{x}_s = \tilde{\alpha} \quad (4.32)$$

Here error integral feedback term has been used to obtain robustness in the control system to parameter uncertainty.

The following Lyapunov function candidate is considered

$$V = \frac{1}{2}S^2 \quad (4.33)$$

Now taking the derivative of Eq. (4.33) with respect to θ yields

$$V' = SS' \quad (4.34)$$

In the preceding Eq.(4.34), S' is obtained by taking derivative of Eq. (4.30) with respect to θ :

$$S' = \tilde{x}_1^{(3)} + p_3\tilde{x}_3 + p_2\tilde{x}_2 + p_1\tilde{x}_1 \quad (4.35)$$

Eq. (4.35) can be rewritten into the following form,

$$S' = \alpha^{(3)} - \alpha_d^{(3)} + p_3(\alpha'' - \alpha_d'') + p_2\tilde{x}_2 + p_1\tilde{x}_1 \quad (4.36)$$

Next the third order derivative of the pitch angle with respect to θ is required for Eq.(4.36), which can obtained as

$$\alpha^{(3)} = \frac{\partial \hat{T}_{ga}}{\partial \alpha} \alpha' + \frac{\partial \hat{T}_{a_{sim}}}{\partial \beta_1} \beta_1' + \frac{\partial \hat{T}_{a_{sim}}}{\partial \beta_2} \beta_2' \quad (4.37)$$

Since the partial derivative $\partial \hat{T}_{ga} / \partial \alpha$ is summation of partial derivative of \hat{T}_g and $\hat{T}_{a_{sim}}$ with respect to α

$$\frac{\partial \hat{T}_{ga}}{\partial \alpha} = \frac{\partial \hat{T}_g}{\partial \alpha} + \frac{\partial \hat{T}_{aSim}}{\partial \alpha} \quad (4.38)$$

Taking partial derivative of \hat{T}_g and \hat{T}_{aSim} given by Eq. (4.3) and (4.12) with respect to α the following equations are obtained,

$$\frac{\partial \hat{T}_g}{\partial \alpha} = -3K \cos 2\alpha \quad (4.39)$$

$$\begin{aligned} \frac{\partial \hat{T}_{aSim}}{\partial \alpha} = C_a C_D \left\{ \Delta_1 \left[-\hat{h}_s \cos(2\alpha + \beta_1) + \hat{l}_s \sin(2\alpha + \beta_1) - \hat{l}_f \sin(2(\alpha + \beta_1)) \right] \right. \\ \left. + \Delta_2 \left[\hat{h}_s \cos(2\alpha - \beta_2) + \hat{l}_s \sin(2\alpha - \beta_2) - \hat{l}_f \sin(2(\alpha - \beta_2)) \right] \right\} \end{aligned} \quad (4.40)$$

Replacing Eq. (4.39) and Eq. (4.40) into Eq. (4.38), one can obtain

$$\begin{aligned} \frac{\partial \hat{T}_{ga}}{\partial \alpha} = -3K \cos 2\alpha \\ + C_a C_D \left\{ \Delta_1 \left[-\hat{h}_s \cos(2\alpha + \beta_1) + \hat{l}_s \sin(2\alpha + \beta_1) - \hat{l}_f \sin(2(\alpha + \beta_1)) \right] \right. \\ \left. + \Delta_2 \left[\hat{h}_s \cos(2\alpha - \beta_2) + \hat{l}_s \sin(2\alpha - \beta_2) - \hat{l}_f \sin(2(\alpha - \beta_2)) \right] \right\} \end{aligned} \quad (4.41)$$

Next taking the partial derivative of T_a with respect to β_j , the following equations :

$$\frac{\partial \hat{T}_{aSim}}{\partial \beta_1} = C_a C_D \Delta_1 \left[-\cos(\alpha + \beta_1) (\hat{h}_s \cos \alpha - \hat{l}_s \sin \alpha) - \hat{l}_f \sin(2(\alpha + \beta_1)) \right] \quad (4.42)$$

$$\frac{\partial \hat{T}_{aSim}}{\partial \beta_2} = C_a C_D \Delta_2 \left[-\cos(\alpha - \beta_2) (\hat{h}_s \cos \alpha + \hat{l}_s \sin \alpha) + \hat{l}_f \sin(2(\alpha - \beta_2)) \right] \quad (4.43)$$

Substituting Eqs.(4.41), (4.42), and (4.43) into Eq.(4.37), $\alpha^{(3)}$ is

$$\alpha^{(3)} = f_s + [B_1 \quad B_2] \begin{bmatrix} u_1 \\ u_2 \end{bmatrix} \quad (4.44)$$

where,

$$f_s = \frac{\partial \hat{T}_{ga}}{\partial \alpha} \alpha', B_1 = \frac{\partial \hat{T}_{aSim}}{\partial \beta_1}, B_2 = \frac{\partial \hat{T}_{aSim}}{\partial \beta_2} \quad (4.45)$$

Now taking $S' = -\eta \operatorname{sgn}(S)$ in Eq. (4.34) yields $V' = -\eta|S|$, which is negative semi-definite of S for positive value of η . So, the proposed control laws are globally stable for assumed Lyapunov Function (4.33). Using Eq.(4.36), Eq.(4.44), and $S' = -\eta \operatorname{sgn}(S)$, we obtain following relations:

$$f_s + [B][u] - \alpha_d^{(3)} + p_3 \tilde{x}_3 + p_2 \tilde{x}_2 + p_1 \tilde{x}_1 = -\eta \operatorname{sgn}(S) \quad (4.46)$$

Rearranging above Eq.(4.46), the control laws can be written as

$$[u] = \mathbf{B}^\top [\mathbf{B}\mathbf{B}^\top]^{-1} \{-f_s + \alpha_d^{(3)} - p_3 \tilde{x}_3 - p_2 \tilde{x}_2 - p_1 \tilde{x}_1 - \eta \operatorname{sgn}(S)\} \quad (4.47)$$

Using above control laws Eq. (4.47) will have chattering in control input response, in order to avoid chattering in control input we have given following control law

$$[u] = \mathbf{B}^\top [\mathbf{B}\mathbf{B}^\top]^{-1} \{-f_s + \alpha_d^{(3)} - p_3 \tilde{x}_3 - p_2 \tilde{x}_2 - p_1 \tilde{x}_1 - \eta \tanh(S)\} \quad (4.48)$$

For the existence of the control law (4.48), $\mathbf{B}\mathbf{B}^\top$ must be non-zero in the region of interest :

$$\mathbf{B}\mathbf{B}^\top = \left(\frac{\partial T_{aSim}}{\partial \beta_1} \right)^2 + \left(\frac{\partial T_{aSim}}{\partial \beta_2} \right)^2 \neq 0 \quad (4.49)$$

The region of $\Omega_s (\Omega_{s_1} \cap \Omega_{s_2})$ singularity in which $\mathbf{B}\mathbf{B}^\top = 0$ is given by

$$\begin{aligned}
 \Omega_{S_1} &= \left\{ \left(\frac{\partial T_s}{\partial \beta_1} \right)^2 = 0 \right\} \\
 &= \left\{ C_a \Delta_1 \left[-\cos(\alpha + \beta_1) (\hat{h}_s \cos \alpha - \hat{l}_s \sin \alpha) - \hat{l}_f \sin(2(\alpha + \beta_1)) \right] \right\}^2 = 0 \\
 &= \left\{ \left[\hat{h}_s \cos \alpha - \hat{l}_s \sin \alpha + 2\hat{l}_f \sin(\alpha + \beta_1) \right]^2 = 0 \right\} \\
 \Omega_{S_2} &= \left\{ \left(\frac{\partial T_s}{\partial \beta_2} \right)^2 = 0 \right\} \\
 &= \left\{ C_a \Delta_2 \left[-\cos(\alpha - \beta_2) (\hat{h}_s \cos \alpha + \hat{l}_s \sin \alpha) + \hat{l}_f \sin(2(\alpha - \beta_2)) \right] \right\}^2 = 0 \\
 &= \left\{ \left[\hat{h}_s \cos \alpha + \hat{l}_s \sin \alpha + 2\hat{l}_f \sin(\alpha - \beta_2) \right]^2 = 0 \right\}
 \end{aligned} \tag{4.50}$$

The control laws (4.48) is well defined as long as the trajectory of the closed-loop system does not enter the region Ω_S .

4.2.4 Results and Discussions

In order to study the performance of the proposed controller, the system response is numerically simulated using Eq. (4.25) where, free molecular aerodynamic torque model Eq.(4.24) is considered in equation of motion, and the control laws Eq. (4.48). The simulation was carried out using MATLAB. The following parameters are assumed for numerical simulation:

Table 4. 1: Parameters for Model-I

Satellite Parameters	$\hat{h}_s = 0.1[m], \hat{l}_s = 0.1[m], \hat{w}_s = 0.1[m],$ $\hat{l}_f = 0.2[m], r_s = 1[m]$
Orbital Parameters	$R = 6878 [km], \mu = 3.986 \times 10^5 [km^3 / s^2],$ $\rho = 6.967 \times 10^{-13} [kg / m^3]$
Initial and Final Attitude Conditions	$\alpha_o = 70^\circ, \alpha'_o = 0.01, \beta_{j_o} = 100^\circ, \alpha_f = 0^\circ$
Control Parameters	$p_1 = 6, p_2 = 12, p_3 = 8, \eta = 0.5$
Free Molecular Aerodynamic Model Parameters	$s = 5, \sigma_n = 0.85, \sigma_t = 0.9, T_\infty = 997.3[K],$ $T_s = 300[K]$
Other Parameters	$C_D = 2$

The effects of mass distribution parameter K , aerodynamic parameter C_a are studied. The satellite attitude response remains almost unaffected with changes in these parameters (Figure 4.3 – Figure 4.4). Here, the satellite attitude maneuver initially starting from $\alpha_o = 70^\circ$ to final $\alpha_d = 0^\circ$ has performed.

The effects of mass moment of inertia distribution parameters (K) on the controller performance (Figure 4.3) are examined first. The value of K is varied from -1 to 1. Here $K=-1$ refers to an unstable gravity gradient configuration while $K=1$ signifies a stable gravity gradient configuration. As the parameter K varies from $K=-1$ to $K=1$, the satellite attitude response remains virtually unaffected. Figure 4.3 shows the satellite attitude and control flap deflection responses obtained for $K=1$, and $K=-1$. As the parameter K varies from $K=-1$ to $K=1$, the satellite attitude response remains virtually unaffected. However, the control flap deflection (β_j) varies with changes in K . As K is increased from $K=-1$ to $K=1$, $|\beta_1|_{\max}$ decrease from 140.3 deg to 117.5 deg, respectively in steady state situation. The large control flap deflection $|\beta_1|_{\max}$ for negative value of K are due to the fact that $K=-1$ corresponds to an

unfavorable gravity gradient configuration while the small control flap deflection $|\beta_1|_{\max}$ for $K=1$ corresponds to a favorable gravity gradient configuration.

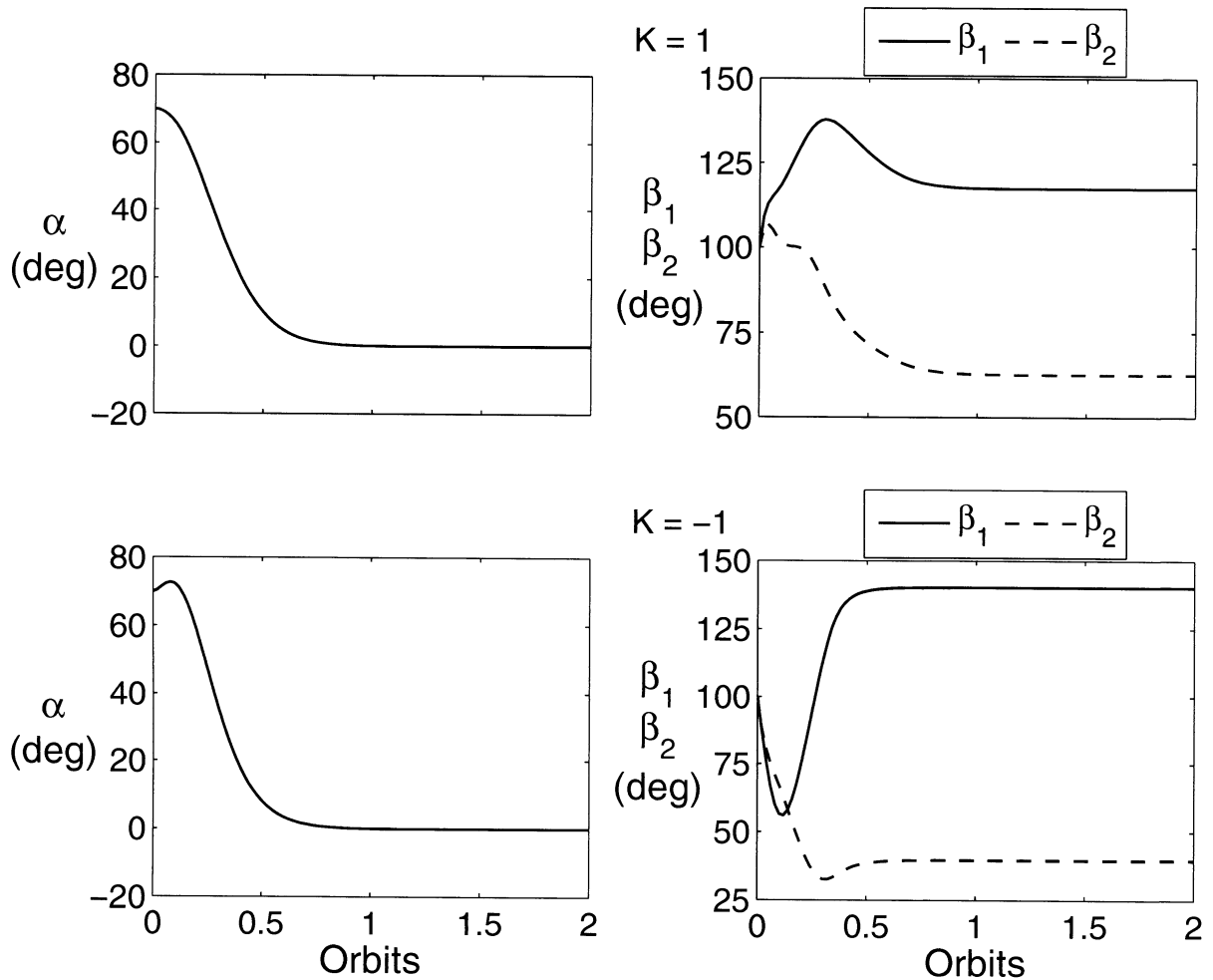


Figure 4.3: Effect of K on system performance and control flap deflection: $C_a = 5$, $\eta = 0.5$, $p_1 = 6$, $p_2 = 12$, $p_3 = 8$, $\alpha_0 = 70^\circ$, $\alpha'_0 = 0.01$.

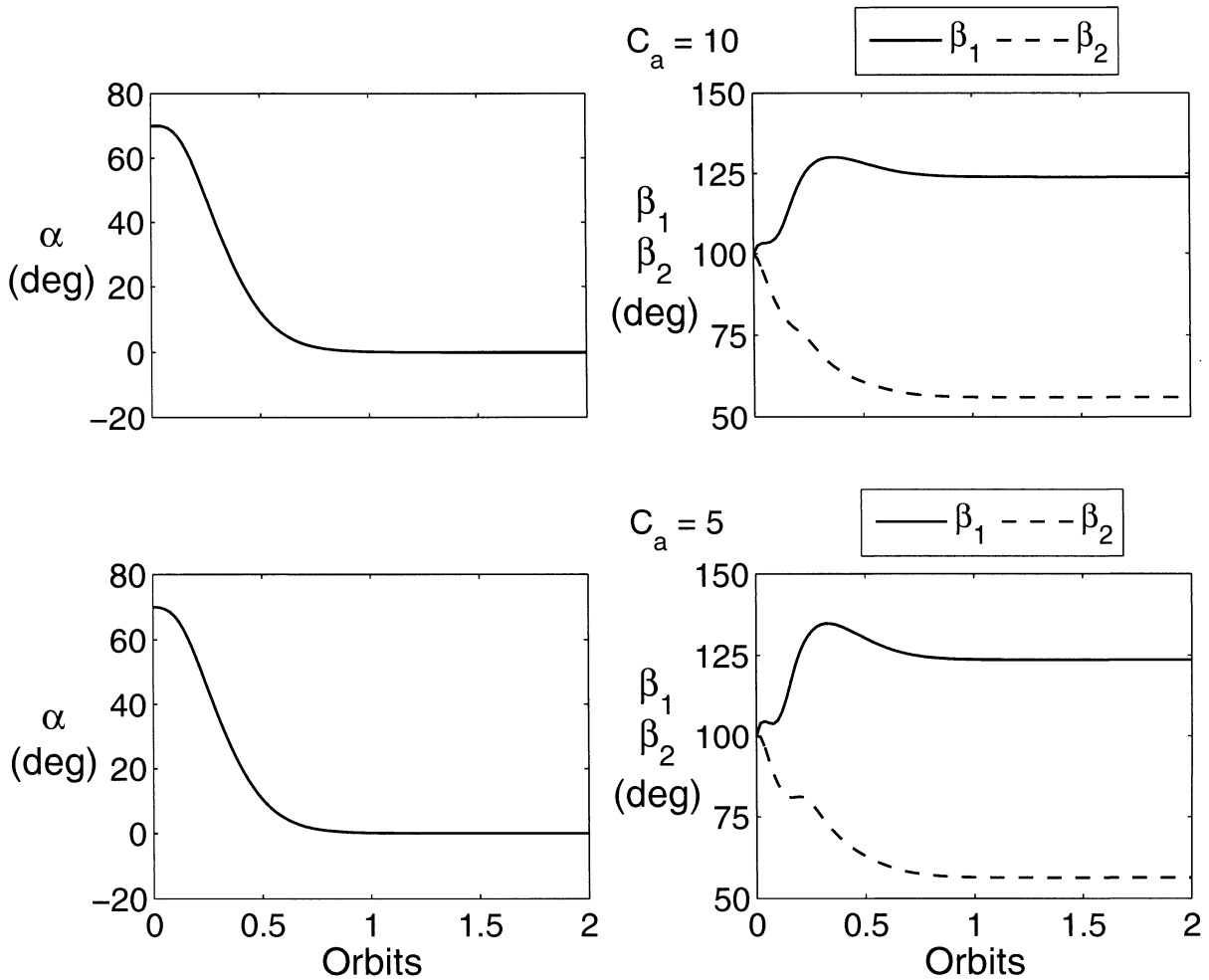


Figure 4.4: Effect of aerodynamic parameter C_a system performance and control flap deflection: $K=0.5$, $\eta = 0.5$, $p_1 = 6$, $p_2 = 12$, $p_3 = 8$, $\alpha_0 = 70^\circ$, $\alpha'_0 = 0.01$.

The effect of the aerodynamic parameter C_a is examined next (Figure 4.4). As the aerodynamic parameter C_a is decreased from 10 to 5, the control flap deflection $(|\beta_1|_{\max}, |\beta_2|_{\max})$ increases from (129.9, 56.06) deg to (134.8, 57) deg. This increase in control input could be explained from Eq. (4.48) where $|u_j|_{\max}$ is inversely proportional to the aerodynamic parameter C_a (i.e. lower C_a corresponds to higher control flap deflection rate). With changes in parameter C , however, the satellite attitude response remains unaffected showing robustness of the proposed controller. The maximum control flap deflection $(\beta_{1\max},$

$\beta_{2\max}$) is given in Table 4.1. It should be noted that with lower aerodynamic parameter C_a the controller requires very large control flap deflection.

Table 4.2: Maximum control flap deflection for different aerodynamic parameter C_a (transient condition)

Aerodynamic parameter (C_a)	Flap deflection (deg)
$C_a = 5$	$ \beta_1 _{\max} = 134.8$ $ \beta_2 _{\max} = 57$
$C_a = 10$	$ \beta_1 _{\max} = 129.9$ $ \beta_2 _{\max} = 56.06$

In order to study the performance of the proposed variable structure control in presence of the parameter uncertainties, the numerical simulation was done in the perturbed modes (Figure 4.5). First, the mass distribution parameter (K) and the aerodynamic parameter (C_a) are decreased by 30% from its nominal values as follows: $K=0.35$ and $C_a=3.5$, respectively in the plant dynamics. In the second case, the mass distribution parameter (K) and the aerodynamic parameter (C_a) are increased by 30% from its nominal values as follows: $K=0.65$ and $C=6.5$, respectively in the plant dynamics. The above parameters are remained same as its nominal values as $K=0.5$ and $C_a=5$ in the VSC controller Eq.(4.48). The results of the numerical simulation are shown in Figure 4.5 for parameter uncertainties into the mass distribution parameter and the aerodynamic parameter. The desired pitch orientation of the satellite is achieved smoothly within 0.7 orbits. Also note that the VSC stabilized the pitch motion without any overshoot in presence of parameter uncertainties. Thus, the proposed VSC is robust against the parameter uncertainties and the numerical simulation verifies the theory presented in Section 3.5.

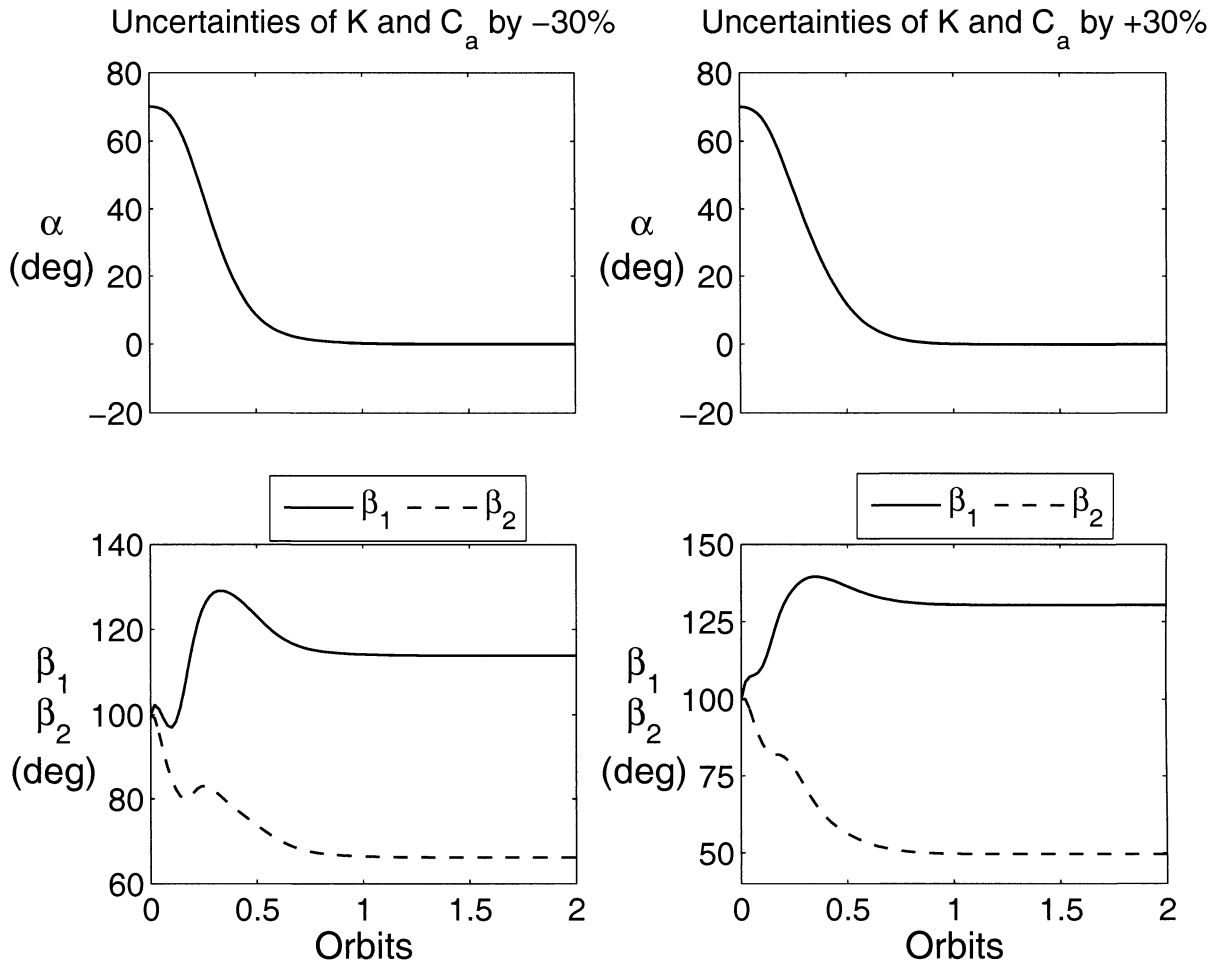


Figure 4.5: Performance of sliding mode control (SMC) in presence of parameter uncertainties into the mass distribution parameter (K) and the aerodynamic parameter (C_a): $K=0.5$, $C_a = 5$, $\eta = 0.5$, $p_1 = 6$, $p_2 = 12$, $p_3 = 8$, $\alpha_0 = 70^\circ$, $\alpha'_0 = 0.01$.

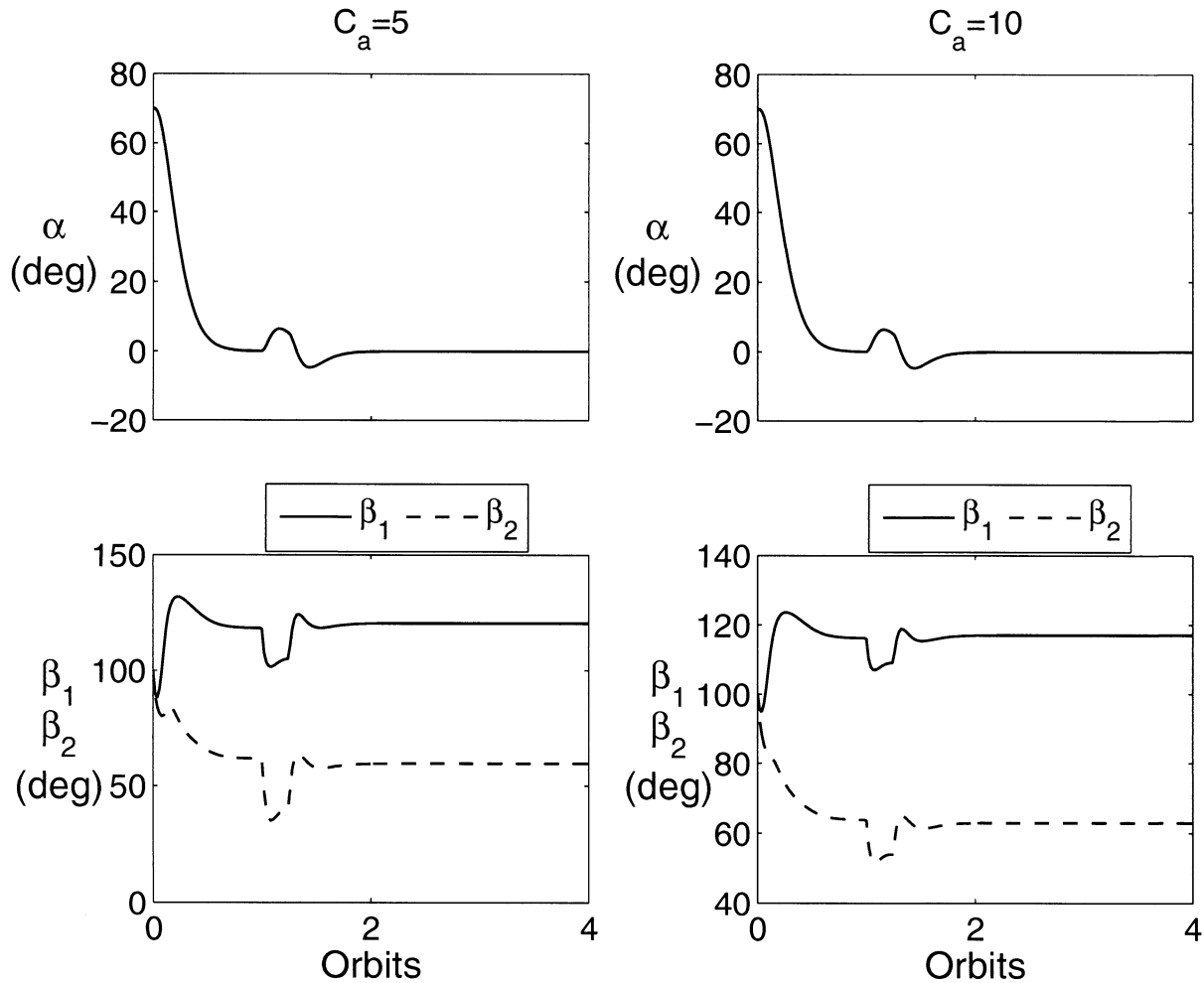


Figure 4.6: Performance of sliding mode control (SMC) in presence of external disturbance: $K=0.5$, $C_a=5$, $\eta=0.5$, $p_1=6$, $p_2=12$, $p_3=8$, $\alpha_0=70^\circ$, $\alpha'_0=0.01$.

Finally, for an appreciation about the effectiveness of the proposed control laws in presence of external disturbance (Figure 4.6), a typical satellite with $I_x=0.00952 \text{ kg}\cdot\text{m}^2$, $I_y=0.00211 \text{ kg}\cdot\text{m}^2$, and $I_z=0.00952 \text{ kg}\cdot\text{m}^2$ are considered [35]. The system may experience disturbance torques due to several factors including aerodynamic torque modeling errors, aero flap misalignment and other environmental forces. The disturbance torque is assumed to be in the order of 10^{-6} for the satellite in the Low Earth Orbits. The external disturbance torque of $3.6 \times 10^{-6} [N\cdot m]$ is applied from 1.0 orbits to 1.5 orbits. This disturbance torque is in fact applied to the system when the system almost reaches its desired pitch angle of 0 deg. Two

cases are considered: the first case with $C_a = 5$ and the second case $C_a = 10$. As shown in Figure 4.6, the desired pitch is successfully attained for both the cases in presence of disturbances with small attitude oscillations between 1 orbit to 1.5 orbits. For the first case the maximum control aerodynamic flap deflection $(|\beta_1|_{\max}, |\beta_2|_{\max})$ decrease to (101.8, 35.46) deg while in the second case it decrease to (107.3, 51.8) deg as compared to the case of no disturbance. The decrease of control flap deflections in both cases are due to the fact that in order to compensate the external disturbances control flap has to generate enough aerodynamic torques by varying control flap deflection. Thus, this simulation verifies the external disturbances rejection property of VSC.

4.3 System Model - II

4.3.1 System Description

A system model that comprises of a satellite with four light-weight aero flaps is placed along the satellite Y-axis. The system center of mass O moving in a circular orbit about the Earth's center E (Figure 4.7) is assumed. The system center of mass O lies on the center of mass of the satellite. For simplicity, the cube satellite is considered with length, width and height given as l_s , w_s , and h_s , respectively. The mass of the aero flaps and other accessories are assumed to be negligible. For the system under consideration, an orbital reference frame $O-X_0Y_0Z_0$ is selected such that the X_0 -axis always points along the local vertical, the Z_0 -axis lies normal to the orbital plane, and the Y_0 -axis represents the third axis of this right handed frame taken. The body-fixed coordinate frame is represented by $O-XYZ$. For top two aero flap- j ($j = 1, 2$), we consider its axis $\vec{n}_j, j = 1, 2$ initially aligned with the X-axis is rotated by an angle $\beta_j, j = 1, 2$ about the Z-axis (normal to the orbit plane Y-Z) in counter clock wise direction. For bottom aeroflap- j , we consider its axis $\vec{n}_j, j = 3, 4$ initially aligned with the opposite to the X-axis and then it is rotated by angle $\beta_j, j = 3, 4$ in clock wise direction. All aero flaps are considered to be made of a light weight material and their total area $\left(A_j = \frac{1}{2} w_s l_f \right)$ facing the incoming air velocity are assumed same.

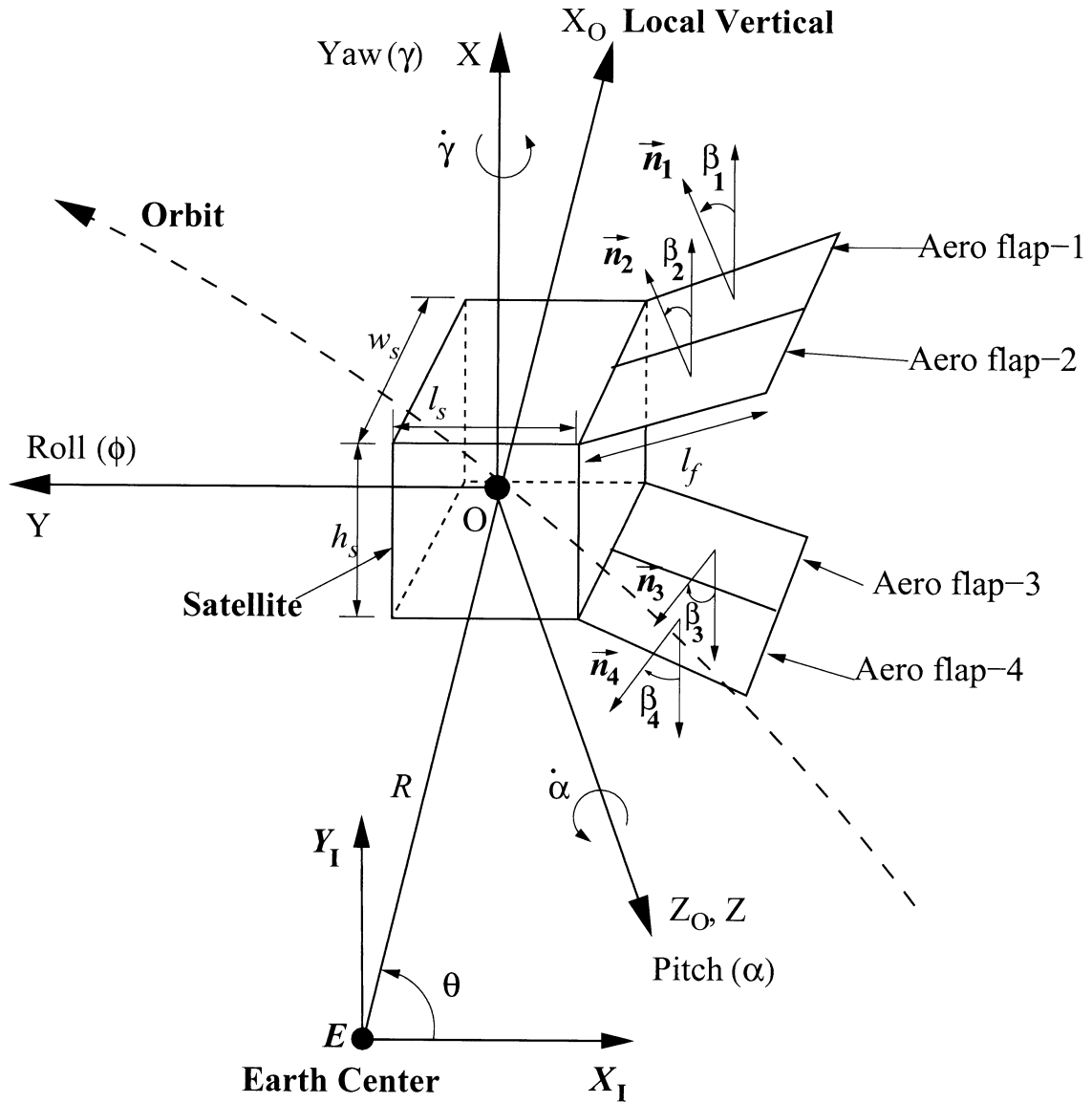


Figure 4.7: Geometry of orbit motion and proposed aerodynamic controller configuration

4.3.2 Kinematics and Equations of Motion

4.3.2.1 Euler Angles

The orientation of a spacecraft with body fixed axes O-XYZ can be specified completely by a sequence of three consecutive rotations about different spacecraft body axes. There are 12 such possible combinations can be used to achieve specify spacecraft orientation. For present

research work we have consider Euler 3-2-1 rotation sequence. Here, 1, 2, and 3 correspond to X, Y, and Z axes, respectively.

It is often useful to perform calculation in the spacecraft's body frame. Therefore, transformations are necessary to translate measurements in one coordinate frame into another. To transform measurements in the orbital frame to the spacecraft's principle axis body frame an Euler 3-2-1 rotation sequence is used to produce the following rotation matrix [2]:

$$R_{321} = \begin{bmatrix} c_\alpha c_\phi & s_\alpha c_\phi & -s_\phi \\ c_\alpha s_\phi s_\gamma - s_\alpha c_\gamma & s_\alpha s_\phi s_\gamma + c_\alpha c_\gamma & c_\phi s_\gamma \\ c_\alpha s_\phi c_\gamma + s_\alpha s_\gamma & s_\alpha s_\phi c_\gamma - c_\alpha s_\gamma & c_\phi c_\gamma \end{bmatrix} \quad (4.51)$$

where, $s_k = \sin k$ and $c_k = \cos k$, for $k = \gamma, \phi, \alpha$

or

$$R_{321} = \begin{bmatrix} \cos \alpha \cos \phi & \sin \alpha \cos \phi & -\sin \phi \\ \cos \alpha \sin \phi \sin \gamma - \sin \alpha \cos \gamma & \sin \alpha \sin \phi \sin \gamma + \cos \alpha \cos \gamma & \cos \phi \sin \gamma \\ \cos \alpha \sin \phi \cos \gamma + \sin \alpha \sin \gamma & \sin \alpha \sin \phi \cos \gamma - \cos \alpha \sin \gamma & \cos \phi \cos \gamma \end{bmatrix}$$

Thus, the transformation from the frame $O-i_o j_o k_o$ to the body fixed frame $O-ijk$ using 3-2-1 Euler angle rotation sequence is

$$\begin{Bmatrix} \hat{i} \\ \hat{j} \\ \hat{k} \end{Bmatrix} = R_{321} \begin{Bmatrix} \hat{i}_o \\ \hat{j}_o \\ \hat{k}_o \end{Bmatrix} \quad (4.52)$$

If it is require transforming the frame $O-ijk$ to the orbital frame $O-i_o j_o k_o$, the following relation is used to get the rotation matrix R_{123} by taking the inverse of the rotation matrix R_{321}^{-1} as follows:

$$R_{123} = \begin{bmatrix} c_\alpha c_\phi & c_\alpha s_\phi s_\gamma - s_\alpha c_\gamma & c_\alpha s_\phi c_\gamma + s_\alpha s_\gamma \\ s_\alpha c_\phi & s_\alpha s_\phi s_\gamma + c_\alpha c_\gamma & s_\alpha s_\phi c_\gamma - c_\alpha s_\gamma \\ -s_\phi & c_\phi s_\gamma & c_\phi c_\gamma \end{bmatrix} \quad (4.53)$$

4.3.2.2 Angular Velocity Vector

In addition to rotation matrix, we need to determine inertial angular velocity of the spacecraft as well. The angular velocity of the spacecraft can be expressed as

$$\vec{\omega} = \omega_x \hat{i} + \omega_x \hat{j}_1 + \omega_x \hat{k} = \dot{\gamma} \hat{i} + \dot{\phi} \hat{j}_1 + (\dot{\theta} + \dot{\alpha}) \hat{k}_o \quad (4.54)$$

where $\dot{\alpha}$ is about the \hat{k}_o axis in the frame $O-X_oY_oZ_o$, followed by $\dot{\phi}$ about the j_1 axis in the intermediate frame $O-X_1Y_1Z_1$ and finally $\dot{\gamma}$ about the \hat{i} axis in the $O-XYZ$.

Using Euler 3-2-1 rotation the angular velocity vector can be obtained as

$$\begin{aligned} \omega_x &= -(\dot{\theta} + \dot{\alpha}) \sin \phi + \dot{\gamma} \\ \omega_y &= (\dot{\theta} + \dot{\alpha}) \cos \phi \sin \gamma + \dot{\phi} \cos \gamma \\ \omega_z &= (\dot{\theta} + \dot{\alpha}) \cos \phi \cos \gamma - \dot{\phi} \sin \gamma \end{aligned} \quad (4.55)$$

or also it can be written as

$$\begin{Bmatrix} \omega_x \\ \omega_y \\ \omega_z \end{Bmatrix} = \begin{bmatrix} 1 & 0 & -s_\phi \\ 0 & c_\gamma & c_\phi s_\gamma \\ 0 & -s_\gamma & c_\phi c_\gamma \end{bmatrix} \begin{Bmatrix} \dot{\gamma} \\ \dot{\phi} \\ \dot{\alpha} + \dot{\theta} \end{Bmatrix} \quad (4.56)$$

4.3.2.3 Attitude Dynamics

The equation of motion of the spacecraft is derived using Euler's Rotational Equations of motion [2]:

$$I \dot{\vec{\omega}} + \vec{\omega} \times I \vec{\omega} = \vec{T} \quad (4.57)$$

This is the general form of Euler's Equation where I is the moment of inertia of the body being analyzed, $\vec{\omega}$ is the angular velocity vector of the spacecraft and T is the external torque acting on the body. The spacecraft moment of inertia is assumed to be principle moment of inertia. The external torque ($\vec{T} = \vec{T}_g + \vec{T}_a$) acting on the spacecraft being analyzed here are the gravity gradient torque (\vec{T}_g), and the aerodynamic torque (\vec{T}_a) being generated by aero-flaps.

Euler's equations of motion can be written in the expanded scalar form as follows:

$$\begin{aligned}
 I_x \dot{\omega}_x - (I_y - I_z) \omega_y \omega_z &= T_x \\
 I_y \dot{\omega}_y - (I_z - I_x) \omega_z \omega_x &= T_y \\
 I_z \dot{\omega}_z - (I_x - I_y) \omega_x \omega_y &= T_z
 \end{aligned} \tag{4.58}$$

Time derivative of the Eq. (4.55) is obtained as

$$\begin{aligned}
 \dot{\omega}_x &= -(\ddot{\theta} + \ddot{\alpha}) \sin \phi - (\dot{\theta} + \dot{\alpha}) \dot{\phi} \cos \phi + \ddot{\gamma} \\
 \dot{\omega}_y &= (\ddot{\theta} + \ddot{\alpha}) \cos \phi \sin \gamma - (\dot{\theta} + \dot{\alpha}) \dot{\phi} \sin \phi \sin \gamma + (\dot{\theta} + \dot{\alpha}) \dot{\gamma} \cos \phi \cos \gamma \\
 &\quad + \ddot{\phi} \cos \gamma - \dot{\gamma} \dot{\phi} \sin \gamma \\
 \dot{\omega}_z &= (\ddot{\theta} + \ddot{\alpha}) \cos \phi \cos \gamma - (\dot{\theta} + \dot{\alpha}) \dot{\phi} \sin \phi \cos \gamma - (\dot{\theta} + \dot{\alpha}) \dot{\gamma} \cos \phi \sin \gamma \\
 &\quad - \ddot{\phi} \sin \gamma - \dot{\gamma} \dot{\phi} \cos \gamma
 \end{aligned} \tag{4.59}$$

4.3.2.4 Equations of motion

Now using Eq. (4.58), Eq.(4.55), and Eq. (4.59), the resulting equations of motion of the spacecraft for the circular orbit can be obtained as

Satellite: Yaw (γ)

$$\begin{aligned}
 I_x \ddot{\gamma} - (I_x \sin \phi) \ddot{\alpha} - I_x (\dot{\theta} + \dot{\alpha}) \dot{\phi} \cos \phi \\
 - (I_y - I_z) [(\dot{\theta} + \dot{\alpha}) \cos \phi \sin \gamma + \dot{\phi} \cos \gamma] [(\dot{\theta} + \dot{\alpha}) \cos \phi \cos \gamma - \dot{\phi} \sin \gamma] &= T_x
 \end{aligned} \tag{4.60}$$

Satellite: Roll (ϕ)

$$\begin{aligned}
 (I_y \cos \gamma) \ddot{\phi} + (I_y \cos \phi \sin \gamma) \ddot{\alpha} + I_y \{ -(\dot{\theta} + \dot{\alpha}) \dot{\phi} \sin \phi \sin \gamma \\
 + (\dot{\theta} + \dot{\alpha}) \dot{\gamma} \cos \phi \cos \gamma - \dot{\gamma} \dot{\phi} \sin \gamma \} - (I_z - I_x) [-(\dot{\theta} + \dot{\alpha}) \sin \phi + \dot{\gamma}] \\
 \times [(\dot{\theta} + \dot{\alpha}) \cos \phi \cos \gamma - \dot{\phi} \sin \gamma] &= T_y
 \end{aligned} \tag{4.61}$$

Satellite: Pitch (α)

$$\begin{aligned}
 (I_z \cos \phi \cos \gamma) \ddot{\alpha} - (I_z \sin \gamma) \ddot{\phi} \\
 - (I_x - I_y) [-(\dot{\theta} + \dot{\alpha}) \sin \phi + \dot{\gamma}] [(\dot{\theta} + \dot{\alpha}) \cos \phi \sin \gamma + \dot{\phi} \cos \gamma] \\
 + I_z \{ -(\dot{\theta} + \dot{\alpha}) \dot{\phi} \sin \phi \cos \gamma - \dot{\gamma} \dot{\phi} \cos \gamma - (\dot{\theta} + \dot{\alpha}) \dot{\gamma} \cos \phi \sin \gamma \} &= T_z
 \end{aligned} \tag{4.62}$$

4.3.2.5 Gravity gradient torques

The external torque acting on the system due to gravity, \vec{T}_g is

$$\vec{T}_g = T_{g_x} \hat{i} + T_{g_y} \hat{j} + T_{g_z} \hat{k} \quad (4.63)$$

where

$$\begin{aligned} T_{g_x} &= -\frac{3\mu}{R^3} (I_y - I_z) C_{x_o,y} C_{x_o,z} \\ T_{g_y} &= -\frac{3\mu}{R^3} (I_z - I_x) C_{x_o,z} C_{x_o,x} \\ T_{g_z} &= -\frac{3\mu}{R^3} (I_x - I_y) C_{x_o,x} C_{x_o,y} \end{aligned} \quad (4.64)$$

Here the direction cosines from the orbital reference frame $O-i_o j_o k_o$ to the body fixed frame $O-ijk$ using 3-2-1 Euler angle rotation sequence as given in Eq.(4.51) can be obtained as

$$\begin{aligned} C_{x_o,x} &= \cos \alpha \cos \phi \\ C_{x_o,y} &= \cos \alpha \sin \phi \sin \gamma - \sin \alpha \cos \gamma \\ C_{x_o,z} &= \cos \alpha \sin \phi \cos \gamma + \sin \alpha \sin \gamma \end{aligned} \quad (4.65)$$

4.3.2.6 Aerodynamic torques

The aerodynamic forces or torques experience by satellites vary with their altitudes. So far in literature researchers are consider two type of model for calculating aerodynamic torques: simplified aerodynamic torque model and more realistic free molecular flow aerodynamic model. Both aerodynamic torque models will be given in this section for Model-II.

Simplified Aerodynamic Force Model

Assuming flat flaps and considering both aerodynamic drag and aerodynamic lift as show in Figure 4.3, the forces acting on the aero flap-j is given by

$$\begin{aligned} \vec{F}_{D_j} &= -\frac{1}{2} \rho \|\vec{V}_R\|^2 C_D A_j |\cos \zeta_j| \hat{V}_R, j = 1, 2, 3, 4 \\ \vec{F}_{L_j} &= \frac{1}{2} \rho \|\vec{V}_R\|^2 C_L A_j |\cos \zeta_j| \hat{F}_L, j = 1, 2, 3, 4 \end{aligned} \quad (4.66)$$

where ρ = density of the atmosphere; \vec{V}_R = The relative velocity of the satellite with respect to the atmosphere in the direction of the orbital velocity; C_D = drag coefficient; C_L = lift coefficient; A_j = total area of the aero flap-j; ζ = angle between the relative velocity \vec{V}_R and the outward unit normal vector \vec{n}_j of the aero flap-j . We assume that the drag force is acting opposite to the local horizontal direction, i.e., $-Y_0$ direction and the lift force is acting in the direction of local vertical for top two aero flaps and in the opposite to the local vertical for bottom aero flaps as show in Figure 4.3.

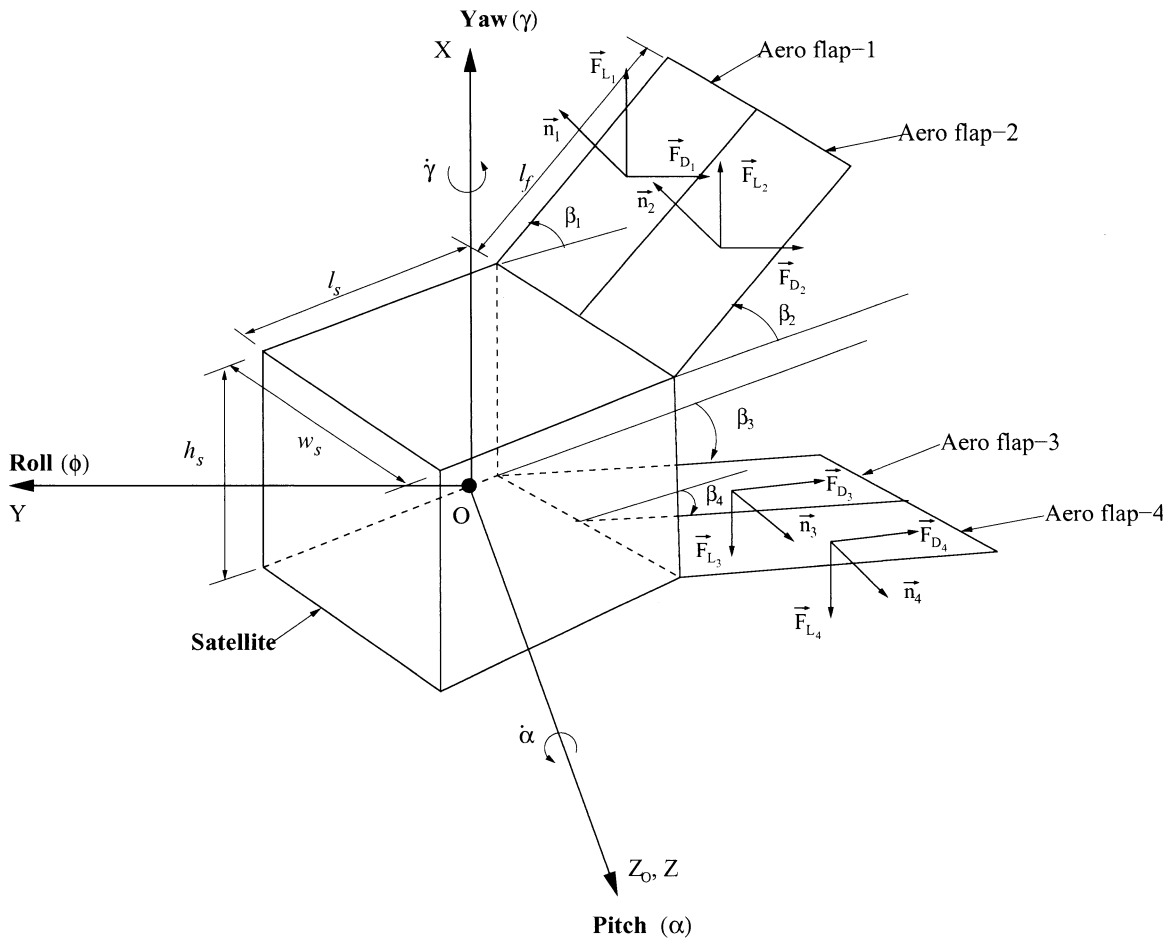


Figure 4.8: Detailed schematic diagram of the spacecraft

In Eq.(4.5), Angle ζ_j is calculated using following relation,

$$\zeta_j = \cos^{-1}(\hat{V}_R \cdot \vec{n}_j) \quad (4.67)$$

Also it should be noted that using Eq.(4.5) for projected area of aero flap-j ,if $\cos \zeta \geq 0$ then there will be aerodynamic forces otherwise for $\cos \zeta < 0$ there will be no aerodynamic forces produced by aero flap-j.

Here \hat{V}_R is the unit vector of the incoming air velocity from atmosphere on the aero flap-j and is expressed in the satellite body-fixed reference frame as

$$\hat{V}_R = R_{321} \hat{j}_o \quad (4.68)$$

Whereas, lift force direction for the top two aero flaps is given by

$$\hat{F}_{L_j} = R_{321} \hat{i}_o, j = 1, 2 \quad (4.69)$$

and for bottom aero flaps is considered as

$$\hat{F}_{L_j} = -R_{321} \hat{i}_o, j = 3, 4 \quad (4.70)$$

The outward unit normal vector of the aero flap-j, \vec{n}_j is given by

$$\begin{aligned} \vec{n}_j &= [\cos \beta_j] \hat{i} + [\sin \beta_j] \hat{j}, \quad j = 1, 2 \\ \vec{n}_j &= -[\cos \beta_j] \hat{i} + [\sin \beta_j] \hat{j}, \quad j = 3, 4 \end{aligned} \quad (4.71)$$

The position vector \vec{r}_j from center of mass O to the center of pressure of the aero flap-j is obtained as

$$\begin{aligned} \vec{r}_j &= \left(\frac{h_s}{2} + \frac{l_f}{2} \sin \beta_j \right) \hat{i} - \left(\frac{l_s}{2} + \frac{l_f}{2} \cos \beta_j \right) \hat{j} + \left((-1)^j \frac{w_s}{4} \right) \hat{k}, \quad j = 1, 2 \\ \vec{r}_j &= -\left(\frac{h_s}{2} + \frac{l_f}{2} \sin \beta_j \right) \hat{i} - \left(\frac{l_s}{2} + \frac{l_f}{2} \cos \beta_j \right) \hat{j} + \left((-1)^j \frac{w_s}{4} \right) \hat{k}, \quad j = 3, 4 \end{aligned} \quad (4.72)$$

where h_s = height of the satellite; w_s = width of the satellite; l_s = length of the satellite; l_f = length of the aero flap-j.

Thus, the torque exerted by the aero flap-j on the satellite is obtained as

$$\vec{T}_{a_{sm}} = \sum_{k=1}^4 \vec{r}_k \times \vec{F}_{a_k} \quad (4.73)$$

where $\vec{F}_{a_k} = \sum_{k=1}^4 \vec{F}_{D_k} + \vec{F}_{L_k}$.

Free Molecular Aerodynamic Force Model

Based on the free-molecular aerodynamic force model [2], the force on a flap surface with area A in the body fixed frame is

$$\vec{F}_{M_j} = A \left[-\bar{n}_j p_j + (\bar{n}_j \sin \chi_j - \hat{V}_R) \left(\frac{\tau_j}{\cos \chi_j} \right) \right] \quad (4.74)$$

where p_j is the total pressure and τ_j is the shearing stress. For analytical simplicity, all flaps were considered to have the same area. The total pressure p_j and shearing stress τ_j are calculated

$$\begin{aligned} \frac{p_j}{q_\infty} = & \left[\left(\frac{2 - \sigma_n}{\sqrt{\pi}} \right) \sin \chi_j + \frac{\sigma_n}{2s} \sqrt{\frac{T_s}{T_\infty}} \right] \\ & \times \left\{ \frac{1}{s} e^{-s^2 \sin^2 \chi_j} + \sqrt{\pi} \sin \chi_j [1 + \operatorname{erf}(s \sin \chi_j)] \right\} \\ & + \left(\frac{2 - \sigma_n}{2s^2} \right) [1 + \operatorname{erf}(s \sin \chi_j)] \end{aligned} \quad (4.75)$$

$$\frac{\tau_j}{q_\infty \cos \chi} = \sigma_t \left\{ \frac{1}{s\sqrt{\pi}} e^{-s^2 \sin^2 \chi_j} + \sin \chi_j [1 + \operatorname{erf}(s \sin \chi_j)] \right\} \quad (4.76)$$

where σ_n and σ_t are normal and tangential accommodation coefficients, T_s is the absolute temperature of the spacecraft surface, T_∞ is the atmospheric temperature, q_∞ is the dynamic pressure given by

$$q_\infty = \frac{1}{2} \rho V_R^2 \quad (4.77)$$

$\operatorname{erf}()$ is the error function defined by

$$\operatorname{erf} = \frac{2}{\sqrt{\pi}} \int_0^x e^{-y^2} dy \quad (4.78)$$

and s is the air speed, non-dimensionalized by the mean molecular speed of the atmosphere

$$s = \sqrt{\frac{M_a V_R^2}{2R^* T_\infty}} \quad (4.79)$$

where M_a is the mean molar mass of the atmosphere and R^* is the universal gas constant.

Thus, the torque exerted by the aero flap-j on the satellite is obtained as

$$\vec{T}_{a_{Mol}} = \sum_{k=1}^4 \vec{r}_k \times \vec{F}_{M_k} \quad (4.80)$$

where $\vec{F}_{a_k} = \sum_{k=1}^4 \vec{F}_{D_k} + \vec{F}_{L_k}$.

4.3.3 Control Laws

The resulting equations of motion Eqs. (4.60)-(4.62) can be written in the following form as

$$[M]\{\ddot{q}\} + \{f_q\} = \{T\} \quad (4.81)$$

where M is the mass matrix, f_q is the force vector which contain centrifugal and coriollis acceleration force terms from equations of motion, q is generalized coordinate as defined by $[\gamma \ \phi \ \alpha]^T$ and T is the external torque vector as defined by $T = T_g + T_{a_{Sim}}$ or $(T_{a_{Mol}})$.

In this section, control laws are derived based on simplified aerodynamic torque model as explained in previous section.

The nonlinear and nonautonomous system equation of motion, Eq. (4.81) is represented in state space form. The following state vector is defined

$$\mathbf{x} = [\gamma \ \dot{\gamma} \ \phi \ \dot{\phi} \ \alpha \ \dot{\alpha} \ \beta_1 \ \beta_2 \ \beta_3 \ \beta_4]^T \quad (4.82)$$

A state space representation of the system (4.81) with a selected controlled output variable $y = \alpha$, is given by

$$\begin{aligned} \dot{\mathbf{x}} &= \mathbf{f}(\mathbf{x}) + \mathbf{g}\mathbf{u} \\ \mathbf{y} &= [\gamma \ \phi \ \alpha]^T \end{aligned} \quad (4.83)$$

where,

$$\mathbf{f}(\mathbf{x}) = [\dot{\gamma}, M_\gamma, \dot{\phi}, M_\phi, \dot{\alpha}, M_\alpha, 0, 0, 0, 0]^T \quad (4.84)$$

$$\mathbf{u} = [\dot{\beta}_1 \ \dot{\beta}_2 \ \dot{\beta}_3 \ \dot{\beta}_4]^T$$

$$\mathbf{g} = [\mathbf{O}_{6 \times 6}, \mathbf{I}_{4 \times 4}]^T \quad (4.85)$$

Here \mathbf{O} and \mathbf{I} denote null and identity matrices of indicated dimensions, and super subscript T denotes the matrix transposition. M_γ , M_ϕ , and M_α denote the decoupled nonlinear equations of motion.

The objectives for the design of control system are: 1) drive the system error to zero without oscillations or overshoots, 2) compensate external disturbances from beginning. To satisfy these objectives, the sliding plane is considered as

$$\mathbf{S} = \ddot{\tilde{\mathbf{q}}} + p_3\dot{\tilde{\mathbf{q}}} + p_2\tilde{\mathbf{q}} + p_1\mathbf{q}_s \quad (4.86)$$

where

$$\tilde{\mathbf{q}} = \mathbf{q} - \mathbf{q}_d, \dot{\tilde{\mathbf{q}}} = \dot{\mathbf{q}} - \dot{\mathbf{q}}_d, \ddot{\tilde{\mathbf{q}}} = \ddot{\mathbf{q}} - \ddot{\mathbf{q}}_d \quad (4.87)$$

Parameters p_1 , p_2 , and p_3 are positive constant, $\tilde{\mathbf{q}} = \mathbf{q} - \mathbf{q}_d$ is the attitude angle tracking error, and \mathbf{q}_s is the integral of the tracking error, that is,

$$\dot{\mathbf{q}}_s = \tilde{\mathbf{q}} \quad (4.88)$$

Here error integral feedback term has been used to obtain robustness in the control system to parameter uncertainty.

The following Lyapunov function candidate is considered

$$V = \frac{1}{2} \mathbf{S}^T \mathbf{S} \quad (4.89)$$

Now taking the derivative of Eq. (4.89) with respect to time yields

$$\dot{V} = \mathbf{S}^T \dot{\mathbf{S}} \quad (4.90)$$

In the preceding Eq.(4.90), $\dot{\mathbf{S}}$ is obtained by taking derivative of Eq. (4.86) with respect to time:

$$\dot{\mathbf{S}} = \tilde{\mathbf{q}}^{(3)} + p_3\ddot{\tilde{\mathbf{q}}} + p_2\dot{\tilde{\mathbf{q}}} + p_1\tilde{\mathbf{q}} \quad (4.91)$$

Eq. (4.91) can be rewritten into the following form,

$$\dot{\mathbf{S}} = \mathbf{q}^{(3)} - \mathbf{q}_d^{(3)} + p_3\ddot{\tilde{\mathbf{q}}} + p_2\dot{\tilde{\mathbf{q}}} + p_1\tilde{\mathbf{q}} \quad (4.92)$$

Next the third order derivative of decoupled equations of motion is required, so using Eq.(4.81), one can obtained following

$$\mathbf{q}^{(3)} = [\mathbf{M}]^{-1} \left(-[\dot{\mathbf{M}}] \{\ddot{\mathbf{q}}\} - \{\dot{f}_q\} + \{f_{s_1}\} + \{f_{s_2}\} + [\mathbf{B}][\mathbf{u}] \right) \quad (4.93)$$

where

$$\begin{aligned} \{\dot{f}_q\} &= \frac{d\mathbf{f}_q}{dt}, \{f_{s_1}\} = \frac{\partial T_g}{\partial \mathbf{q}} \dot{\mathbf{q}}, \{f_{s_2}\} = \frac{\partial T_{a_{sim}}}{\partial \mathbf{q}} \dot{\mathbf{q}} \\ \boldsymbol{\beta} &= [\beta_1, \beta_2, \beta_3, \beta_4]^T, [\mathbf{B}] = \frac{\partial T_{a_{sim}}}{\partial \boldsymbol{\beta}} \dot{\boldsymbol{\beta}} \end{aligned} \quad (4.94)$$

Now taking $\dot{\mathbf{S}} = -\eta \operatorname{sgn}(\mathbf{S})$ in Eq.(4.90) yields $\dot{V} = -\eta |\mathbf{S}|$, which is negative semi-definite of \mathbf{S} for positive value of η . So, the proposed control laws are globally stable for assumed Lyapunov Function (4.89). Using Eq. (4.92), Eq. (4.93), and $\dot{\mathbf{S}} = -\eta \operatorname{sgn}(\mathbf{S})$, the following relations are obtained

$$[\mathbf{M}]^{-1} \{ \mathbf{f}_s + [\mathbf{B}][\mathbf{u}] \} - \mathbf{q}_d^{(3)} + p_3 \ddot{\tilde{\mathbf{q}}} + p_2 \dot{\tilde{\mathbf{q}}} + p_1 \tilde{\mathbf{q}} = -\eta \operatorname{sgn}(\mathbf{S}) \quad (4.95)$$

Here $\mathbf{f}_s = -[\dot{\mathbf{M}}] \{\ddot{\mathbf{q}}\} - \{\dot{f}_q\} + \{f_{s_1}\} + \{f_{s_2}\}$.

Rearranging above Eq.(4.95), the control laws can be written as

$$[\mathbf{u}] = \mathbf{B}^T [\mathbf{B}\mathbf{B}^T]^{-1} \left\{ -\mathbf{f}_s + [\mathbf{M}] \left[\mathbf{q}_d^{(3)} - p_3 \ddot{\tilde{\mathbf{q}}} - p_2 \dot{\tilde{\mathbf{q}}} - p_1 \tilde{\mathbf{q}} - \eta \operatorname{sgn}(\mathbf{S}) \right] \right\} \quad (4.96)$$

Using above control laws Eq. (4.96) will have chattering in control input response, in order to avoid chattering in control input we have given following control law

$$[\mathbf{u}] = \mathbf{B}^T [\mathbf{B}\mathbf{B}^T]^{-1} \left\{ -\mathbf{f}_s + [\mathbf{M}] \left[\mathbf{q}_d^{(3)} - p_3 \ddot{\tilde{\mathbf{q}}} - p_2 \dot{\tilde{\mathbf{q}}} - p_1 \tilde{\mathbf{q}} - \eta \tanh(\mathbf{S}) \right] \right\} \quad (4.97)$$

For the existence of the control law(4.97), $\mathbf{B}\mathbf{B}^T$ must be non-zero in the region of interest :

$$\mathbf{B}\mathbf{B}^T \neq 0 \quad (4.98)$$

4.3.4 Results and Discussions

In order to study the performance of the proposed controller, the system response is numerically simulated using Eq. (4.81) where, free molecular aerodynamic torque model (4.80) is considered in equations of motion, and the control laws Eq.(4.97). The simulation was carried out using MATLAB. The following parameters are assumed for numerical simulation:

Table 4. 3: Parameters for Model-II

Satellite Parameters	$h_s = 0.1[m], l_s = 0.1[m], w_s = 0.1[m],$ $l_f = 0.1[m], I_x = 0.0952, I_y = 0.00211, I_z = 0.0952$
Orbital Parameters	$R = 6878 [km], \mu = 3.986 \times 10^5 [km^3 / s^2],$ $\rho = 6.967 \times 10^{-13} [kg / m^3], \omega_E = 7.27 \times 10^{-5} [rad / s]$
Initial and Final Conditions	$\gamma_o = 40^\circ, \phi_o = 20^\circ, \alpha_o = 40^\circ,$ $\beta_{i_o} = 45^\circ, \gamma_f = 0^\circ, \phi_f = 0^\circ, \alpha_f = 0^\circ$
Control Parameters	$p_1 = 0.97 \times 10^{-6}, p_2 = 2.94 \times 10^{-4}, p_3 = 0.0297,$ $\eta = 0.01$
Free Molecular Aerodynamic Model Parameters	$s = 5, \sigma_n = 0.85, \sigma_t = 0.9, T_\infty = 997.3[K],$ $T_s = 300[K]$
Other Parameters	$C_D = 2, C_L = 0.2$

The first case is looked at where a satellite is required to maneuver from arbitrary reference attitude to desired attitude (Figure 4.9 and Figure 4.10) using aerodynamic torques only. The time history of pico-satellite orientation is given in Figure 4.9. The time history of the control flap deflection of pico-satellite is given in Figure 4.10. Figure 4.9 shows that the desired final orientation was achieved about 0.25 orbits. Here pico-satellite attitude maneuver from 40 deg in yaw, 20 deg in roll, and 40 deg in pitch is performed. Figure 4.10 shows the control flap

deflection is needed in order to maneuver satellite. The control flaps are finally settles down to some angles when satellite reaches to its desired orientation.

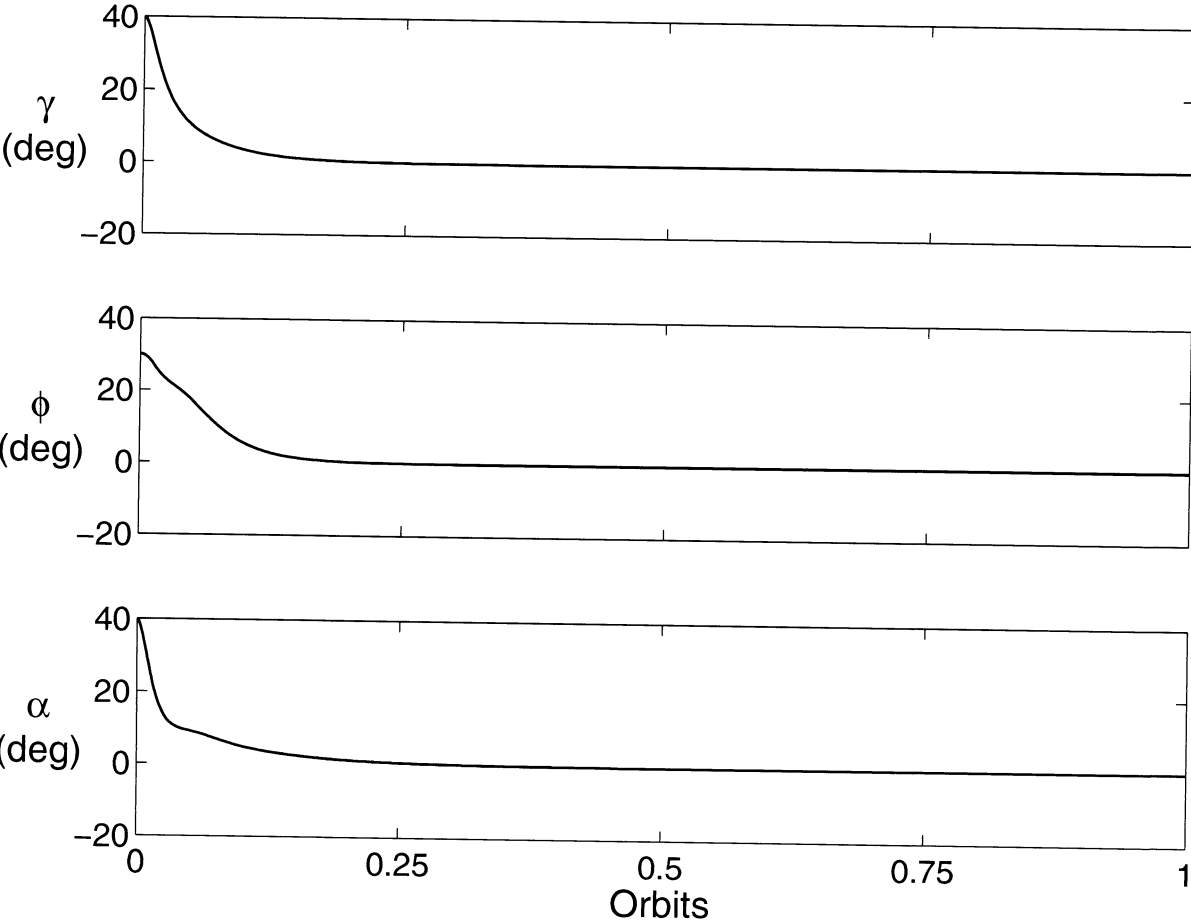


Figure 4.9: Pico-satellite attitude response

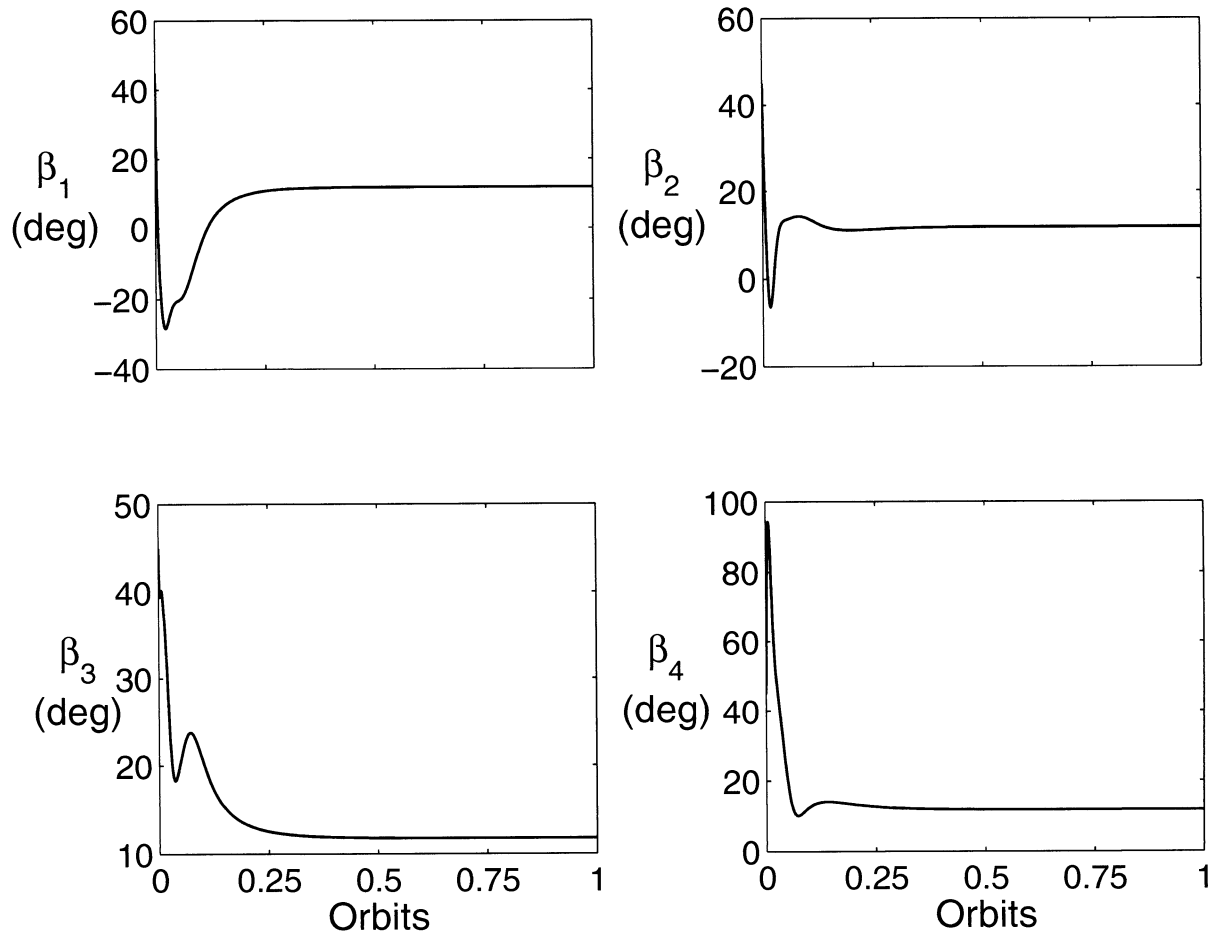


Figure 4.10: Pico-satellite control flaps deflections

In order to study the performance of the proposed VSC in presence of the parameter uncertainties, the numerical simulation was done in the perturbed modes (Figure 4.11 – Figure 4.14). First, the principal moment of inertias ($I_k, k = x, y, z$) are decreased by 30% from its nominal values as follows: $I_x = 0.0067, I_y = 0.0015,$ and $I_z = 0.0067$ in the plant dynamics. In the second case principal moment of inertias ($I_k, k = x, y, z$) are increased by 30% from its nominal values as follows: $I_x = 0.0124, I_y = 0.0027,$ and $I_z = 0.0124$. The above parameters are remained same as its nominal values as $I_x = 0.00952, I_y = 0.00211,$ $I_z = 0.00952$ in the VSC controller Eq.(4.97). The results of the numerical simulation are shown in Figure 4.11 – Figure 4.14 for parameter uncertainties into the principal moment of

inertias. The desired attitude orientation of the satellite is achieved smoothly within 0.25 orbits for both cases as shown in Figure 4.11 and Figure 4.13. Also note that the VSC stabilized the satellite attitude motion without any overshoot in presence of parameter uncertainties. Thus, this numerical simulation verifies the parameter uncertainties rejection properties of the proposed VSC.

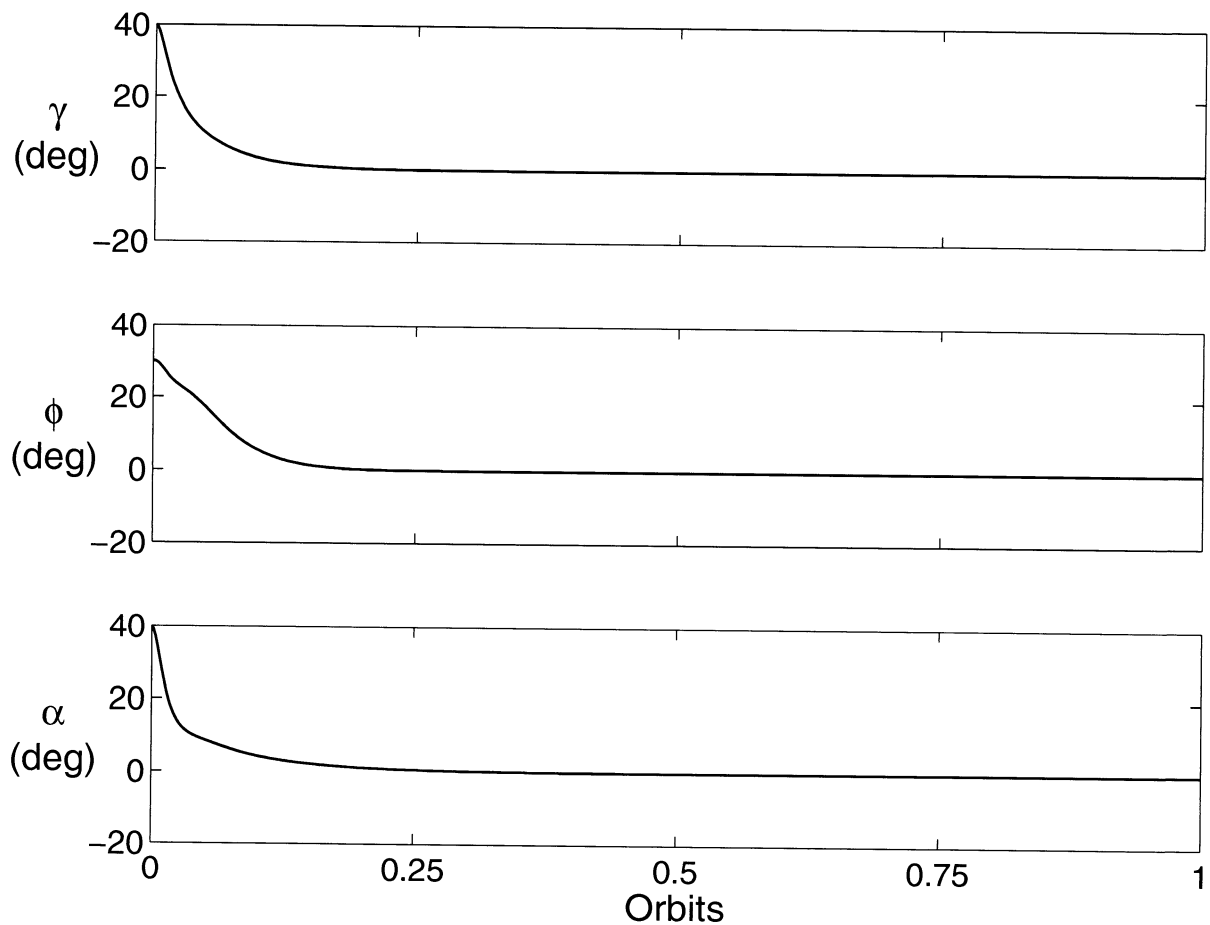


Figure 4.11: Satellite attitude response in presence uncertainties in principle moment of inertia(30% decrease)

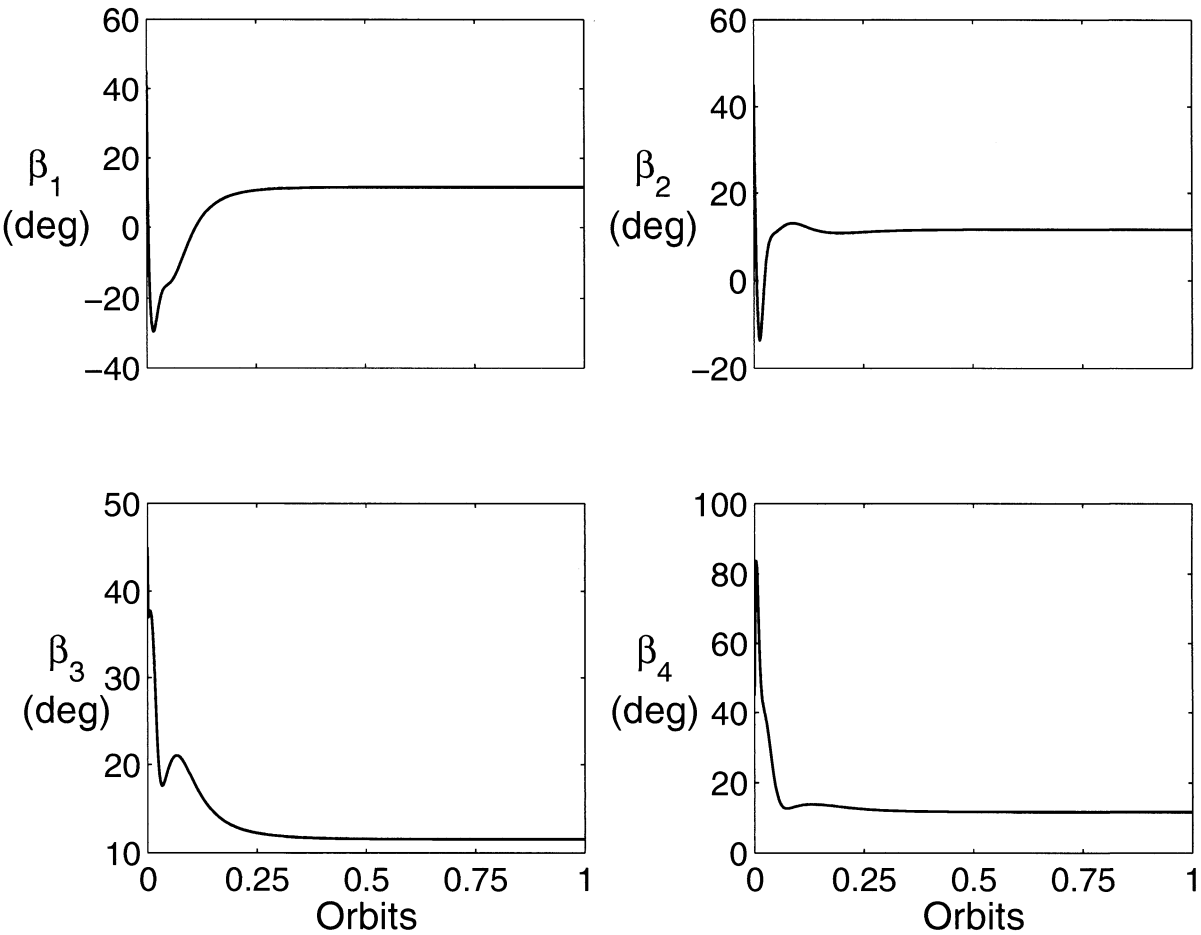


Figure 4.12: Control flaps response in presence of uncertainties in principle moment of inertia(30% decrease)

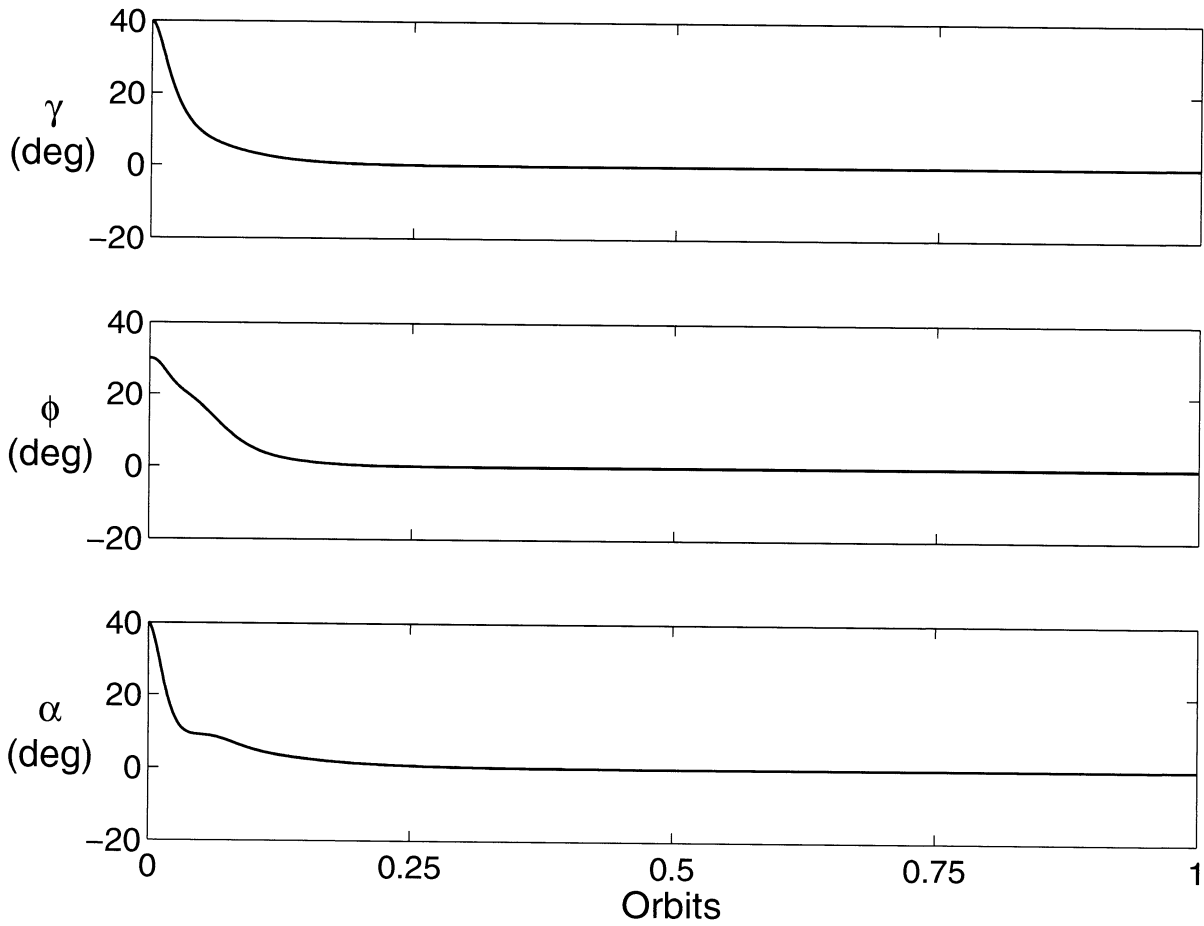


Figure 4.13: Satellite attitude response in presence of uncertainties in principle moment of inertia (30% increase)

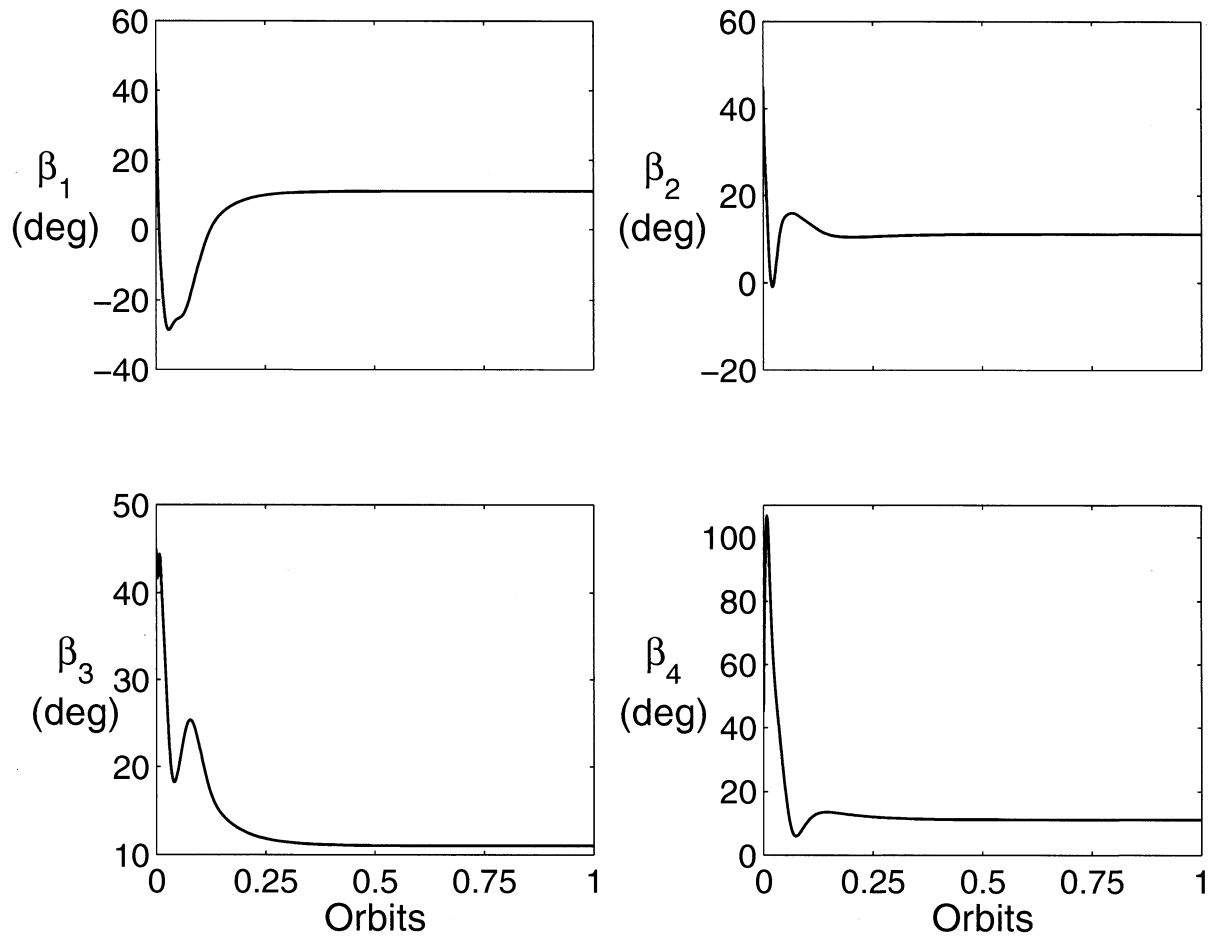


Figure 4.14: Control flaps response in presence of uncertainties in principle moment of inertia (30% increase)

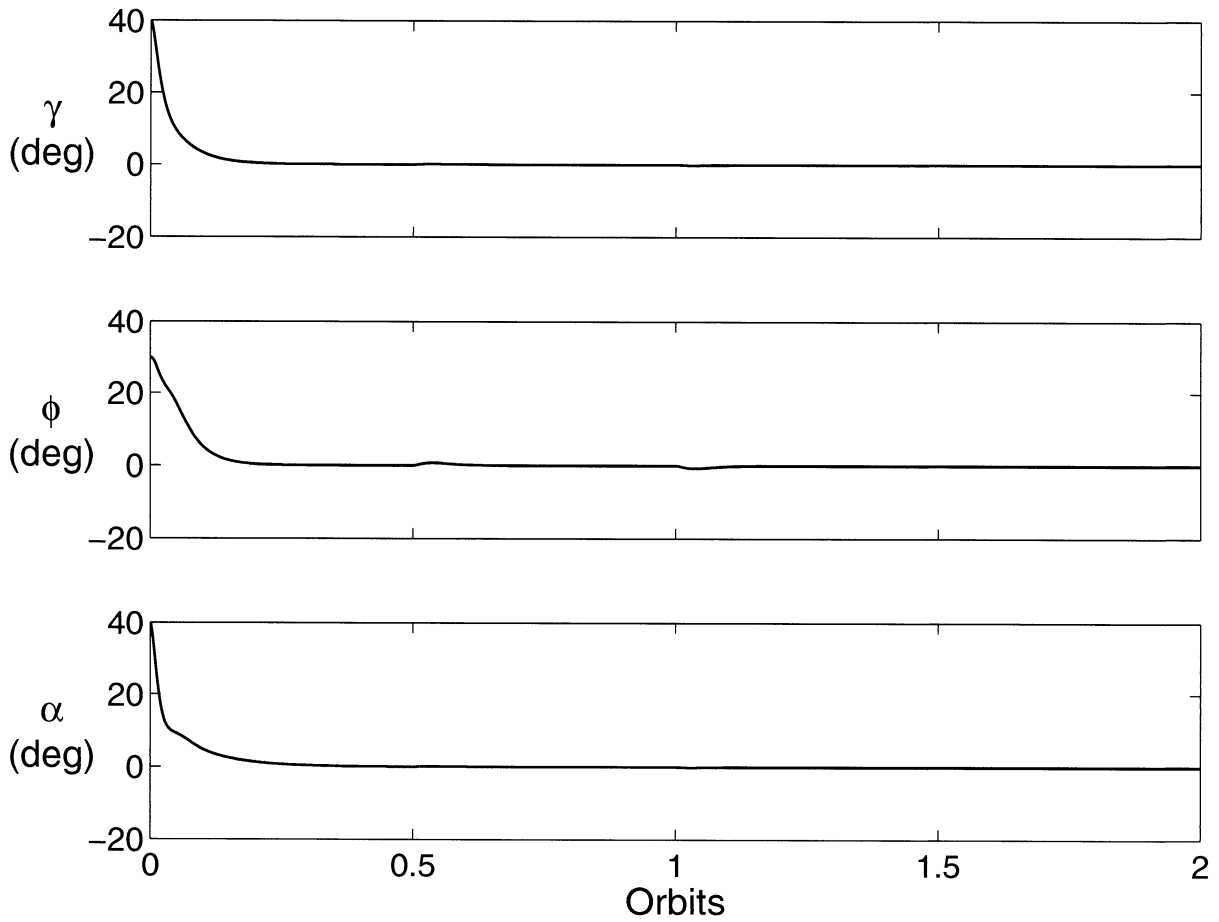


Figure 4.15: Satellite attitude response in presence of external disturbances

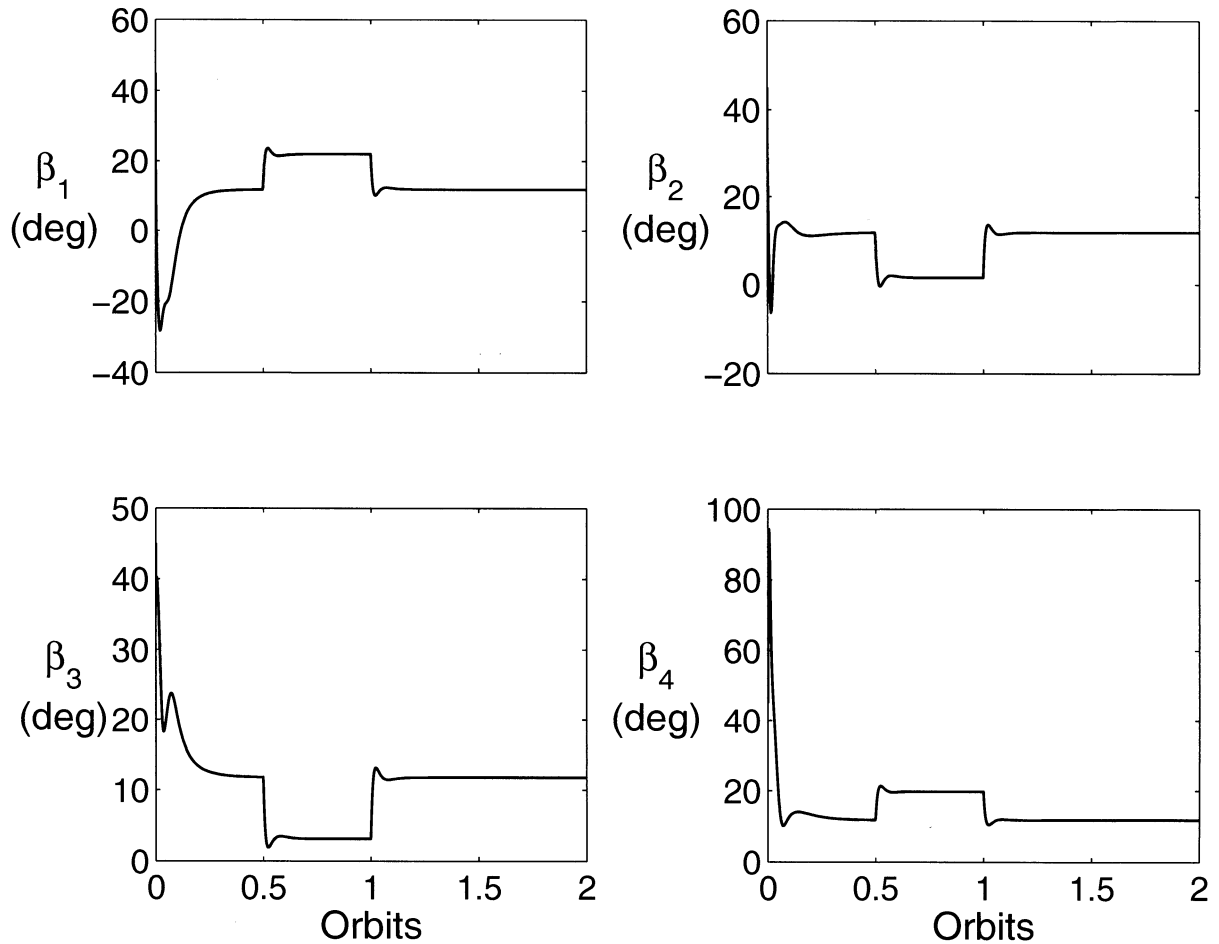


Figure 4.16: Control flaps response in presence of external disturbances

Finally, for an appreciation about the effectiveness of the proposed control laws in presence of external disturbance (Figure 4.15 – Figure 4.16), satellite with external disturbance are considered. The disturbance torque is assumed to be in the order of 10^{-8} for the pico-satellite in the Low Earth Orbits. The disturbance torques of $1 \times 10^{-8} [N.m]$ is applied from 0.5 orbits to 1.0 orbits for all three axis. This disturbance torque is in fact applied to the system when the system almost reaches its desired attitude angle of 0 deg. As shown in Figure 4.15, the desired satellite attitude is successfully attained in presence of disturbances with small attitude errors between 0.5 orbits to 1.0 orbit. Figure 4.16 shows that the control flap deflections. All control flap deflections are changing from their final settling position between 0.5 orbits to 1 orbit. This changes in β_j is due to the fact that in order to

compensate external disturbances control flaps have to generate more aerodynamic torques by varying control flap deflection. Thus, external disturbances rejection property of the proposed VSC verifies the theory presented in Section 3.5.

4.4 Summary

This chapter examines the attitude control of satellites using aerodynamic forces. The synthesis of closed-loop control laws for suitably rotating aero flaps is developed using variable structure control to utilize proper aerodynamic torques for desired attitude response. The control flap deflection β_j is continuously adjusted as per the control laws. The satellite attitude response remains virtually unaffected with changes in mass distribution parameter K and aerodynamic parameter C_a for Model-I. However, the control flap deflection has significant effect as these parameter changes. As K is increased from $K=-1$ to $K=1$, $|\beta_1|_{\max}$ decrease from 140.3 deg to 117.5 deg, respectively in steady state situation. As the aerodynamic parameter C_a is decreased from 10 to 5, the control flap deflection $(|\beta_1|_{\max}, |\beta_2|_{\max})$ increases from (129.9, 56.06) deg to (134.8, 57) deg. Three-axis attitude control for pico-satellite is achieved using only aerodynamic forces. Furthermore, the proposed VSC controllers are found to be robust against parameter uncertainties and external disturbances for both models considered here. The proposed aerodynamic control strategy for attitude control can be implemented for small satellite mission.

Chapter 5

Conclusions

5.1 Conclusions

5.1.1 Solar Radiation Pressure Torques Stabilized Satellite

The present thesis examines the attitude control of satellites using SRP in Chapter 3. The synthesis of closed-loop control laws for suitably rotating solar flaps is developed using VSC to obtain proper SRP torque for satellites operating in circular and elliptic orbits (Section 3.3). The proposed controllers are very effective in presence of initial attitude tracking errors (Section 3.6) for both controllers. The satellite attitude response remains virtually unaffected with changes in orbital eccentricity e , solar parameter C , solar aspect angle ψ , mass distribution parameter K , and orbital inclination i . However, the control solar flap deflection has significant effect as these parameters change. Section 3.6.2 illustrates that as the orbital eccentricity e increases the control solar flap deflection (β_j) increases. It is noted from the results and discussions (Section 3.6) that for lower solar parameter C , the system requires very large solar flap rotation which is not practical. Such large solar flap rotation gives certain limitation on the application of SRP for attitude control of satellites. It is found that solar flap deflection increases with increase in orbit inclination. The VSC is very effective in controlling the satellite harmonic chase-maneuvers which was shown in numerical simulation (Section 3.6). However, as the period of desired harmonic attitude decreases, more control effort is required resulting in increase in solar flaps deflection rates. With regard to SMC and TSMC presented in Section 3.6.2 for satellites in elliptic orbits, the control solar flap deflection almost matches during transient whereas in the steady state the control solar flap deflection differs. Advantage of TSMC is its precise tracking error in finite time was verified in Section 3.6.2. Furthermore, from the analysis it is found that VSC is more robust against external disturbances and parameter uncertainties and its performance is superior in

comparison to other strategies proposed in the literature. The proposed control strategy is augmented with the existing attitude control system of the satellite to extend the life of the space mission experiencing attitude actuator failures.

5.1.2 Aerodynamic Torques Stabilized Satellite

This thesis studies the attitude control of satellites using Aerodynamic forces in Chapter 4. Two aerodynamic models are considered: simplified aerodynamic model and more realistic free molecular aerodynamic torque model for planar case (Model-I) and three dimensional case (Model-II). The closed-loop control laws for suitably rotating aerodynamic flaps are developed using VSC based on simplified aerodynamic torque model to utilize proper aerodynamic torques for desired attitude response in Section 4.2 and Section 4.3, respectively. The large angle attitude maneuver is attained by rotating aero flaps. The effect of aerodynamic parameter C_a and mass distribution parameter K on satellite attitude response is studied in Section 4.2.4 for Model-I and it is found that attitude response remains virtually unaffected with changes in these parameters. However, the control aero flap deflection has significant effect as these parameters changes. As K is increased from $K=-1$ to $K=1$, aerodynamic control flap deflection decreases whereas decrease in the aerodynamic parameter C_a require more control flaps deflection was shown in Section 4.2.4. Three-axis satellite attitude control using only aerodynamic torques by rotating four aero flaps was accomplished in Section 4.3. Here a satellite attitude maneuver from arbitrary reference attitude to desired attitude for pico-satellite is achieved in Section 4.3.4. In order to study the performance of the proposed VSC laws for three-axis attitude control in presence of the parameter uncertainties, the numerical simulation was done in the perturbed modes in Section 4.3.4 for uncertainties in principle moment of inertias. It is shown that controller was successful to achieve desired attitude response in presence of parameter uncertainties. The effectiveness of the controller in presence of external disturbances is also presented in Section 4.3.4 for pico-satellite with large angle attitude maneuver. The proposed control strategy is attractive for small satellite mission to stabilize satellite three-axis control using only aerodynamic forces.

5.2 Future Works

In the future work, the proposed concept for SRP stabilized satellite can be extended for three-axis attitude control of the satellite using different configurations. Failure of the control solar flaps can also be studied as extension of this research work. If one of the control flaps fails then it is difficult for the control system to stabilize a satellite attitude without knowing failure. Therefore, it is required to investigate such controllers which will consider these cases. Recently, researchers are studying fault tolerant controllers; these controllers can be applied for the failure cases. Furthermore, this study can be extended to an aerodynamic stabilized satellite. Also shadowing of the control flaps by a satellite body can be considered for the proposed three-axis aerodynamic controller, because there are many situations where aerodynamic control flaps may enter into the shadow of the satellite body.

References

- [1] W.J. Larson, J.R. Wertz (Editors), Space Mission Analysis and Design, Kluwer Academic Publishers, Third Edition, Dordrecht, Boston, London (1999).
- [2] K. D. Kumar, Fundamentals of Dynamics and Control of Space Systems, Ryerson University Press, First Edition, Toronto (2006).
- [3] W.E. Frye, E.V.B. Stearns, Stabilization and attitude control of satellite vehicles, ARS Journal 29 (1959) 927-931.
- [4] R.L. Sohn, Attitude stabilization by means of solar radiation pressure, ARS Journal 29 (1959) 371-373.
- [5] R.R. Hibbard, Attitude stabilization using focused radiation pressure, ARS Journal 31 (1961) 844-845.
- [6] L.A. Ule, Orientation of spinning satellites by radiation pressure, AIAA Journal 1 (1963) 1575-1578.
- [7] M.C. Crocker II, Attitude control of a sun-pointing spinning spacecraft by means of solar radiation pressure, Journal of Spacecraft and Rockets 7 (1) (1970) 357-359.
- [8] J. Falcovitz, Attitude control of a spinning sun-pointing spacecraft by means of a grated solar sail, Technical Report CSR-TR-66-17, MIT Center for Space Research, (1966).
- [9] V.J. Modi and K.C. Pande, Solar pressure control of a dual-spin satellite, Journal of Spacecraft and Rockets 10 (1) (1973) 355-361.
- [10] V.J. Modi and K.C. Pande, Solar pressure induced librations of spinning axisymmetric satellites, Journal of Spacecraft and Rockets, 10 (9) (1973) 615-617.
- [11] K.C. Pande, Attitude control of a spinning spacecraft by radiation pressure, Journal of Spacecraft and Rockets, 13 (1) (1976) 765-768.
- [12] V.J. Modi and K.C. Pande, A bang-bang solar pressure attitude control system, Journal of the Astronautical Sciences, 22 (1974) 1-20.
- [13] K.C. Pande, M.S. Davies, and V.J. Modi, Time optimal pitch control of satellite using solar radiation pressure, Journal of Spacecraft and Rockets 11 (1) (1974) 601-603.
- [14] K.C. Pande and R. Venkatachalam, Semipassive pitch attitude control of satellite using solar radiation pressure, IEEE Transactions on Aerospace and Electronic Systems 15 (2) (1979) 194-198.

- [15] K.C. Pande and R. Venkatachalam, Solar pressure attitude stabilization of earth-pointing spacecraft, *IEEE Transactions on Aerospace and Electronic Systems* 17 (6) (1981) 748-756.
- [16] K.C. Pande and R. Venkatachalam, Inertially fixed pitch stabilization of satellites by solar radiation pressure, *Acta Astronautica* 7 (2) (1980) 155-167.
- [17] K.C. Pande and R. Venkatachalam, Optimal solar radiation pressure attitude control of spacecraft-I: inertially fixed attitude stabilization, *Acta Astronautica* 9 (9) (1982) 533-540.
- [18] R. Venkatachalam, R. and K.C. Pande, Optimal solar radiation pressure attitude control of spacecraft-II: large angle attitude maneuvers, *Acta Astronautica* 9 (9) (1982) 541-545.
- [19] R. Venkatachalam, Large angle pitch attitude maneuver of a satellite using solar radiation pressure, *IEEE Transactions on Aerospace and Electronic Systems*, 29 (4) (1993) 1164-1169.
- [20] S.N. Singh and W. Yim, Feedback linearization and solar pressure satellite attitude control, *IEEE Transactions on Aerospace and Electronic Systems* 32 (2) (1996) 732-740.
- [21] B.W. Stuck, Solar pressure three-axis attitude, *Journal of Guidance and Control*, 3 (2) (1980) 132-139.
- [22] V.J. Modi and K. Kumar, Attitude control of satellites using the solar radiation pressure, *Journal of Spacecraft and Rockets*, 9 (9) (1972) 711-713.
- [23] V.K. Joshi and K. Kumar, New solar attitude control approach for satellites in elliptic orbits, *Journal of Guidance and Control* 3 (1) (1980) 42-47.
- [24] K. Kumar, A solar attitude controller for extending operational life-span of communication satellites, *Acta Astronautica* 17 (1) (1988) 61-67.
- [25] J.R. Scull, Mariner IV revisited or the tale of the ancient mariner, *Proceedings of the 20th International Astronautical Federation Congress, Argentina* (1969) 747-758.
- [26] U. Renner, Attitude control by Solar Sailing-A promising experiment with OTS-2, *European Space Agency Journal* 3 (1979) 35-40.

- [27] K.D. Kumar, H.C. Bang, and M.J. Tahk, New attitude control approach for satellite in elliptical orbits using solar radiation pressure, *Acta Astronautica* 59 (6) (2006) 462-473.
- [28] V. J. Modi and S. K. Shrivastava, Optimized Performance of a Semipassive Aerodynamic Controller, *AIAA Journal* 11 (8) (1973) 1080-1085.
- [29] R. Ravindran and P. C. Hughes, Optimal Aerodynamic Attitude Stabilization of Near-Earth Satellites, *Journal of Spacecraft and Rockets* 9 (7) (1972) 499-506.
- [30] K.C. Pande and R. Venkatachalam, On Optimal Aerodynamic Attitude Control of Spacecraft, *Acta Astronautica* 6 (1979) 1351-1359.
- [31] V. A. Sarychev, Aerodynamic Stabilization System of the Satellites, *Proceedings of the International Colloquium on Attitude Changes and Stabilization of Satellites, Paris* (1968) 177-179.
- [32] R. R. Kumar, D. D. Mazanek, and M. L. Heck, Simulation and Shuttle Hitchhiker Validation of Passive Satellite Aerostabilization, *Journal of Spacecraft and Rockets* 32 (5) (1995) 806-811.
- [33] Y. H. Chen, Z. C. Hong, C. H. Lin, and J. S. Chern, Aerodynamic and gravity gradient stabilization for microsattellites, *Acta Astronautica* 46 (7) (2000) 491-499.
- [34] R. Wisniewski, Optimal Three-Axis Satellite Attitude Control with the Use of Magnetic Torquing, *Proceedings of AIAA Guidance, Navigation, and Control Conference, New Orleans* (1997).
- [35] M. L. Psiaki, Nanosatellite Attitude Stabilization Using Passive Aerodynamics and Active Magnetic Torquing, *Journal of Guidance, Control, and Dynamics* 27 (3) (2004) 347-355.
- [36] V. J. Modi and K. C. Pande, Aerodynamic-solar hybrid attitude control of near-earth satellites, *Journal of the Astronautical Sciences* 22 (1974) 36-54.
- [37] K. D. Kumar, M. J. Tahk, and H. C. Bang, Satellite Attitude Stabilization Using Solar Radiation Pressure and Magnetic Torquer, *IEEE Trans. on Aerospace and Electronic System* (2005). (under review, TAES-200501603).
- [38] V. Utkin, *Sliding Modes and Their Applications in Variable Structure Systems*, MIR Publishers, Moscow (1977).

- [39] V. Utkin, J. Gulnder, and J. Shi, Sliding Mode Control in Electromechanical Systems, Taylor & Francis Ltd., London, Philadelphia (1999).
- [40] W. Perruquetti and J. P. Barbot, Sliding Mode Control in Engineering, Marcel Dekker Inc., New York (2002).
- [41] Z. Man and X. H. Yu, Terminal sliding mode control of MIMO linear systems, IEEE Transactions on Circuits and Systems 44 (11) (1997) 1065-1070.
- [42] T. Yu, Terminal sliding mode control for rigid robots, Automatica 34 (1) (1998) 51-56.
- [43] F. Yong, X. Yu, and Z. Man, Non-singular terminal sliding mode control of rigid manipulators, Automatica 38 (12) (2002) 2159-2167.
- [44] C. W. Tao, J. S. Taur, and M.-L. Chan, Adaptive fuzzy terminal sliding mode controller for linear systems with mismatched time-varying uncertainties, IEEE Transactions on Systems, Man, and Cybernetics 34 (1) (2004) 255-262.
- [45] S. Janardhanan and B. Bandyopadhyay, On discretization of continuous-time terminal sliding mode, IEEE Transactions on Automatic Control 51 (9) (2006) 1532-1536.
- [46] C.-K. Lin, Nonsingular terminal sliding mode control of robot manipulators using fuzzy wavelet networks, IEEE Transactions on Fuzzy systems 14 (6) (2006) 849-859.
- [47] S. Sastry, Nonlinear Systems: Analysis, Stability, and Control, Springer-Verlag New York Inc., New York, London (1999).
- [48] J.-J. E. Slotine and W. Li, Applied Nonlinear Control, Prentice-Hall, New Jersey (1991).
- [49] M. J. Sidi, Spacecraft Dynamics & Control, Cambridge University Press, First Edition, Cambridge, New York, Melbourne (2002).
- [50] P. C. Hughes, Spacecraft Attitude Dynamics, Dover Publications, Second Edition, New York (2004).
- [51] B. Wie, Space Vehicle Dynamics and Control, American Institute of Aeronautics and Astronautics Inc., Reston (1998).

List of Publications From Present Research

- [1] T. R. Patel, K. D. Kumar, and K. Behdinan, "Satellite attitude control using solar radiation pressure based on non-linear sliding mode control," *Proc. IMechE Vol. 222 Part G: Journal of Aerospace Engineering*, December, 2007, (accepted for publication).
- [2] T. R. Patel, K. D. Kumar, and K. Behdinan, "Variable structure control for satellite attitude stabilization in elliptic orbits using solar radiation pressure," *International Journal of Control*, February, 2008, (under review, TCON-2008-0095).
- [3] T. R. Patel, K. Behdinan, and K. D. Kumar, "Satellite attitude control using aerodynamic forces based on variable structure control," *IEEE Trans. on Aero. and Electr. Sys.*, May, 2008, (submitted).
- [4] T. R. Patel, K. D. Kumar, and K. Behdinan, "Satellite three-axis attitude control using aerodynamic force based on nonlinear sliding mode control," will be submitted to *Journal of Spacecrafts and Rockets* by May, 2008, (under writing).

